UNIVERSITY OF
BIRMINGHAM

Toward Autonomous Cell Recognition and Manipulation for Intra-cytoplasmic Sperm Injection

By

Amir Mohammad Hajiyavand

A thesis submitted to

The University of Birmingham

for the degree of

DOCTOR OF PHILOSOPHY

School of Engineering

University of Birmingham

Birmingham, United Kingdom

March 2018

Dedicated to

My lovely family

for all their great support

Abstract

Micromanipulation and microinjection of biological cells are two of the most useful techniques for manipulating cells for different applications. One of these applications, employed for infertility treatments, is intra-cytoplasmic sperm injection. The current set-up for this application is designed to be operated manually by an embryologist. In this method, a single sperm is deposited into an oocyte. There are a number of non-clinical factors affecting the success rate of fertility. These factors can cause cells to be damaged at the time of injection and resulting in its degeneration after sperm deployment. This thesis focuses on analysing these factors, in particular the creation of deformation of the cell at the time of injection. The speed of injection has been considered as critical factors linked to the creation of oocyte deformation during injection. The main aim of this research is to develop an autonomous cell manipulation and injection system whilst minimising cell deformation during injection. A proposed set-up is designed to manipulate a single oocyte in three dimensional space to the desired location using a minimal number of operations. After the operation, the injection of sperm proceeds and is delivered into the desired position inside the oocyte. New software has been designed for the polar body and oocyte position and orientation recognition. Furthermore, an FE model has been developed to help the analysis of different factors affecting the injection process and provides information on the injection force and deformation creation during the injection.

Acknowledgment

I would like to express my sincere gratitude to my supervisor Dr Mozafar Saadat who has been very supportive during this research. Without his patient and enormous support this thesis would not have been possible. I would like to appreciate Dr Artemis Stamboulis for her great support and being a fantastic friend in all aspects. Also I would like to thank Dr Paris Keynejad who helped me to learn the medical section of this project.

I would like to thank Ferhat and Alessandro, who have been a great friend and very supportive. I would also like to thank all my colleagues and friends in Mechanical Engineering who have been encouraging during this research.

I would like to thank Sebastian at the Birmingham Halal Centre and Peter Jones in Biomedical Service Unit within University of Birmingham who helped me by providing the sheep ovarian samples and Zebrafish embryo sample. Additionally, I would like to thank Mr Simon Rowan who assist me considerably by manufacturing the system.

This thesis was copy edited for conventions of language, spelling and grammar by Janet's Proofreading Service and Miss Elspeth Insch.

I would like to express my sincere thanks to Liudmyla who has supported me in every step during writing this thesis and make the hardness of this path smooth for me.

Finally, I would like to express my deepest appreciation to my lovely parents, Abbas and Shahla, and my brother Arya whose words of encouragement and persistent motivation assisted me throughout this research.

Contents

List of Illustrations

List of Tables

List of Symbols

Title	Symbol	Unit
circular segment	S	µm
Spring constant	K	N/m
Damping constant	C	N .m / s
Force	F	N
Stress	σ	N/m2
Elastic modulus	E	N/m2
Speed	V	µm/s

List of Abbreviations:

GV: Germinal vesicles

ICSI: Intra-cytoplasmic sperm injection

IUI: Intrauterine insemination

IVF: In vitro fertilization

MFAR: Maximum force amplitude ratio

List of Medical Terms:

Cytoplasm: a dense liquid inside an oocyte.

Embryo: oocyte after being fertilised.

In vitro fertilization (IVF): Infertility method to put sperm and oocyte beside each other in incubator and let the sperm fertilise the oocyte.

Intra-cytoplasmic sperm injection (ICSI): introducing a single sperm into an oocyte

Intrauterine insemination (IUI): infertility method to spray sperms on oocyte in fallopian tube.

Oocyte: female cell of reproductive system.

Oolemma: the inner layer of an oocyte which protect the cytoplasm.

Perivitelline space: a space between oolemma and zona pellucida.

Sperm: female cell of reproductive system.

Zona pellucida: the most outer layer of an oocyte consists of glycoproteins which protects the oocyte.

CHAPTER 1

INTRODUCTION

Infertility is defined for a couple who cannot get pregnant, despite trying for more than six months for young couples and for a year for those aged over 40. Around one out of seven couples may face difficulties with pregnancy in the UK and one out of four in developed countries [1, 2]. The chance for a couple who are trying to have a baby for more than three years is less than 25% without receiving any treatment. Different causes of infertility have been reported and these can originate either from the man or the woman. The main cause of infertility in women is lack of regular ovulation and in men is poor quality of semen. There are different methods used for the treatment of infertility. Besides medical treatments, there are three methods which are suggested for treatment of infertility which usually caused by male factor deficiencies. These treatments are named as intrauterine insemination (IUI), *in vitro* fertilization (IVF) and intra-cytoplasmic sperm injection (ICSI). Intra-cytoplasmic sperm injection is an invasive method to the cell and considered as a microinjection procedure [1, 2].

Microinjection is one of the most suitable techniques in introducing foreign material into a biological cell. Intracytoplasmic sperm injection (ICSI) is an application of microinjection used for infertility treatment. The current set-ups have certain drawbacks and may harm the oocyte at the time of the injection. This project focuses on the needle/oocyte interaction and is aimed at developing a novel integrated technology to address the current deficiencies.

There are many researchers who focus on improving the success rate of pregnancy using ICSI. They mostly concentrate on the drawbacks of the current methods. There are a number of different factors affecting this success rate, including clinical factors and non-clinical factors (engineering factors).

This project involves with the improvement of the current ICSI operation from an engineering point of view. Analysing the mechanical properties of the biological cell (oocyte) at the time of injection would be the very first stage of this project in terms of understanding the harm inflicted on the oocyte at the time of injection.

The deficiencies of the current methods and their effects on the oocyte at the time of the injection will be mechanically analysed in this project. The research starts with the mechanical tests of a real oocyte to obtain it's the mechanical properties. These properties can help to simulate and model the injection process. The next step will focus on the design of a new set-up for ICSI, which will eliminate the existing drawbacks. This set-up will include a holder/injector integrated unit. Reducing the deficiencies of the process in the new set-up will be achieved by using the holding and injecting factors. After the engineering modelling of the cell and the ICSI procedure, a new design will be proposed for the new set-up. The injector and the holding system will be completely automated and controlled by a computer based on an integrated injection force feedback system. This set-up would have the capability of simultaneous multi injections.

The other advantages of force feedback will be used for a haptic system to give the embryologist the sense of injection by magnifying the amount of the injection force. Moreover, this can help to develop an appropriate tele-manipulation system.

The proposed design is an integrated system which includes the cell holder and injector. Additive manufacturing, which is 3D printing, is proposed as the fabrication method.

1.1 ***Motivation***

The conventional method of cell injection normally involves a human operator who relies on visual feedback using a microscope and also employing two manual joysticks to process the injection procedure. To achieve expertise in cell injection it requires a long and complex training period (approximately one year) and still the success rate is not high enough to trust [3]. Some of the factors considerably affecting the success rate are accuracy, speed and also trajectory of the micropipette [4]. Consequently, developing automated systems is useful in advancing the cell injection process.

Developing an automated system needs different factors to be considered; expanding image processing software which is a capable of working with the system, is essential as a detector. On the other hand, many researchers focus on developing a mechanical model that can: mimic the cell behaviour under the external load, which is the injection force; and predict the amount of deformation that may be caused by mentioned factors such as speed, as deformation is considered as major damage to the cell. This also provides more controllable manipulation of biological cells, considering the injection speed and its role in potential mechanical damage to the cell.

These factors motivate this research to develop an automated system integrating with vision detection software which is able to process the injection and manipulation and minimise the damage applied to the cell.

1.2 *Research aim and objectives*

The aim of this research is to develop the underpinning principles of the design of a novel 3D manipulation and injection technique. The proposed ICSI method is designed with the purpose of minimizing the mechanical damages (i.e. deformation) to the oocyte during injection. In addition, it is designed with the capability of automatically manipulating the oocyte into the desired position followed by single sperm injection into it. In particular this research focuses on the design, the development of the technique as well as modelling and analysing the factors affecting the injection procedure. The research objectives are fourfold, as in the following:

- To derive and develop cell deformation analysis caused by the injection load during the microinjection procedure.
- To develop an FE model to analyse the speed of the injection as an important factor for the creation of deformation. Additionally, injection speed will be analysed in real experiments on zebrafish embryos. The injection forces will be measured to investigate the effect of speed on the injection force.
- To develop an oocyte and polar body detection software. This software is essential for directing the manipulation of the cell; it can be adapted with different

microscopes. The experimental data from images obtained from different microscopes will be discussed.

- To design and analyse a 3D micromanipulation system. This will involve the design and analysis of a 3D cell micromanipulation and injection system which is able to manipulate the oocyte and position it in the right direction and orientation with the minimum number of operations. The conceptual design will be developed and the operational process will be analysed in detail.

1.3 *Research methodology*

In this research, a novel method of micromanipulation of the cell is introduced. This is a first report of a system which can manipulate and inject at the same time fully automatically in one unit. A proposed model is developed to predict the creation of the deformation of the embryo's membrane based on the indentation force during the cell microinjection procedure. The real experiment is conducted to understand the effect of injection speeds on deformation create and find the optimum injection speed which makes minimum damages. Then vision detection software is developed that is compatible with different inverted microscopes and can detect the position of the oocyte and polar body as well as the orientation of the polar body. Finally, an automated system is proposed and the method of manipulation has been analysed for manipulating the oocyte to position the polar body with the minimum number of operations.

1.4 *Thesis structure*

This thesis is divided into seven chapters. The structure of the rest of the thesis is as follows:

Chapter 1 covers the introduction of this thesis, and presents the aims, objectives, methodology and total structure of thesis.

Chapter 2 covers the literature review of different methods of cell injection in the application of intra-cytoplasmic sperm injections and factors influencing the injection procedure and also different systems of cell manipulation for orienting and positioning the cell in any appropriate and desired location.

Chapter 3 concerns the analytical modelling of the cell deformation and how it affects the degeneration of cells after the sperm injection using current methods. Cell deformation analysis helps to find the best methods to decrease the damage to the cell at the time of injection. Also this chapter will consider the methods of sperm injection into the oocyte. The injection plays a significant role in creating the damage to the cell in intra-cytoplasmic sperm injection. Different methods of injection will be analysed in this chapter. These methods will be compared and the creation of deformation by each method will be discussed.

Chapter 4 covers the speed analysis and effect of different speeds on the creation of deformation. The results of this chapter are obtained from the zebrafish embryo injections for six different speeds. Also an experimental set-up is designed and developed for the speed injection tests. A finite element analysis for the injection process which was developed to analyse the effect of different speeds. Accessing real samples is difficult and

the purpose of developing this FE model is to analyse the effect of speed in the creation of deformation. The model is validated with the experimental results.

Chapter 5 reports on the cell vision recognition and integration to the newly designed manipulation. In this chapter, the detection method is discussed which is newly developed and can recognize the oocyte and its polar body position and then calculate the optimum number of actions based on the manipulator end-effectors to deliver the oocyte to the right position and orientation. Also the integration of this software to the system will be discussed to make it adaptable to this newly developed system.

Chapter 6 considers the manipulator system's design and control. The design of the manipulators for manipulating the oocyte by an optimum number of actions will be discussed in this chapter. Inverse kinematics, and dynamics are the main factors for the design of the manipulators; after discussing the design, the control methods and how the manipulators operate in real time will be analysed in the second part of this chapter.

Chapter 7 concludes the thesis and suggests future works for this application by employing suggested methods.

CHAPTER 2

LITERATURE REVIEW

2.1 *Introduction*

An intra-cytoplasmic sperm injection is a method of delivering a single sperm inside an oocyte which is considered for couples who are not able to have a baby naturally. This method is mainly employed for couples where the male has a fertility problem. In this method, an embryologist selects a single sperm based on its morphological shape and motility and then delivers it to the collected oocyte by using a microinjection set-up. The current devices function with two manual micromanipulators which are directed by two handles to control the movement of the injection micropipette. Also, other joysticks are employed to hold the cell in place during the injection procedure.

The injection procedure is a sensitive operation. The injection must not happen through a specific part of the oocyte called the polar body. The polar body is an intracellular object located in the perivitelline space. The injection must not happen through this polar body as it would cause deficiencies to the baby. Consequently, the same set-up is used to manipulate the oocyte to the correct position and orientation for the desired location.

There are many researchers who have been focused on improving the success rate of pregnancy by developing various methods for injections in ICSI. The schematic view

of ICSI is represented in Figure 2-1. They have mostly concentrated on the drawbacks of the current methods. They strongly believe there are various factors affecting this success rate, including clinical factors and non-clinical factors (engineering factors). Non-clinical factors are crucial in the failure of the ICSI outcome and recently they have been the main focus of both clinicians and engineers. There have been a small number of developed set-ups and some methods of injections reported in the literature, which will be demonstrated in the following sections.

2.2 *Oocyte presentations*

Oocytes are developed and released from a female organ called the ovary. Each female has two ovaries and these ovaries are connected to the uterus via fallopian tubes. Each month, a female produces a single oocyte which travels from the ovary to the uterus via a fallopian tube. Pregnancy occurs when a single sperm enters the oocyte and an embryo is formed.

Oocytes are trapped at an early stage of the first meiotic divisions prior to being released from the ovaries. Following maturation and during each menstrual cycle, pituitary gonadotrophin replicates the completion of the first meiosis a day before ovulation (as represented in Figure 2-2). Early oocytes are immature and are also known as germinal vesicles (GV) or as being at the metaphase I (MI) stage. The GV breakdown specifies a continuation of meiosis and polar body extraction signals the completion of the first meiotic division in a human oocyte. The released oocyte is surrounded by a thick layer called the zona pellucida which has the responsibility of enveloping the intracellular objects from the environmental adversity.

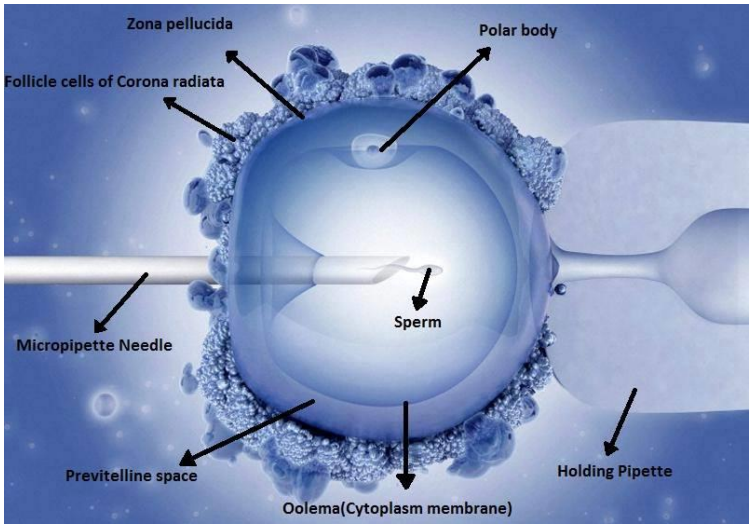

Figure 2-1. Schematic view of ICSI process indicating oocyte parts [5]

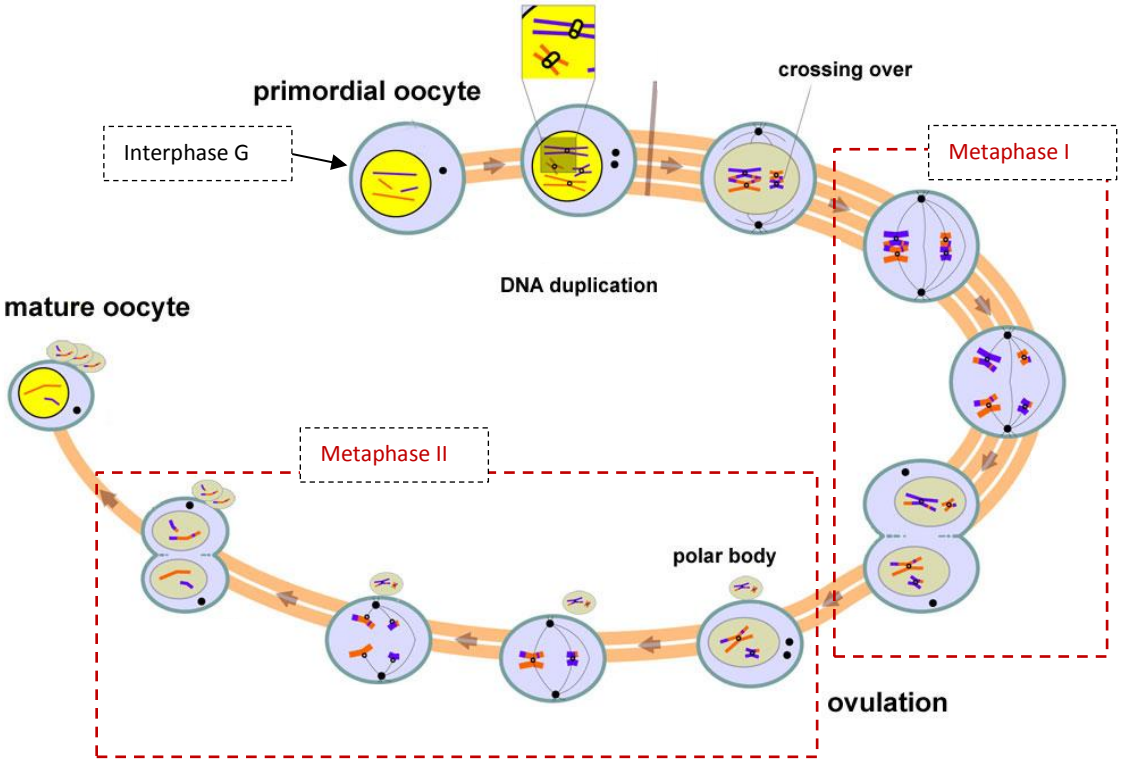

Figure 2-2. Oocyte developmental stages [6]

The polar body is a small intracellular cytoplasmic exclusion object which is formed to surround the DNA and is created during the oocyte meiosis. The oocyte which extracts the polar body is called an oocyte in stage II or metaphase level II. There is another thin layer inside the oocyte named as the oolemma. This layer is much thinner than the zona pellucida but more stretchable. The oolemma covers the cytoplasm inside in addition to the nucleolus. This layer is also called the vitelline membrane. The cavity area between the oolemma and the zona pellucida is called the perivitelline space. The polar body is located in the perivitelline space.

2.3 *ICSI background*

During the past decade, the infertility treatment field has been a major focus of the researchers in the area of fertility in both clinical and non-clinical aspects. There are three different methods considered for the treatment of infertility non-clinically: intrauterine insemination (IUI), *in vitro* fertilization (IVF), intra-cytoplasmic sperm injection (ICSI) [5-7]. Among all the problems causing infertility, the main reason stems from the male factor, which consequently leads to an *in vitro* operation for treatment [8-12]. IUI and IVF are general treatments for the infertility in these cases, but are not proposed for low sperm deficiencies [13].

In the last decade different techniques have been proposed for treatments for the couples who suffer from severe immobility of the sperm. The intra-cytoplasmic sperm injection was proposed as a treatment for this type of infertility. Low sperm production, low maturation and low motility are three considerable factors causing infertility of this

type. This means the sperm is immature, abnormally shaped, unable to reach the oocyte, or not able to penetrate the zona pellucida [14-16].

Microinjection is one of the most suitable techniques for introducing and injecting foreign materials into biological cells. ICSI is one of the applications of the microinjection. This method was first proposed in 1992 and 1993 and there were reports of success for couples who had difficulty in fertilization using IVF. The ICSI has had a rapid acceptance around the world [17-19].

In this method, the oocyte is collected from the female patient and subjected to the injection using a micropipette to deliver the sperm. This method is currently used for infertile couples. The current method has some deficiencies which reduce the success rate. These deficiencies can be divided into two main categories: clinical issues and non-clinical issues [20]. In the proposed set-up, attempts were made to solve the mechanical issues by suggesting different methods of injections. The success rate of ICSI in 2010, from the NHS, is as the following [21, 22]:

- 32.2% for women under 35
- 27.7% for women aged 35-37
- 20.8% for women aged 38-39
- 13.6% for women aged 40-42
- 5% for women aged 43-44
- 1.9% for women aged over 44

As mentioned in the reasons for infertility, there are two main groups of factors affecting the outcome of ICSI: clinical factors and non-clinical factors. This project is

focused on solving the non-clinical factors in detail; the clinical factors are not included here.

2.4 *Oocyte deformation analysis and ICSI methods*

Micro injection of a biological cell is a crucial step in ICSI systems as a tiny excessive force can lead to potential damage to the cell during injection. From the point of view of the characteristics, the survival rate of an oocyte depends on the characteristic structure of oolemma which is changing with respect to the hormonal environment [23]. Therefore, each oocyte's membrane reacts in its own way to the injection needle such as, normal breakage, sudden breakage and difficult breakage [23, 24]. In this case, estimating the oocyte membrane hardness and oocyte quality during the micro-injection task would be useful in order to have less oocyte degeneration [25]. However, the characteristic structure of an oocyte is an important consideration on cell deformation creation which is uncontrollable in nature from the engineering point of view. However, numerous injection methods have been proposed by researchers to overcome this deficiency, such as laser-assisted (LA-ICSI), piezo-assisted (PA-ICSI) and rotationally oscillating drill (ROS-Drill) intra-cytoplasmic sperm injection with the purpose of minimizing cell damage during the injection task.

In conventional ICSI, a micropipette penetrates the oolemma through the zona pellucida, which causes significant deformation of the oolemma. An excessive indentation force in conventional ICSI leads to higher deformation creation which is a potential cause of damage to the cell leading to degeneration [26]. This deformation would increase the internal hydrostatic pressure in the oocyte during injection. By

increasing the internal pressure, the emission of the cytoplasm from the oocyte is induced after extraction of the injector and this contributes to oocyte degeneration and therefore the oocyte's death [26, 27]. This deficiency has motived researchers to propose different methods of injection to minimise the damage applied to the oocyte during injection. Piezo assisted ICSI was proposed to overcome this deficiency leading to increases in the success rate greater than the conventional ICSI results [26]. This technique employs a piezo-activated axial force applied to the pipette to inject the zona pellucida very smoothly and then the oolemma is penetrated causing minimal damage during the injection process. This technique requires a small amount of mercury in order to decrease the lateral vibration at the micro pipette tip when piezo electric pulses are applied [28]. However, mercury will cause a toxicity issue on the cell and therefore failure of the process [29, 30]. To overcome this toxicity issue and high lateral motion of the micro pipette, mercury-free technology, which is called rotationally oscillation drill ICSI, was proposed [31, 32]. In the proposed system, a micropipette containing alcohol is used and driven by a microprocessor-controlled rotationally oscillating drill without mercury or piezo. In this technique, in order to drill the cell membrane by minimizing the cell deformation, a high speed rotation micro injector is used which has rotational vibration at the micro pipette tip. The main advantage of this technique is to have less deformation on the oocyte along with exclusion of mercury. Despite this technique having a very low deformation and similar high success rate as in piezo assisted ICSI, unbalanced eccentricity of the injector pipette causes a whirling effect which is not a desired.

Laser assisted intra-cytoplasmic sperm injection is another method employed to overcome the damage applied to the cell at the time of injection. In this method, a hole with a diameter of 5-10 μm is created on the zona pellucida using a laser beam to facilitate

penetration through the membranes of the oocyte without needing a deformation indication. Consequently, the success rate of the oocyte's survival significantly increases [33, 34]. The major problem of LA-ICSI is the impossibility of localizing the laser-generated hole at the developmental stages [34] in addition of causing the wound on the membrane of the cell.

The previously mentioned techniques have been developed to enable the ICSI procedure to penetrate the zona pellucida and oolemma effectively and deliver the sperm to the oocyte with minimal damage applied to the cell (i.e. less deformation created on the oocyte during the injection procedure). Although it has been reported that the deformation may cause degeneration of the cell in numerous researches, the detailed investigation on this deformation creation remains deficient. The mechanical models have been developed to understand the cell response to any technique and obtain the mechanical properties of the cells.

It is essential to consider the mechanical properties of the cells to recognize their physiology and to model the procedure applied. The mechanical behaviour of the cells in different animals varies and also it changes before and after fertilization. Usually the creation of deformation is one of the significant behaviours of the cell under an external load [35-38].

Several methods already exist to understand the mechanical behaviour of biological cells. However, it is not possible to perfectly model the mechanical behaviour of a biological cell since the cell membrane presents nonlinear characteristics which vary over time [39, 40]. Consequently, different types of mechanical modelling have been reported to demonstrate the oocyte's mechanical behaviour during the injection procedure

[41-43]. These models are divided into two main categories. There are two popular models for bio-membrane behaviour which have been reported as the contact mechanics model and the micropipette aspiration model. In the contact mechanics model, the elastic behaviour of the cell is considered by utilising atomic force microscopy. Young's modulus of the sample is calculated by pushing the tip of the cantilever towards the membrane of the cell and analysing the force-distance curves. Micropipette aspiration is another method of recognizing the properties of the membrane. These properties are essential in modelling any type of cell [31]. The properties are obtained by applying a negative pressure on the cell membrane through a micropipette. Both of these models consider the cell membrane as a solid body, which is insufficient to provide more accurate understanding of cell behaviour. Additionally, the analysis of these models is just for small local deformation and the global geometry of the cell remains unchanged. This assumption is not sufficient to model the real injection procedure.

Understanding of the mechanical behaviour of biological cells has been developed by proposing different models and validating them. The membrane point load model is a mechanical model developed in 2003 which explains the membrane's behaviour under a concentrated load [44]. In this model, the outer membrane of the cell is assumed to be a thin film and is subjected to hydrostatic pressure from the inner cytoplasm. The proposed force sensing technique and point load model can be implemented for examinations of the mechanical properties of other cell types. This model was developed to characterise the mechanical properties of the membrane as well as predicting the deformation creation on the outer membrane [45, 46]. However, it is assumed the residual stress of the bio membrane is zero which is not the situation in the reality. The nonlinear bio-membrane cell model proposed in 2008 [47] suggests that the hyper-elastic Mooney-Rivlin material

equation should be employed to model the bio-membrane and solved by using the Runge-Kutta numerical method. In the proposed model, uniform hydrostatic pressure of the cytoplasm exerted on the membrane is assumed. However, the large yolks inside the embryos is are overlooked which is an essential consideration.

A biological cell's response to the external load is usually divided into three categories: elastic, viscoelastic and hyper-elastic which refer to the properties of the membrane and its behaviour when it is subjected to the external load. Elastic and hyper-elastic behaviour is not very suitable for cell modelling, as its properties cannot be defined for the behaviour of the cell. As a result, most of the models consider the cell as viscoelastic; which means that a cell has both elasticity and viscosity properties and behaviour. The most suitable representatives for the viscoelastic materials are springs and dampers. Different models were proposed based on different configurations. There are three established configurations proposed for the behaviour modelling of the cell known as the Maxwell, Kelvin-Voigt and Zener standard solid models. In the Maxwell model, the spring and damper is connected in series, while the Kelvin-Voigt model indicates a configuration with the spring and damper connected in parallel. [48]

With the purpose of modelling the cell, it is essential to understand the properties of the cell membranes during the injection. As mentioned earlier, the pattern of oolemma breakage is a significant factor affecting deformation. Based on previous studies, there are three different patterns of oolemma breakage: normal breakage, sudden breakage and difficult breakage. Group I indicates no resistance to breakage by the oolemma when the micropipette enters the oocyte. This group belongs to the specific type of oocytes which have fragile membranes. Oocytes with this type of membrane has less ability to extrude the second polar body and decondense the cytoplasm inside; consequently, they

degenerate. Group II indicates mild resistance which is in the category of normal breakage. The micropipette enters the oocyte with gentle resistance from the membrane. Group III belongs to the difficult breakage or high resistance category, where the micropipette faces high resistance from the membrane at the time of injection and creates a funnel shape. Figure 2-3 shows a visual comparison between these categories. Rupturing with mild resistance (second category) results in a significant increase in the fertilization rate of 87%; in comparison to the other two categories, which are 55% and 70% for group I and group III respectively [23, 24].

Figure 2-3 . Different groups of membranes' responses to the micropipette: (a) Sudden breakage, (b) Normal Breakage, (c) Difficult breakage [23, 24]

2.5 *Injection speed effects on cells*

Biological cell injection is a laborious process within different areas of research which introduces a foreign material into a biological cell with various applications such as DNA, ICSI, and cell biopsy. Current cell injection (particularly in ICSI) procedures are suffering from low success rates. The conventional method of cell injection is operated by a human who relies on visual feedback from the optic devices. The conventional method is performed manually using two manual joysticks. In this method,

the tip, of the micropipette is moved towards the oocyte to the point it touches the zona pellucida and then the oolemma membranes. Afterwards, it moves rapidly until it pierces the membrane and delivers foreign material into the desired location in the oocyte [53, 54]. This method is prone to errors as it relies on the skills of an operator who was guided by optical devices. During cell injection, there are some factors which are not possible to control manually using joysticks and which have a high impact on the success rate of the procedures. During the injection procedure the ICSI needle creates excessive deformation of the oocyte. Excessive deformation may induce emission of the cytoplasm into the perivitelline space after injection [55]. This causes an increase in the internal pressure of the oocyte and therefore leads to oocyte degeneration. Other causes of the low success rate are excessive force, which causes additional deformation, and hand tremor. Automating the entire process has been the main focus in the literature [56, 57] in order to eliminate human involvement and therefore deformation due to excessive cellular force.

Automating and mechanising the whole process aside including haptic feedback to the operator in the ICSI operation has been reported in [58-60] as haptic information allows the operator to minimize physical damage to the cellular structure and increase the success rate of the cell development procedure. Since biological cells are highly deformable and irregular in conformation, the biological cells could be damaged seriously during non-controlled injection procedure [61]. Various force sensing techniques were proposed by researchers to improve cell survivability rates in the microinjection process [62, 63]. Cellular force measurement is also essential for evaluating the stiffness of the cell membrane which exhibits viscoelastic behaviour during the injection process and a 3D mathematical model can be derived [64, 65]. Therefore, having force feedback is a

prior concern in micro injection tasks so that the operator can achieve better control over the micro injection process [66, 67].

Although a combination of vision and force feedback provided to operator induce a higher success rate in cell injection tasks compared to visual feedback alone [67], regulating the penetration force in a desired force trajectory at the time of injection becomes more important to increase the cell survival rate [68]. Precise real-time force sensing is a requirement for reliable automatic cell injection processes [69]. However, the actual role of the indentation force on cell deformation and how this affects the success rate of the injection task remains deficient.

Despite the great developments above, numerous factors playing considerable roles in the process have not been entirely discovered while improving the microinjection task. Sufficient penetration force, penetration speed and an accurate injection point are the key factors to achieve successful penetration in the microinjection process which requires sensitive control methods [70]. The role of microinjection speed, force feedback on cell deformation in cell penetration tasks is well recognized [71]. However, it has not been comprehensively studied.

Following the role of contact force in micro injection and how it affects the outcome of the system, analysing the effect of injection speed in microinjection on cell deformation is a must to reduce the deformation of a cell and improve cell survivability rate. Since the micropipette is in contact with a cell at different indentation speeds, the contact force and deformation rate are also changing. There is a complex dynamical relation among contact force, injection speed and cell deformation. Although, speed analysis in microinjection is a promising way to obtain better outcomes in the context of

getting less deformation on cells in comparison to constant injection speed [71], force and speed analysis on deformation creation in cell injection tasks remains a gap in the literature.

2.6 *Cell detection methods*

Positioning and orienting the polar body in conventional ICSI is controlled by an embryologist. Currently, cell manipulation in conventional ICSI has been manually operated by well-trained embryologists. The oocyte is manipulated by using a micropipette and inducing negative pressure to hold and relief the oocyte repeatedly until the polar body is positioned in the desired location. This type of manipulation is known as a trial-and-error course of action [74]. During the conventional operation, a single cell is touched several times until it is located in the desired place and preparing it for injection. In cell manipulation, some of the researchers tried to develop this operation to an automated process. There are various research projects focusing on automating 3D manipulations of biological cells [75-78]. Robotic cell manipulation with a good success rate and high degree of accuracy has been reported in some previous publications [77, 79-81]. However, there are some deficiencies introduced in each method, such as lack of correct detection of oocyte. Different methods of manipulations have been reported in research which is Lab-on-a-chip using micro fluidic flow advances [82-86], optical tweezers [87] and micromechanical grippers [88-91].

Cell detection is an essential method towards 3D cell manipulation. In the proposed application in this chapter, image processing is focused on the oocyte and polar body

recognition. The first attempt at a vision detection software for cell manipulating purposes was designed to use morphological factors and Bayesian assessment as a classifier of texture and shape [92]. The major problem with this method is that it is computationally very expensive. Another method, the Hough cell detection algorithm (HCDA) utilised high pass filtering to detect the edges of the holding pipette and determine the oocyte size value [85]. In this method, polar body detection has not been developed. Again, the computational time for this method is high for a real time application which is 22 s in detection time. Different algorithms have been proposed for detecting the polar body during the manipulation. However, the early stages of these detections recognized the polar body when in plane [93]. This method involves the Otsu adaptive algorithm and morphological operator for fitting the circle to the cell. Otsu is a clustering based image threshold technique which is employed to convert the greyscale image to a binary image. A linearization method was employed here for the polar body recognition [94]. The failure of this technique happens when the gray scale of the polar body and the oocyte are in the same level of surroundings in the image. Later, an algorithm was added to this method that estimated the polar body location out of plane using frame by frame motion analysis [93].

Image binarization is a method developed to detect the polar body. However, this method is highly dependent on the gray level of the neighbourhood pixels in the image. Inaccuracy occurs when the gray levels are similar in the surrounding pixels [85]. Another method of polar body detection was based on the polar body's texture data. Oocyte texture deficiencies and microscope light regulation limitation are two main disadvantages of this technique which cause low accuracy [95]. Here the polar body and oocyte detections were proposed based on a machine learning method using image classification. In this method,

the improved Histogram of Oriented Gradient (HOG) algorithm is used to extract features of polar body images for the prediction of the polar body position in the image, determination of this position, and finally detection [96, 97]. Recently, a method has been proposed for oocyte and polar body detection which employs template matching followed by morphological operations and thresholding [78]. The method is computationally expensive based on the sizes of the template and may need new templates.

Visual detection algorithms for the purpose of cell injection automation have involved the Hough transform to detect the polar body [98], roundness and elongation calculations following segmentation to detect the oocyte and injector respectively [99]; and a connected neighbourhood method for oocyte detection [100].

A new detecting technique for the oocyte and polar body has been proposed by our group which is developed using images detection rather than continuous frame tracking using video and employs a gradient-weighted Hough transform in the application of ICSI. In addition, a new method of gradient based on elliptical fitting has been developed for this software [73].

2.7 *Three-dimensional manipulation of a single cell*

The interaction between the manipulator and a cell leads to mechanical stress on the cell membrane in the micromanipulation task. Hence, the stiffness and Young's modulus of the cell becomes a significant consideration in cell manipulation as well as the cell transportation task. Due to the sensitive interaction between a manipulator and a cell, cell micromanipulation systems have been developed to prevent the potential damage and drawbacks in the current systems [108-112]. Cell micromanipulation has

been the focus of research in the last few years. Micromanipulation is defined as a combination of tools and techniques for the purpose of cell rotating and positioning. The micromanipulation technique plays an important role in the development of devices in assisted reproductive technology [13]. There are different applications for three-dimensional rotation and manipulation of biomaterials in biomedical applications: such as ICSI, polar body biopsy and cloning [82-84, and 86].

Currently, cell manipulation in conventional ICSI has been manually operated by well-trained embryologists. The oocyte is manipulated by using a micropipette and applying negative pressure [114] to hold and release the oocyte frequently until the polar body is positioned in the desired location. This type of manipulation is known as a trial-and-error course of action [74]. The method of sucking the cell with negative pressure can be utilized to model the cell with an aspiration technique. There are various research projects focusing on automating 3D manipulations of biological cells [125-128]. Robotic cell manipulation has been reported in a few publications with a considerable success rate and high accuracy [79, 117]. However, there are some deficiencies introduced in each method, such as lack of correct detection.

MEMS micro gripper is a form of contact manipulator fortified with a force sensor [118-121]. Actuation of a micro gripper could be either electro-thermally [122] or piezo-electrically [120].

Microfluidics is a form of a non-contact manipulation. Technology has recently been developed for the cell manipulation task. It provides a higher success rate in comparison to conventional methods since it is economical, compact and requires less fluidic medium for the cell [123]. Microfluidics can be utilized for cell injection, cell immobilization, and

cell transportation etc. Lab-on-a-chip is a proposed method for cell manipulation on a small chip using micro fluidic flow advances [82, 86, 124]. Lab-on-a-chip technology combines all necessary micro injection steps into one small chip [114, 125, and 126]. This method leads to minimum damage as it is non-contact and also reduces the chance of contamination [127-129]. The drawback of using microfluidics is that it is a difficult procedure for precise fluid handling. As the lab-on-a-chip method is difficult to use with end effectors, another method is proposed which utilises micromechanical grippers for pick and place purposes and securing the cell position [88-91, 130].

Cell manipulation using optical tweezers is another method used for three-dimensional rotation of the cells; it uses an infrared laser beam to provide a tangential force on the cell in order to rotate it [87]. A single axis rotation, as well as cell various sizes are the limitations of this method [131]. In addition, the oocyte is exposed to the laser beam which causes damage to the cell. Then a combination technique was proposed which employed the combination of optical tweezer technology and an image guide robotics technique which saved the cell from a direct attack by the laser and the manipulation happens indirectly [132].

Ultrasonic vibration technique as a non-contact manipulation provides acoustic radiation force fields produced by a piezoelectric mechanism [133] to the suspended cell in a fluid. Produced acoustic radiation force fields align the cells into a straight line. After that, the aligned cell can be grasped by a MEMS actuator. The drawback of this method is that the required voltage to supply the system is high which is a cause of potential damage to the cell and reduces the success rate of the manipulation task.

Sun et al. proposed an autonomous set-up for the application of biological cell injection. This was a 3DoF micro robotic system to direct the injector towards the cell. In the proposed system, the holding pipette is assembled on a manual micromanipulator. A vision system is also employed to detect the micropipette motion [134]. Then this system was developed to an automation system for oocyte positioning and orienting [135].

Automating the manipulation of the oocyte in collaboration with injection and integrating a vision detection system have been focused on during the last decade [134-137]. Although there have been many researchers working in this area, still there are some difficulties in the manipulation methods, as well as in the integration of the vision software and manipulation in addition to the injection.

2.8 *Conclusion*

ICSI is one of the most useful techniques in infertility treatments. Certain technical aspects in the injection procedure would affect the developmental stages of the embryo after injection. This chapter covers different potential damages reported in the literature which are applied to the cell during injection emphasising on deformation. To minimize these types of damage, some methods have been proposed by researchers; such as laser assisted intra-cytoplasmic sperm injection, piezo assisted intra-cytoplasmic sperm injection and rotationally oscillating drill intra-cytoplasmic sperm injection. Each of the reported techniques have their own advantages and disadvantages which are discussed.

Different types of mechanical modelling have been reported to model the oocyte's mechanical behaviour during the injection procedure. The most suitable representatives

for the viscoelastic materials are springs and dampers. The different models were proposed based on different configurations. There are three established configurations proposed for the behaviour modelling of the cell known as Maxwell, Kelvin-Voigt and Zener standard solid models.

Also different method of cell manipulation systems have been reported. Currently, cell manipulation in conventional ICSI has been manually operated by well-trained embryologists. Robotic cell manipulation has been reported in a few publications with a considerable success rate and high accuracy. In addition, there are other different techniques which have been proposed for manipulating the oocyte. Lab-on-a-chip is a proposed method for cell manipulation on a small chip using micro fluidic flow advances. Cell manipulation using optical tweezers is another method used for three-dimensional rotation of the cells.

CHAPTER 3

DEFORMATION ANALYSIS AND METHODS OF DEFORMATION ELIMINATION

3.1 *Introduction on deformation analysis*

Micro injection of a biological cell is a crucial step in ICSI systems as a tiny excessive force can lead to potential damage to the cell during injection. Prevention of any oocyte deformation as a potential will reduce the mechanical stresses and applied forces on it, which leads to minimising the internal hydrostatic pressure increased during injection. Consequently, this leads to minimisation of the mechanical damage during injection which therefore reduces the chance of deformations and, therefore, failures of the procedure occurring. Despite the improvements in the literature with the objective of minimizing the cell deformation during the injection task, the actual role of cell deformation from either a negative or positive point of view remains deficient in the literature. So in this chapter, initially, a theory is developed to analyse the geometrical aspects of the injection procedure. Then the experiments are conducted to validate the hypothesis and theoretical model.

3.2 *Deformation theoretical analysis*

As mentioned earlier, this chapter mainly focuses on analysis of the shape and geometry of an oocyte before and at the time of injection to illustrate deformation creation and its effects on the cell during the penetration of the cell membranes. During cell injection, the microinjector moves toward the grasped cell. The injection time is defined for the duration when the microinjector pushes the membrane until penetration happens. When the injector moves towards the cell as shown in Figure 3-1, it then pushes the cell towards the holding pipette. At this stage, the pipette holder acts as a supporting wall which provides the counter balance force to the injection force. There are a few mechanical damages during the injection which causes the degeneration of the cell after being fertilised. Consequently, modelling of this procedure and analysing the cell deformation plays important roles in recognising the deficiencies and solving the problems. This chapter explains the mechanical behaviour of the cell membrane under uniform hydrostatic pressure subject to microinjection.

There are some assumptions for the modelling of the cells as follows:

- deformed cell membrane is axisymmetric;
- two outer membranes are assumed for each cell named as the zona pellucida and oolemma;
- the inner layer encapsulates the cytoplasm;
- the cytoplasm is incompressible, so the total volume does not change;
- flexural rigidity is negligible and the membrane stretches during the deformation;
- there are no initial stresses on the membrane; and
- cell behaviour is linearly elastic.

Deformation occurs during the time the needle touches the outer membrane of the oocyte (ZP). The main created deformation on the cell happens on the oolemma layer as deformation on Zona pellucida is negligible. Consequently, this mechanical model is focused on the deformation of the oolemma which is causing the post emission after needle removal. The deformation is analysed in two dimensional form from the vision obtained from cell injection and demonstrated in three dimensional form to provide better understanding of the phenomenon that happens in this procedure.

The deformation causes elasticity in the membrane of the cell. This elasticity varies in different sections of the cell during the injection. The elongation in the membrane nearer to the injection pipette is greater in comparison to other sites. This means that the membrane enters the plastic region of its material, behaviour which is not willing to revert the deformation in this section and the funnel is remained remains after pipette removal. On the other hand, in the other sites of the cell, the stretches are not entering into the plastic region and are willing to return to the original shape. The difference between the areas of these two regions causes the emission.

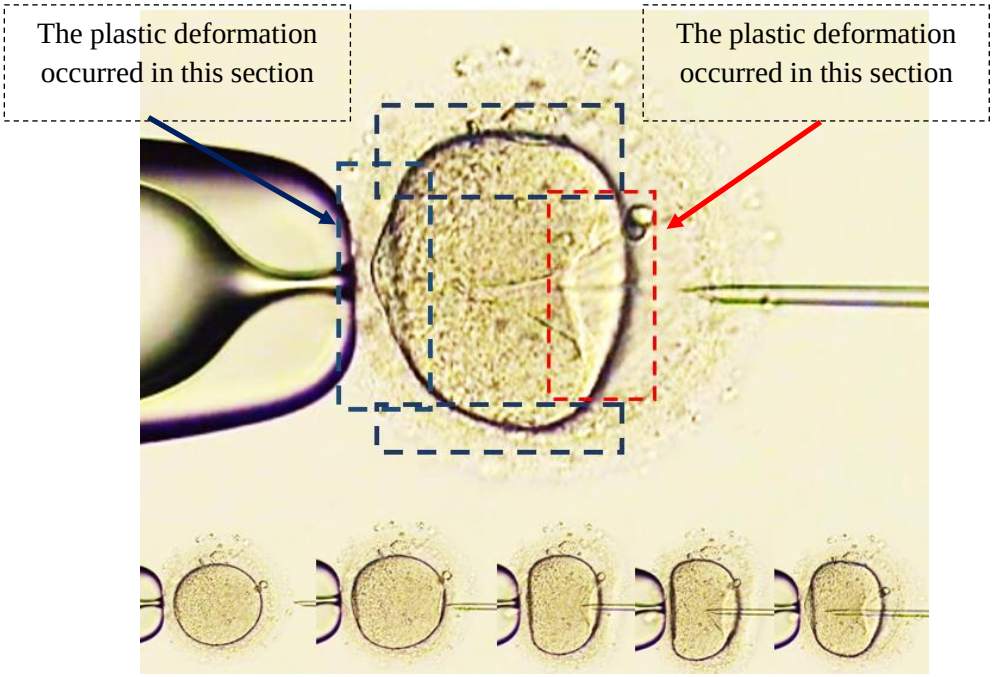

Figure 3-1. A human oocyte subjected to the injection in ICSI and induced cell deformation

As mentioned earlier, the internal cytoplasm of the cell is incompressible, so the total cell volume does not change during the injection. This would be applicable in 2D analysis as the total area of the cell does not change. The membrane stretches during the injection once the microinjector creates the deformation. This is because of a created triangle at the position of injection.

The original shape of the cell is considered as a circle. The circumference of this circle is the initial length of the membrane before the injection. A rounded rectangle is considered to calculate the circumference of the deformed shape as is indicated in Figure 3-2. This geometry consists of two circular segments and two lengths of rectangle deducted by the geometry of triangle. The arc length and perimeter of the deformed cell are obtained from Equation 3.1 and 3.2.

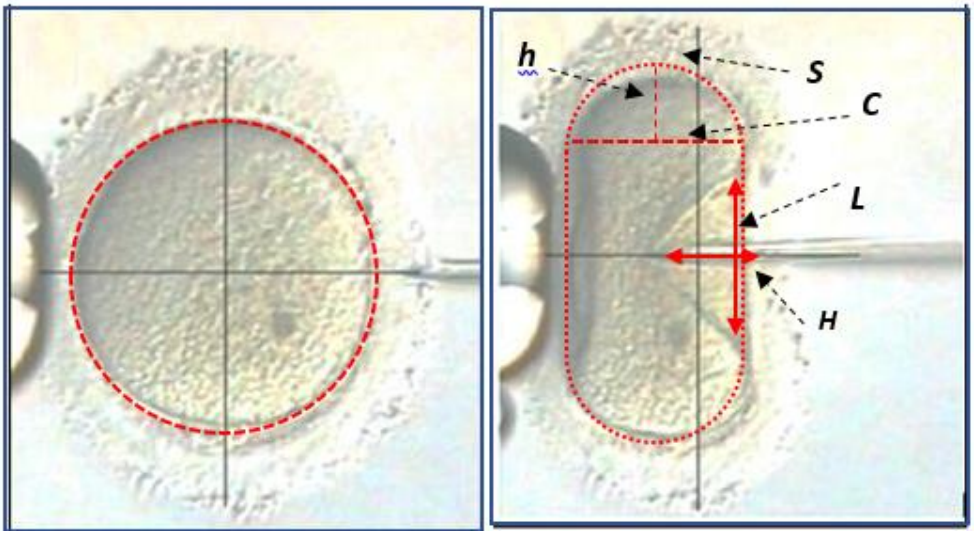

Figure 3-2. Human oocyte before injection and at the time of injection and variable presentations (Oocyte image from [25])

$$S = \frac{\alpha}{180^{\circ}}\pi R = \theta R = arcsin\left(\frac{c}{h+\frac{c^2}{4h}}\right)\left(h + \frac{c^2}{4h}\right) \quad (3.1)$$

$$P_{Deformed\ Cell} = 2S + 2 \times (2a) - L + \sqrt{L^2 + 4H^2} \quad (3.2)$$

where S is circular segment, L, h and a are indicated in Figure 3-2. The elongation of the cell circumference is obtained by the difference between the circumferences of the original circle and deformed cell geometry.

$$X = Membrane\ Elongation = P_{deformed\ cell} - 2\pi r \quad (3.3)$$

Oocytes are trying to compensate for the elongation after the injector removal. Consequently, the membrane applies excess force to the internal cytoplasm which is increasing the internal hydrostatic pressure which it is believed would then cause cytoplasmic emission to perivitelline space. Figure 3-3 illustrates the amount of the forces applied to the internal cytoplasm to compensate this elongation.

As the cell membranes are viscoelastic material, the Maxwell model is the most suitable model to represent this behaviour due to the simplicity of this model. This model

consists of Newtonian damper and Hookean elastic spring connected in series. Figure 3-3(a) exhibited the reaction forces preventing the injector which is the main cause of the deformation and Figure 3-3(b) illustrates the compensation forces to recover the elasticity of the [72].

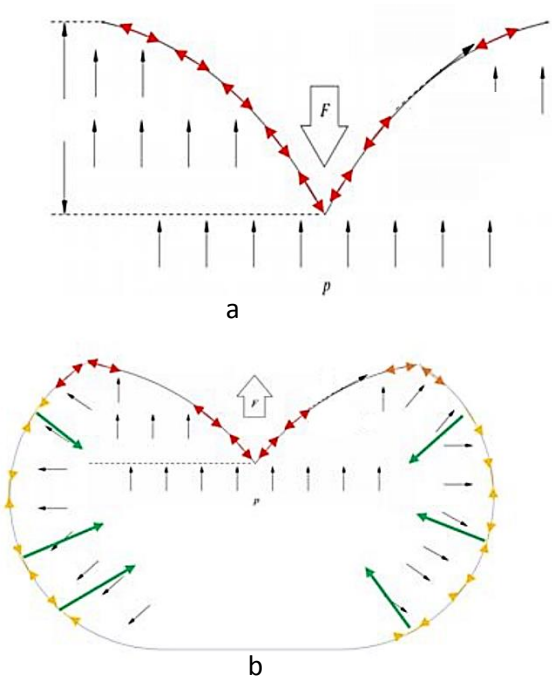

Figure 3-3. Schematic view of membrane reaction and created forces due to deformation [72]

The total force on each element exerted on the membrane is shown in Equation 3.4.

$$F = KX + C\frac{dx}{dt} \tag{3.4}$$

where C and K are damping and spring constants. The exerted force on the membrane is located on the surface of a circle which provides an angle between forces in the vicinity which blocks as is indicated in Figure 3-4. The resultant of these forces is the amount of force exerted on the cytoplasm to recover the deformation which causes emission.

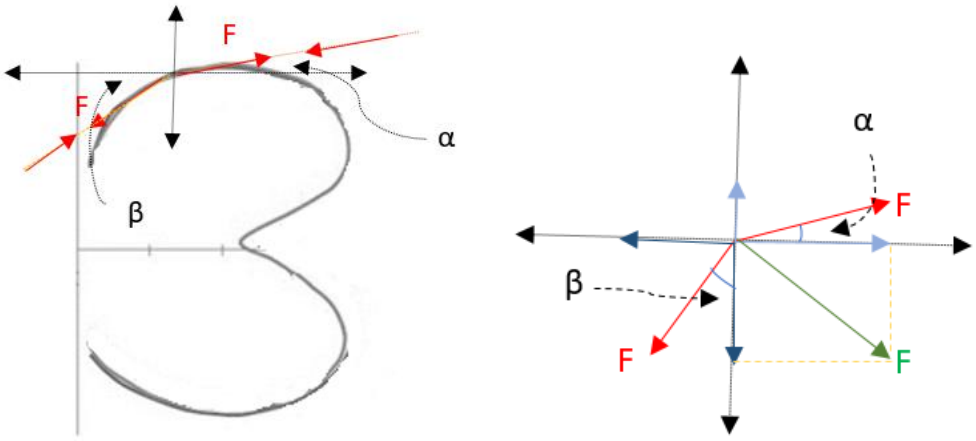

Figure 3-4. Force analysis on membrane and resultant force acting on the cytoplasm inside the cell

$$F_e = \sqrt{(Fcos\beta)^2 + (Fcos\alpha)^2} \tag{3.5}$$

F_e is the force exerted to the cytoplasm caused by the membrane during the compensation phase. Next, in the 3D analysis section, the overall cell membrane volume is considered as fully spherical before loading with a radius of r before it is compressed. Consequently, the volume of the cell is as mentioned in Equation 3.6. This volume also indicates the total volume of the cytoplasm which is not compressible. The cell inner structure is uniform and the shape of the compressed cell remains axisymmetric during injection.

$$Volume\ of\ Cytoplasm = Initial\ volume\ of\ Cell = \frac{4}{3}\pi R^3 \tag{3.6}$$

During the injection, the micro injector occupies a certain amount of volume by pressing the membrane towards the centre of the cell. This volume has a similar geometry to a cone. Consequently, the total volume of the new geometry is the addition of the initial volume and exerted cone volume as indicated in equation.

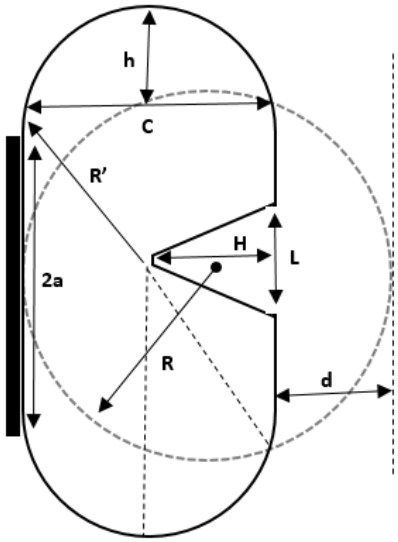

Figure 3-5. Schematic view of deformed cell after injection and variable presentations

Figure 3-5 indicates the schematic view of the compressed cell under injection. Point A illustrates the centre of the un-deformed cell and point B indicates the centre of new geometry created at the time of penetration. The cell is in contact with the support, which is holding pipette here, at point C. The parameters R and R' is the radius of the un-deformed and deformed cell respectively. As it is illustrated in Figure 3-5, a, h, and d are contact radius, lateral extension and injection depth respectively. The lateral surface profile is considered as spherical geometry. By utilising the variables mentioned earlier, the surface area of cell can be obtained from the following [51]:

$$dA = \int_0^{360} (R' d\theta) \,.\, (R' cos\theta) d\vartheta \tag{3.7}$$

$$A_T = 4\pi R'^2 \frac{R-d}{\sqrt{R'^2-(R-d)^2}} cos\theta \tag{3.8}$$

where A_T is the total surface of the capsule under injection at the time of penetration. However, this is not showing the surface area of the cell in 3D. The total surface area of the cell at this time is the subtraction of total surface from the cone base and addition to

the surrounding the cone. Equation 3.9 indicates the total surface area of the cell at the time of piercing.

$$A_{Cell} = 4\pi R'^2 \frac{R-d}{\sqrt{R'^2-(R-d)^2}} cos\theta + \pi \frac{L}{2}\left(\sqrt{H^2 + {L}/{2}^2}\right) \quad (3.9)$$

The new surface area of the cell is demonstrating the expansion of the membrane due to deformation. The volume of the capsule is determined from this as following:

$$V = 2\pi \left[R'^2(R-d) - \frac{(R-d)^3}{3}\right] - \pi \left(\frac{L}{2}\right)^2 \frac{H}{3} \quad (3.10)$$

Due to volume balance and consistency of the cytoplasm as it is incompressible, the obtained volume in the equation should be equal to the initial volume of the total cytoplasm before injection. So:

$$V = 2\pi \left[R'^2(R-d) - \frac{(R-d)^3}{3}\right] - \pi \left(\frac{L}{2}\right)^2 \frac{H}{3} - \frac{4}{3}\pi R^3 = 0 \quad (3.11)$$

For a biological cell as a soft material under the injection, the volume of the penetration path will be reduced. However, this volume reduction is transferred to the later surface side which is initially compression free and causes extension of the lateral surface. This extension causes stresses on the membrane.

As the wall thickness of the cell is small in comparison to the diameter (r/t>10) and the internal pressure exceeds the external pressure, thin shell theory is applied for the analysis of the stress which is caused by changing the surface area of the cell during penetration. The membrane of the cell is subjected to uniform tensile stresses in all directions as illustrated in Figure 3-6.

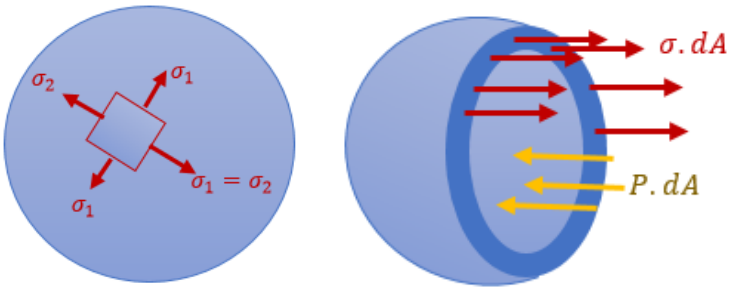

Figure 3-6. Exerted stresses on the cell membrane

Similarly, as mentioned in the previous section, it has been reported that the membrane of the cell is either viscoelastic or hyperelastic. In the majority of the area, further to the penetration point, the surface tension exists in the elastic zone of the oocyte membrane; then after removal of the external force, the membrane reverts to the original shape, which is the major cause of emission. Consequently, the distribution of the stress and strain in the deformed membrane is not uniform. The outer limits of the deformed area tolerate maximum stress in the membrane. At the dimple top, therefore, the membrane strain was equivalent to zero. On the deformed cell membrane, as shown in Figure 3-7, the strain membrane is on the top of the deformed shape at its most extreme and gradually reduces alongside the arched boundary towards the location of the injection. The stress is at its maximum level in the location of the injection and gradually decreases to its minimum level at the top of the dimple.

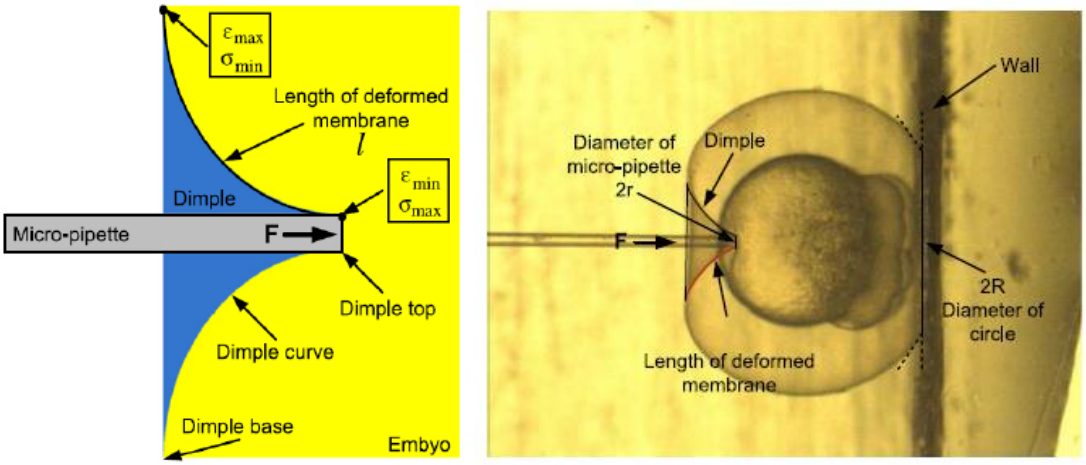

Figure 3-7. (a) Distribution of stress and strain in deformed membrane (b) parameters description [49]

As a result the stress applied to the cell due to expansion of membrane during the injection is:

$$\sigma_1 = \sigma_2 = \frac{F_{Hydrostatic\ pressure}}{A} \tag{3.12}$$

where A is the extended area. The exerted force on the surface is calculated from the following:

$$F = \sigma . dA = \sigma . dX . dX \tag{3.13}$$

where dX is the elongation of the membrane in each direction.

3.3 *Experimental results*

In this section, the hypothesis is examined based on testing the theory and also real-time experiments. Analysing the deformation using the developed theory was facilitated by using ImageJ software. As illustrated in Figure 3-5, all required dimensions of both geometry of the original oocyte and at the time of injection were examined and

recorded. The obtained results indicates that the overall surface extension of the cell during injection is 25±7% which is a considerable figure. This means the membrane will need to compensate for the extension of the cell in the elastic area which will cause emission of the cytoplasm from the injection hole as the membrane in the plastic zone is not compensated.

A series of experiments was conducted to demonstrate the effect of deformation on increasing internal hydrostatic pressure [50] which will cause cytoplasm discharge and validate the hypothesis of this research which was the negative effect of the deformation on cell survival in cell injections. To examine the emission of the cytoplasm due to deformation creation, low injection speeds were proposed by to inject a zebrafish cell. It should be noted that the selected injection speeds for this experiment are not the optimised speed which is suitable for injection. The aim was to select slow speeds to verify the deformation effects.

The zebrafish is an appropriate model for the human oocyte in terms of the response and mechanical behaviour. The cells were treated with standard embryo preparation procedures [52] and examined randomly to generalise any effect that may cause any defect. The zebrafish embryos were at the stage of six to seven hours after fertilization.

In this experiment, two sets of zebra fish embryos were injected with constant speed of 50, 100, and 200µm/s and the force and deformation recorded. The experimental setup comprises of a precision injection system integrated with an accurate and sensitive loadcell to measure the indenting force of a zebrafish embryo. A data acquisition device is employed to convert the analogue outputs from the loadcell to digital. The obtained

data are analysed using computer software and raw data has been defined as the force unit. Figure 3-8 demonstrates the schematic of the experimental set up.

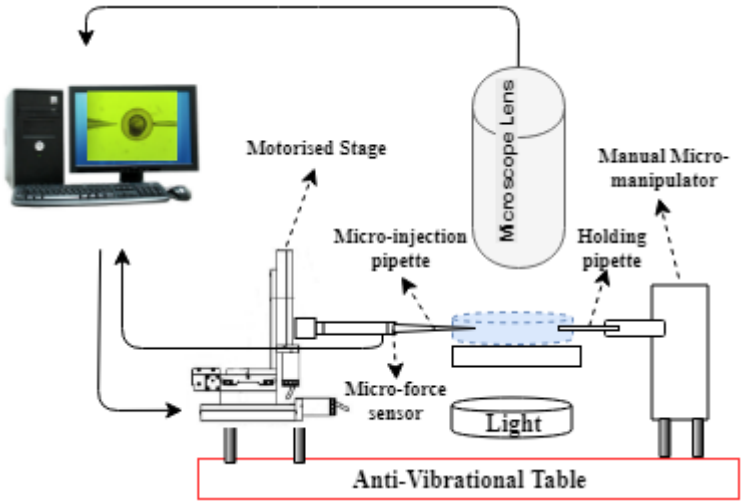

Figure 3-8. Schematic sketch of test rig for deformation experiments

During the experiments, the random selected zebrafish embryo was placed under the focal zone of microscope and held in place using 2.5KPa negative pressure through a holding micropipette. The embryos were injected automatically using constant injection speed controlled by a fully automated injection system and injection force recorded using a SS2 Sherborne Ultra Low Force sensor with a capacity of 0.5886 N and resolution of 1 mN which is utilised for measuring the membrane reaction force during the injection. The amount of deformation and force are analysed using computer aided software. The amount of deformation is the same as the distance travelled by the micropipette from the moment the chorion is touched till the moment the reported force suddenly drops.

The zebrafish embryos exhibited in Figure 3-9 illustrate the three experimental sets. Two captured images on each set are shown which demonstrate the moment before puncturing, the time of puncture, and the graph of force deformation. As illustrated in the

figures, the experiments conform to the initial hypothesis which was the negative effect of deformation. Additionally theory justified the extension of the membrane during the injection due to deformation. The graph of force-deformation demonstrates the behaviour during deformation creation in three different speeds. Also it reports the value of deformation when the injection speed increases. Figure 3-9 a visually exhibits the amount of cytoplasm emission after puncturing in the lowest speed. This amount is reduced while the deformation is reduced by increasing the injection speed.

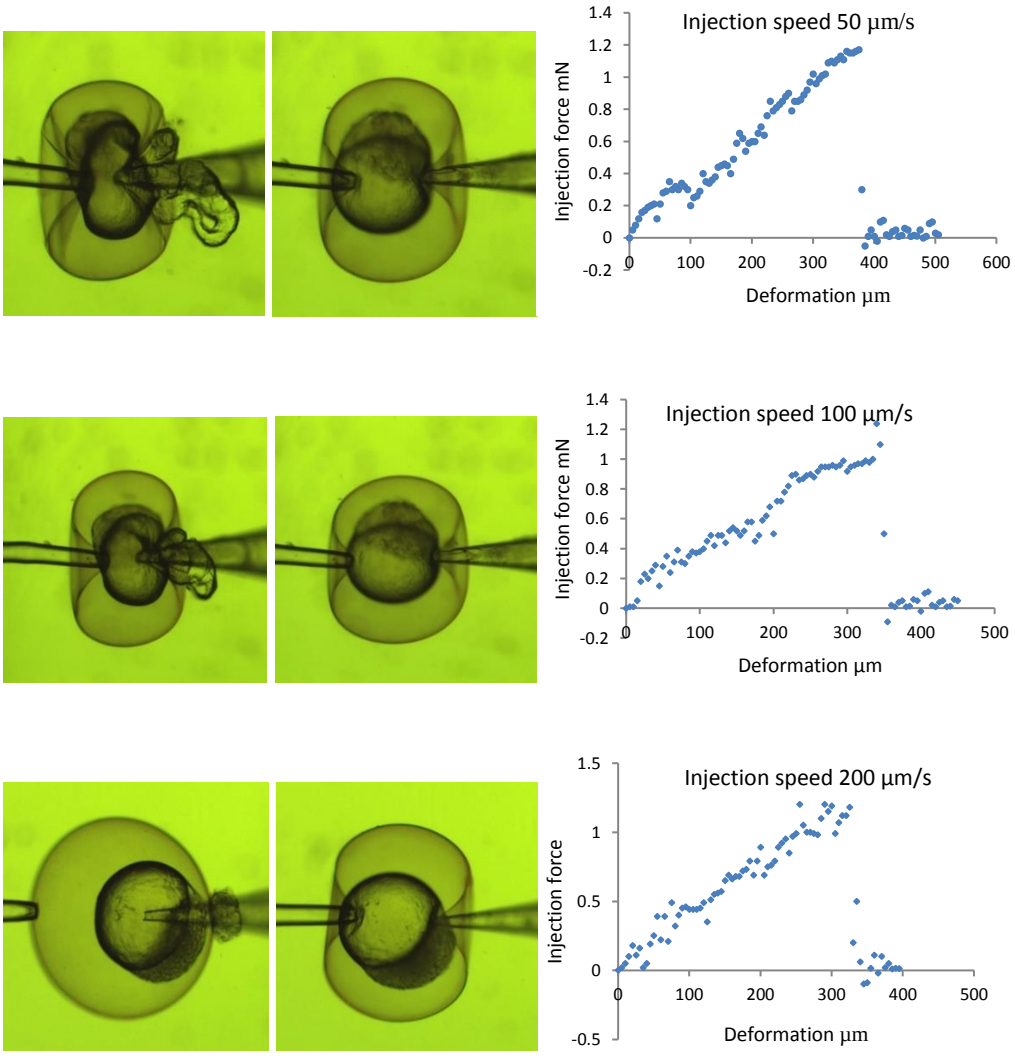

Figure 3-9. Experimental results of the deformation creation due to various speed

Additionally, Figure 3-9 illustrates that the higher speed causes less deformation which produces less emitted cytoplasm. Figure 3-9(a) has the lowest speed in the experiment which has higher deformation. Also, the injection force is higher in comparison to other injection speeds. This illustrates that greater deformation is providing less injection force. However, the differences between the injection forces are not large as illustrated in the following table:

Table 3-1 deformation creation results based on various speed and comparison of the reduction in deformation and force increase by changing the speed

Injection speed (µm/s)	Deformation		Force	
	Magnitude	Reduction	Magnitude	Increase
50	375 µm	0%	1170 µN	0%
100	340 µm	10%	1240 µN	6%
200	310 µm	21%	1265 µN	7%

In table 3-1, the deformation reduces initially to 10% of the original deformation where it is created by the injection speed of 50µm/s. Then, by doubling the speed, this deformation decreases to 21%. This reduction is an important step to minimise cytoplasm leakage due to deformation. On the other hand the injection force increases initially by 6% and 7% with respect to the recorded force in 50um/s injection speed. The emission of the cytoplasm in the images recorded from the experiments is as indicated in the Figure 3-9(b). The greater amount of cytoplasm emitted from the lowest speed injection is while this is decreased by increasing the injection speed which is results in deformation decrease.

Once the external force is removed from the cell, the elastic part tries to compensate for the stretches. As two phases occur in the cell, the elastic sections go back to their original place and the plastic section remains. So the differences between the areas

will be equivalent to the amount of area that is emitted from the wound created by the injector.

3.4 ***Conclusion***

Cell deformation is a dynamical response to the injection which is highly dependent on dynamical factors of injection along with cell properties. Understanding the effect of deformation is essential to improve the cell injection success rate. In this chapter, cell deformation was analysed theoretically and experiments were conducted to demonstrate the negative effect of deformation. Cytoplasm emission is the main drawback of induced deformation on the membrane during the injection which causes death. Based on the developed theory and experimental data which is employed by theory, the membrane surface tension is 25±7% in comparison to the original surface. Additionally, decreasing the deformation by 21% by increasing the injection speed causes a 7% increase in injection force. The emission of cytoplasm is exhibited by testing zebrafish embryos using the same speed sets. This can be a platform for the researcher and practitioner to develop their novel methods to overcome this problem with the aim of increasing the pregnancy percentage.

CHAPTER 4

THE EFFECTS OF SPEED OF INJECTION ON DEFORMATION

4.1 *Introduction*

Cell deformation during the injection procedure causes increases of the internal hydrostatic pressure which may cause degeneration after cytoplasm emission. Consequently, it is essential to study the potential factors which cause this deformation and methods that assist in minimising this deformation during the injection. Deformation of the cell during injection is highly dependent on numerous factors such as cell morphology and operation procedure. Dynamic factors are considered as major procedural elements which may cause cell damage and lead to degeneration. The injection speed, as the main dynamic factors, is considered as the magnitude of the speed at the point where the tip of the micropipette touches the outer membrane of the cell (chorion here) to the point of piercing. The displacement of the micropipette tip within the referred time is exactly equal to the deformation created upon this displacement. This chapter aims to recognize the optimum injection speed to feed automated injection procedures to minimise the damage during injection. This speed is fully controlled by the operator of the injection system.

In this section, analysis of injection speed as a significant factor on deformation creation is the aim. Here, it is hypothesized that a higher injection speed would cause lower deformation although the speed threshold needs to be analysed. A theory, finite element (FE) and experiments have been developed and have validated this hypothesis. In this chapter, the FE has been developed to be compared with static theory and also provide a reliable platform for further research on the cell injections. The material properties for this model have been obtained from literature. Further to this, the FE model is able to receive the material properties from the experiments to adapt itself for new cells. The dynamic section of the theory is developed to propose a unique equation to demonstrate the relation between injection force, deformation creation and velocity. This equation will predict the cell behaviour by changing the speed. Finally an experiment has been conducted to validate the results obtained from theory and FE.

4.2 *Theory development*

This research specifically analyses the injection speed, obtained forces and induced deformation due to the speed variation. The aim is to propose a method to find the optimum injection speed. This analysis includes theory, FE and experiments to demonstrate and predict the mentioned drawbacks.

The cell injection procedure theory is demonstrated by static and dynamic models. The dynamic model is developed to illustrate the relation between speed, deformation and injection force to predict the deformation created by using various speeds. The static

model is developed to calculate Young's modulus and explain the cell-needle interaction model.

In the model development, the following assumptions have been considered and taken into account for both theory and FE models:

- the cell is considered as a proper spherical shape;
- there is a uniform hydrostatic pressure exerting on the cell membrane;
- the thickness of the cell membrane is considered as uniform thickness, homogenous and isotropic before the injection;
- the cytoplasm inside is defined as incompressible and the cell volume has been kept uniform; and
- the elasticity of the membrane is changing linearly.

In theory, deformation created on cell membrane depends on external factors (dynamics of injection) along with unique characteristics of the individual cell at the time of injection. These characteristics are related to the morphological shape of the cell and maturation level which varies between cells. Here the demonstrated theory focuses on the mentioned factors separately and then relates them together. Elastic modulus, as one of the material factors, is considered as an important element affecting cell behaviour in response to external load during injection. On the other hand, this is an essential factor to be considered in FE modelling. The Maxwell-Wiechert model is employed to demonstrate the cell response behaviour. This model has both Hookean spring and Newtonian dashpot which represents the elasticity and viscousity behaviours of the cells respectively. The adopted Maxwell-Wiechert model

contains two standard linear forms of Maxwell parallel to a one spring as demonstrated in Figure 4-1.

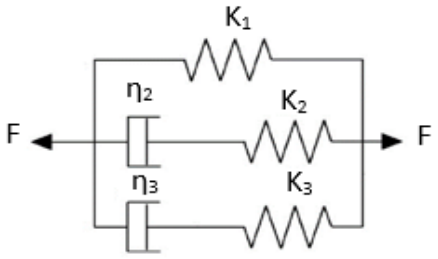

Figure 4-1. Maxwell-Wiechert Model representation

During the needle insertion, all elements are compressed by X amount which illustrates the value of the deformation. Consequently, the spring and dashpot equation is written as:

$$F = KX \qquad and \qquad F = CV = C\frac{dX}{dt} \tag{4.1}$$

where K and C are spring and dashpot constants respectively. The overall displacement on each arm is equivalent. However, the displacement of the spring and dashpot individually is equal to the summation of displacements. The force acted on each arm of Maxwell is mentioned as following:

$$F(t) = KX_t \exp(-\frac{Kt}{C}) \tag{4.2}$$

where

$$X_t = X_s + X_d \tag{4.3}$$

where Xs and Xd are spring and damper respectively. The resultant force for Maxwell-Wiechert model is demonstrated as:

$$F(t) = K_1X + K_2X_t \exp\left(-{}^{K_2t}/_{C_2}\right) + K_3X_t\exp(-{}^{K_3t}/_{C_3}) \tag{4.4}$$

As the induced force on each arm applies the same amount to both spring and dashpot, then:

$$K_s X_s = C_d \frac{dX_d}{dt} \tag{4.5}$$

$$F(t) = K_1 X + C_2 V \exp\left(-{}^{K_2 t}/_{C_2}\right) + C_3 \mathrm{V}\exp(-{}^{K_3 t}/_{C_3}) \tag{4.6}$$

Equation 4.6 illustrates the relation between speed, deformation and exerted forces. The constant values mentioned in the model have been obtained from the experimental results.

In dynamical analysis, the material factors are considered for development of the relevant equation. In this, the membrane deformation is presented due to applied forces during injection. The Point load model has been employed to model this created deformation on the membrane. Considering the assumption mentioned earlier, the force balance on the membrane surface is modelled using n Newton's second law. As the injection happens with constant speed, the motion is considered as no acceleration.

$$\sum F = m\frac{dV}{dt} = 0 \tag{4.7}$$

As it is illustrated in Figure 4-2, the injection force is balanced by the reaction of the internal hydrostatic pressure preventing the injection. This prevention additionally creates the stress on membrane. Consequently, Equation 4.8 demonstrates the equilibrium condition:

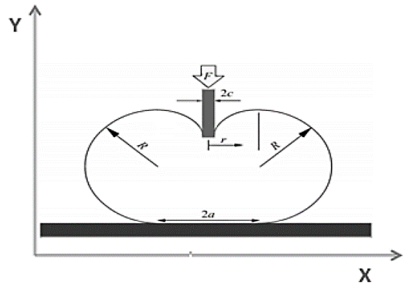

Figure 4-2. The point load model of injection [39]

$$F = \pi r^2 p + \sigma_d 2\pi r h \frac{dw}{dr} \quad (4.8)$$

where F is the injection force in N, Fp is the internal pressure acting on the outer surface of the artificial oocyte and σ_d is the stress at the injection section. Also the dimple profile is changing due to the changing in radius.

Elastic modulus of the chorion of zebrafish has been calculated to feed the FE model. In order to estimate the elastic modulus of the chorion of the zebrafish embryo, a bio-membrane mechanical model is proposed in Equation 4.9. This equation assists to find in finding the elastic modulus obtained from the information provided by experiments. This modulus will feed FE as a material property. The equation is developed that indicates the relation between membrane elastic modulus, and force during injection.

$$F = \frac{2\pi E h \omega_d^3}{a^2(1-\vartheta)}\left[\frac{3-4\zeta^2+\zeta^4+2ln\zeta^2}{(1-\zeta^2)(1-\zeta^2+ln\zeta^2)^3}\right] \quad (4.9)$$

where ζ=c/a; and F is the injection force; H is the membrane thickness (chorion thickness); w is deformation depth; a and c are the geometric parameters and have been obtained by the image analysis. The membrane thickness is considered as 3 μm; the Poisson ratio is considered as 0.5.

4.3 ***Finite element model***

Finite element model development assists the researcher to examine the cell reactions by changing the dynamical factors such as speed during the injection regardless of real experiments. However, defining the appropriate mechanical properties for the relevant cell is the most challenging segment of the FE model development.

In this chapter, a three-dimensional finite element model has been developed using Abaqus 16.1. This model employed dynamical explicit analysis to simulate zebrafish embryo indentation using three different indentation speeds as 100, 600 and 1000μm/s which are considered as low, medium and high injection speeds. A number of 4287 shell elements (S4R elements) have been employed to simulate the embryo; while the micropipette and the holding pipette have been simulated as rigid. A finer mesh has been used near the contact points of the cell with the micropipette and the holding pipette, with mesh density decreasing moving towards the centre of the cell. The minimum element length is 8 μm, while the maximum is 40 μm. The thickness associated with the shell elements has been set to 3 μm. The cell's radius is 400 μm, while the micropipette's radius is 30 μm. A 2.5KPa has been applied to the contact area of the holding micropipette and cell to make it clamped in the three-dimensional space.

The general contact algorithm has been utilised to simulate the contact among different parts of the model; and the Coulomb friction model has been used with a friction coefficient of 0.3. The friction allows maintaining of the position of the cell, avoiding it slipping due to the compression force applied by the micropipette. The embryo has been simulated as linear elastic with Young's modulus function of the impact velocity.

4.4 *Experiment design and test rig*

The experimental setup comprises of a precision injection system integrated with an accurate and sensitive loadcell to measure the indenting force of a zebrafish embryo. A data acquisition device is employed to convert the analogue outputs from the loadcell to digital. The obtained data are analysed using computer software and raw data has been defined as force unit. A SS2 Sherborne Ultra Low Force Load Cell with capacity of 0.5886 N and resolution of 1 mN is utilised for measuring the membrane reaction force during the injection. Figure 4-3 demonstrates the schematic of the experimental set up.

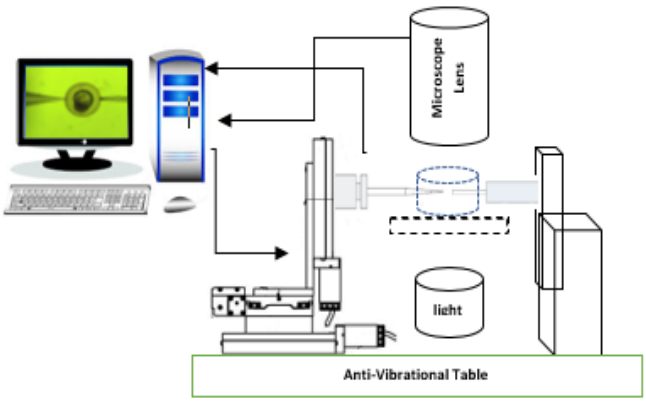

Figure 4-3. Schematic view of the experiment set up

During the experiment, a sample dish is placed within the focal zone of microscope. Then the oocyte is restrained and the injection pipette is set toward the centre of the embryo within a distance from the chorion. This distance allows the injector to achieve the desired speed before the tip of the pipette touches the chorion. The micropipette stops the motion once the breakage of membrane reports a sudden drop of the recoded indentation force. The total deformation and position of the cell were reported to the controller using visual feedback [73]. The micropipette movement is controlled for various speeds, namely 100 to 1200µm/s. Image 2 indicates periods of the injection for

zebrafish. The total amount of micropipette movement during recording force until a sudden drop of force is considered as deformation. The data information obtained from the experimental model will feed both mechanical and FE models. Hence, the experiment results are discussed initially in this chapter.

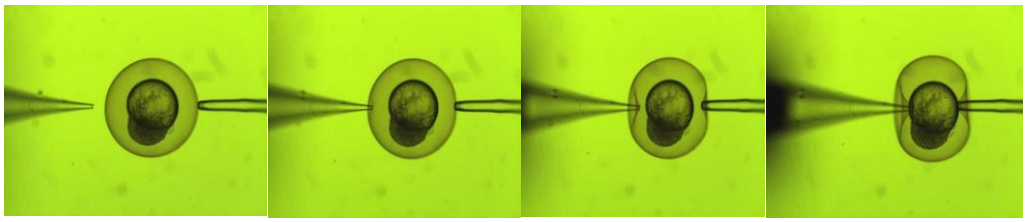

Figure 4-4. Different stages of the zebrafish embryo injection with a constant speed. This figure indicates the deformation creation stages

4.5 *Zebrafish embryo collection*

In biological research, some animals' oocytes and embryos are vertebrate models as they have exceptional properties compared with other models. The zebrafish embryo is a reliable model for the mechanical tests and response behaviour analysis. Additionally, it is a dominant model to realize the genes' role during the development stage. The other advantages of the zebrafish embryo are transparency, high productivity and being of a decent size for mechanical experiments. Zebrafish embryos are collected freshly with the protocol mentioned in guidance for the laboratory use of zebrafish (the zebrafish book as reference). The embryo samples were transferred to the laboratory on the days of the experiments [52].

4.6 *Experimental results*

This section will mainly discuss the results obtained from experiments for various indentation speeds and discuss the validation of the proposed FE model. The main aim of these results is demonstrating the effect of speed on deformation creation and developing an analytical model to be validated by the experiments to assist the researchers in obtaining the speed effect on deformation without existing biological samples. Figure 4-5 demonstrates the graphic user interface for controlling the injection system. This GUI can control the coarse and fine movement of the stage which assisted enabled us to control the speeds. However, the force is also demonstrated on this window to exhibit the force increase during the injection procedure. The designed software can be adjusted for acceleration, deceleration and speed.

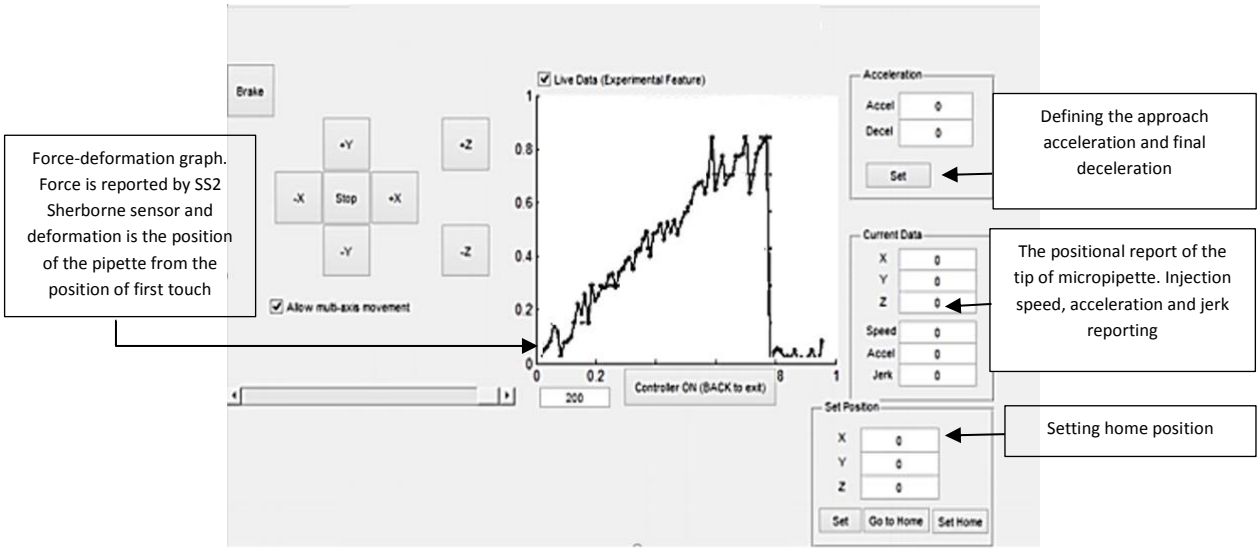

Figure 4-5. The graphic user interface for the injection system

The experimental results are demonstrating the deformation creation on the cell during the injection among six sets of different speeds to identify the potential damage to

the cell while the needle pierces the cell. Table 4-1 compares the deformations created by different speeds along with associated forces generated on the membrane utilising variant speed. Two experiment sets, five cells each, were carried out for each speed.

Table 4-1 Injection speed, created deformation and indentation force comparison

Experiment	Speed µm/s	Deformation µm	Indentation Force mN
Set 1	0.05	379.5	1.145
Set 2	0.1	341	1.23
Set3	0.2	328.5	1.19
Set 4	0.4	316	1.26
Set 5	0.6	281.5	1.335
Set 6	1	249	1.41

As is illustrated in Table 4-1, the deformation reduces with the speed increase. On the other hand, the indentation force is increased by increasing the speed. However, increasing speed may cause an increase in vibration and force fluctuation. This increase in force is expected based on the work equations W=F.d. When the deformation is decreasing by increasing the speed, the force needs to be increased to compensate. Consequently, the deformation is decreased by approximately 35% and forces increased by 23%.

$$W = F.d = \frac{1}{2}mv^2 \tag{5.10}$$

The recorded force is presented versus deformation in Figure 4-6 for six different speeds. The noises that occurred during the experiments were filtered. These graphs are the average values of the recorded data for different speeds and indicate the behaviour of the cells in response to the speed changing. As exhibited here, the fluctuations reported

on the forces are increased by speed increase. The highest force oscillation is reported in 1mm/s which makes this speed unsuitable although it minimises the deformation.

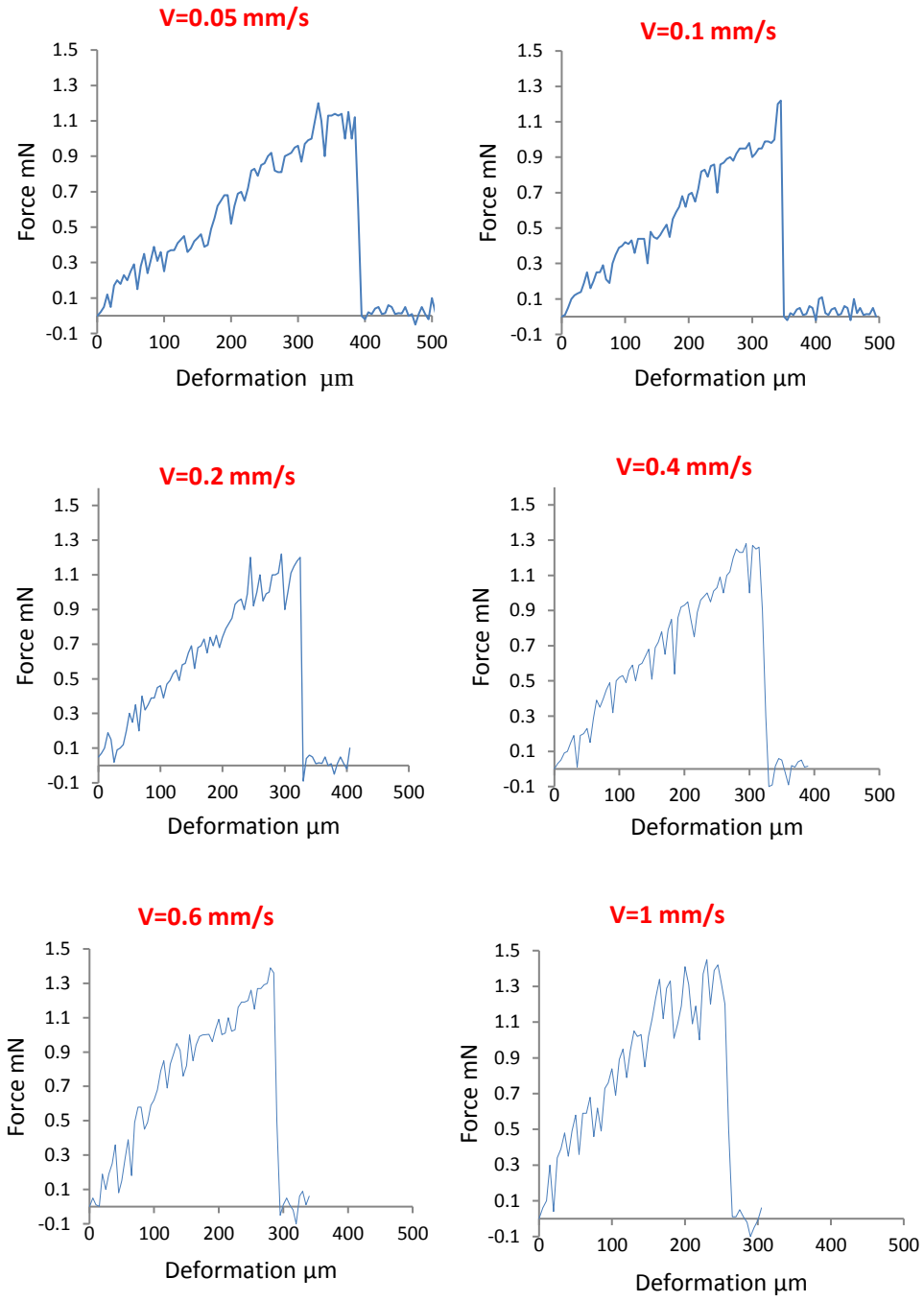

Figure 4-6. Experimental results for various injection speed

The experimental results of the injection speed versus deformation are presented in Figure 4-7. These results agree with the developed dynamical model presented in the previous section and indicates that a higher speed causes smaller deformation on the zebrafish embryo. It can be seen that the rate of the deformation decreases as the injection speed increases. The rate of deformation reduction between 0.1 and 0.4 is slow, however, the sudden decrease occurs between 0.4 and 1 mm/s. On the other hand, 1 mm/s causes considerable amount of fluctuation, which will be discussed next. Therefore 0.6 mm/s is concluded as an optimum speed for zebrafish injection.

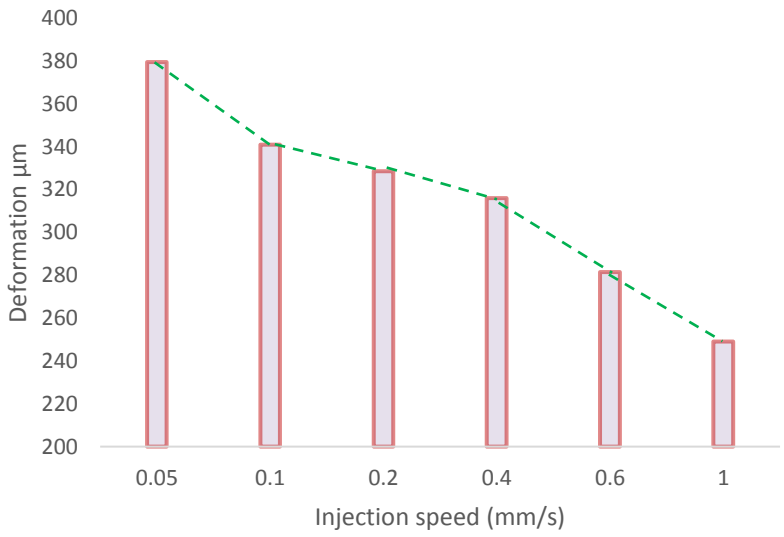

Figure 4-7. Deformation of Zebrafish embryo using different constant injection speed

By increasing speed, the force fluctuation increases which demonstrates the greater vibrations during the injection procedure as illustrated in Figure 4-8. The fluctuation reported on forces are presented the amount of vibrations during the injection as it is illustrated in Figure 4-8. It was expected to face vibration based on the simulation. This vibration is considered as lateral and axial vibration. The result of these two types of vibration is exhibited by force fluctuation. These fluctuations are growing during speed increase. The variation in the forces is acceptable within 25% of total reported force. This limitation satisfies the speed with maximum of 0.6µm/s. More fluctuation indicates more vibration which may cause cell damages.

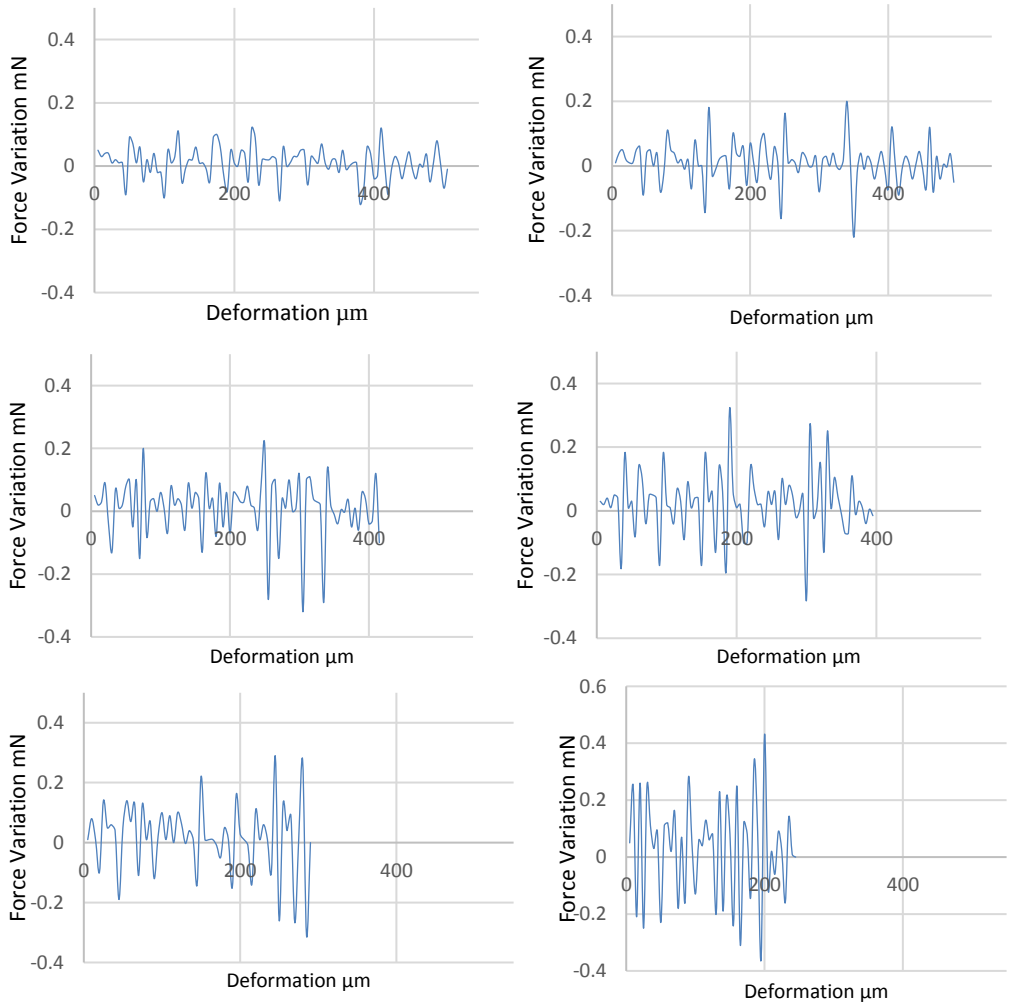

Figure 4-8. Force fluctuation obtained from experimental data

The Young's modulus for the chorion has been calculated using equation 4.9. The average of this Young modulus will feed the FE to model the cell for injection analysis purposes. The results for elastic modulus are consistent and indicate the number of 1.36±0.23 MPa which is very close to the reported modulus in table 4-2 [72] which is 1.51±0.07 MPa.

Table 4-2. The comparison between the obtained experimental results from reported information in literature

Category	Stage	Mean Modulus	Standard Deviation
Literature	Blastula	1.51 MPa	0.07 MPa
In-house experiment	Blastula	1.32 MPa	0.24 MPa

In the previous section, a FE model has been proposed to assist the researcher in modelling the injection process and analyse the mechanical factors without actual experiments. The material constants as input for this FE model have been received from experiments with comparison with literature. For the validation of the model, the experiment results of three speeds have been selected, which are 0.1 mm/s, 0.6 mm/s and 1mm/s. The reason for the selection of these speeds was to validate with the lowest, medium and highest speed of injection in our tests to examine the FE model and its capability of working in these speed categories within the range of low to high injection speed as in Figure 4-9.

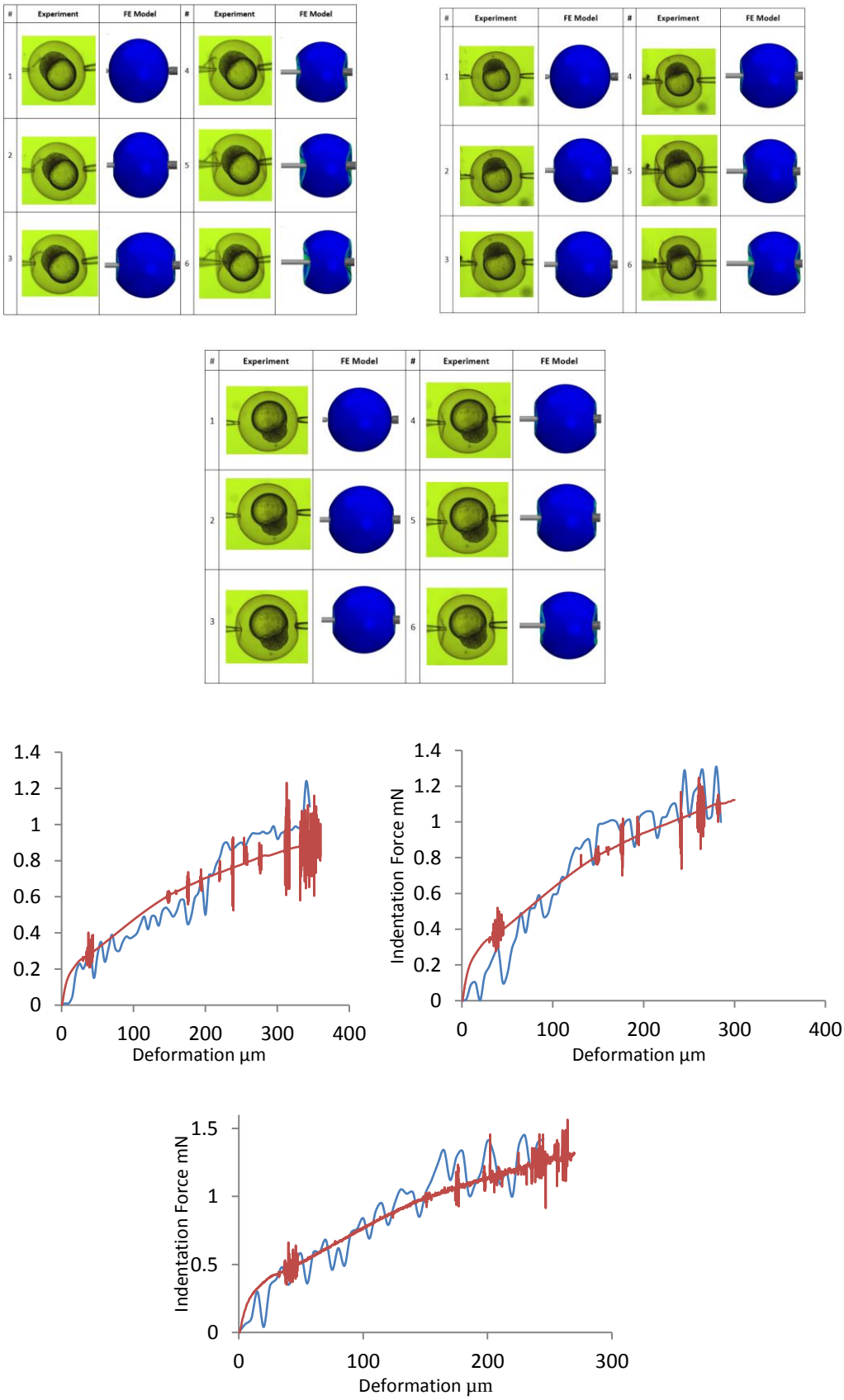

Figure 4-9 comparison between the results of FE and Experimental for three various speeds

Figure 4-10 demonstrates the results obtained from FE for a specific injection speed of 0.6µm/s. Additionally, the real time experiment results are presented to compare between experiment and finite element models during the injection. This figure indicates the force-deformation graphs for three different speeds examined in the FE model.

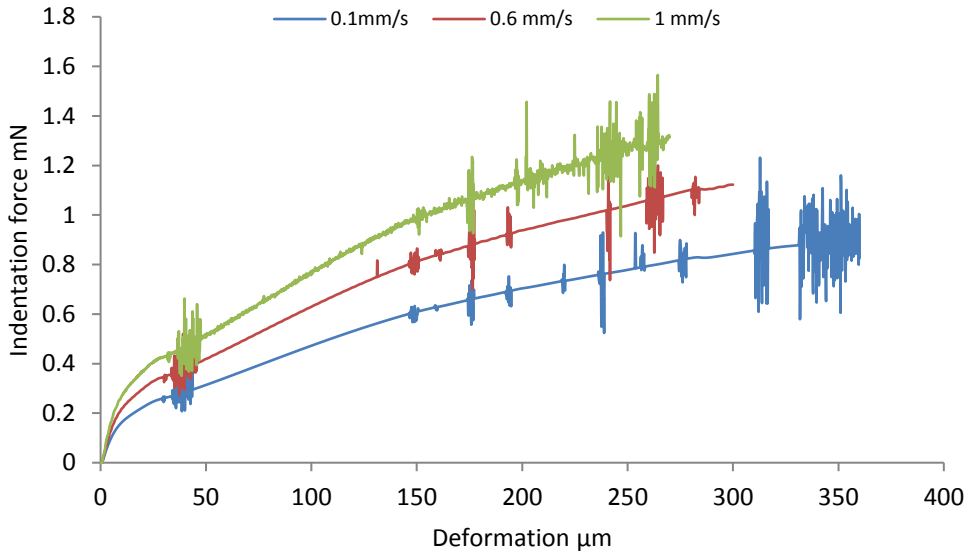

Figure 4-10 The FE results for three speeds

The results obtained from FE indicate that the increase in speed is causing less deformation and the higher indentation force including more fluctuations. These results are close to the results obtained from experiments.

4.7 *Discussion*

The main purpose of this research is analysing the effects of various dynamical factors on cell deformation. The developed theory and FE software are validated by experiments. In theory development, the coefficients are needed to be calculated using experimental results. There are five un-known coefficients mentioned in Equation 4.6. To find these coefficients, the data for each experiment considered by its assigned speed were imported to MATLAB. Then the average of obtained coefficients for each speed was calculated. The final equation using the retrieved coefficients is demonstrated in Equation 4.11. This equation is demonstrating the relation between injection force, deformation and velocity.

$$F(t) = 0.30X + 0.125V\exp\left(-{}^{0.356t}/_{0.125}\right) + 4.74\text{Vexp}(-{}^{0.668t}/_{4.74}) \qquad (4.11)$$

The developed FE and theory can be adapted for different biological cells provided that the properties of the cells have been previously ascertained by different experiments. Injection speed, injection force and deformations were the three main variables which were discussed in the results section. The results from the experiment indicates that by increasing injection speed, force is increased which causes some considerable fluctuations. These fluctuations are considered as potential lateral and axial vibrations which may cause harm to the cell. This has been visually reported in the FE model too.

An increase in inaction force caused by increasing the speed is causing the increasing stress on the membrane. However, there is no report on the negative/positive effect of this stress. Figure 4.9 indicates the accuracy of the developed software justified

by experiments. This figure explains the behaviour of the FE model which is very similar in pattern to the data created experimentally.

Figure 4-11 illustrates the comparisons between changes in increased force, maximum force amplitude ratio and deformation creation among various injection speeds. Maximum force amplitude ratio (MFAR) is a ratio of the maximum amplitude recorded during the injection to the maximum force reported in the same set which is the indentation force. This variable indicates that maximum fluctuation happens during the injection which indicates the total force changing based on vibration. A is demonstrated in the table, the maximum force amplitude ratio reported is 25% for the first five sets which have the injection speed less than 0.6 mm/s. However, it has a dramatic increase in set 6 as 55% fluctuations occur during the injection which indicates the high vibrations. The indentation force has been increased gently up to 12 % in comparison to 0.05 mm/s during the first five sets and has a dramatic jump to 24% in set six. Although the MFAR and indentation force have been slightly increased during first five sets, deformation decreased by 10% which is almost 100µm for set 5. Although this value is 130µm for set 6, there is no feasibility of injection for this speed due to high vibrations.

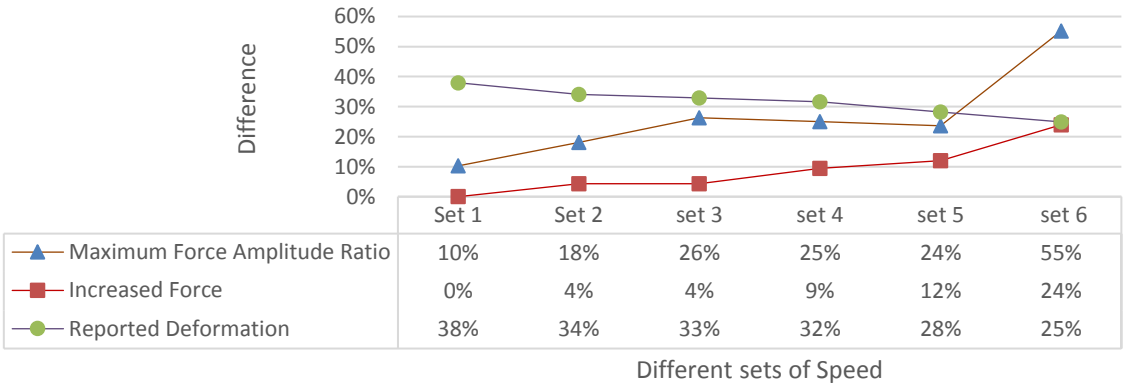

	Set 1	Set 2	set 3	set 4	set 5	set 6
Maximum Force Amplitude Ratio	10%	18%	26%	25%	24%	55%
Increased Force	0%	4%	4%	9%	12%	24%
Reported Deformation	38%	34%	33%	32%	28%	25%

Figure 4-11. The comparison of the results for force amplitude, force increase and deformation

5.8 ***Conclusion***

This chapter illustrates the results obtained to analyse various speed effects on cell deformation during the injection. However, it's been believed that changing the speed during the injection may harm the cell. Consequently, it has been decided to apply fundamental research to investigate this dynamical factor during injection. The obtained results indicate that by increasing the injection speed, the deformation decreases and the injection force increases. However, increasing the speed causes additional vibration which is considered as a negative aspect. The optimum speed based on vibration, force and deformation consideration is obtained and reported to be 0.6 mm/s. This is reported for zebrafish injection as an appropriate mode. However, an FE software and a mathematical equation have been developed for the modelling of injections capable of expanding for different cell types by changing the Young's modulus defined in both models. Our proposed software is capable of recognising the Young's modulus after a set of injections using defined speed and adapting the FE and Theoretical model with that particular cell. The proposed FE model is satisfied by the experiment data environments.

CHAPTER 5

CELL VISION RECOGNITION FOR AUTOMATIC MANIPULATION AND POSITIONING

5.1 *Introduction*

Polar body position detection is a necessary process in the automation of micromanipulation systems specifically used in Intra-Cytoplasmic Sperm Injection (ICSI) applications. The polar body is an intracellular structure, which accommodates the chromosomes, and the injection must not only penetrate this structure but be at the furthest point away from it too. This chapter aims to develop a vision recognition system for the recognition of the oocyte and its polar body in order to be used to inform the automated injection mechanism to avoid the polar body. The novelty of the chapter is its capability to determine the position and orientation of the oocyte and its polar body. The gradient-weighted Hough transform method was employed for the detection of the location of the oocyte and its polar body. Moreover, a new elliptical fitting method was employed for size measurement of the polar bodies and oocytes considering potential shape difference for the oocytes and polar bodies. The proposed algorithm has been designed to be adaptable with typical commercial inverted microscopes with different criteria. The successful experimental results for this algorithm produce maximum errors of 5% for detection and 10% for reporting respectively.

The aim of this chapter is to discuss the previously mentioned methods and the process of its development. Image processing techniques will be discussed initially and then the proposed detection method will be discussed as a follow up to previous work in this area [101]. Experimental results will demonstrate the accuracy of the software. This chapter will be concluded by validation of the software.

5.2 *Image processing techniques and filtration*

The new developed software is proposed with the purpose of detecting oocyte and polar bodies using the images taken by the microscope camera. The detection is based on the microscope's global reference to find the position and orientation of the polar body and oocyte centre point. All the images used in this chapter are from oocytes in metaphase II state and taken from different resources. The oocyte was clearly denudated of all excess surrounding cumulus. The microscope was adjusted to have a clear view of the cell (oocyte) and surrounding (polar body). The oocyte and polar body are commonly circular but may be presented as ovular/elliptical with eccentricity values similar to that of a circle [101]. The detection procedure has been divided into three stages; as are pre-processing, segmentation and feature extraction which will be discussed in the following sections.

5.2.1 *Pre-processing*

The pre-processing procedure has three stages; conversion of the colour, contrast enhancement and spatial filtering.

Digital colour images represent the standard colour model. The most common model for this is RGB which represents red, green and blue; these are the three principal components for each pixel of an image. The level of each of these components identifies the colour for each image. For example, a greyscale image is an image for intensity ranges from black to white, which indicates equal RGB in each pixel. Greyscale conversion from an RGB image would be achieved by Equation 5.1 which makes the level of each component equal by averaging the RGB for each pixel and computes the greyscale intensity.

After conversion of RGB image to grayscale image, the obtained images have low, medium or high gray values. These values will indicates how dark or light our image is. This information can be obtained from the image's histogram.

$$Greyscale_{Intensity} = \frac{R(x,y)+G(x,y)+B(x,y)}{3} \tag{5.1}$$

Greyscale has different dynamic ranges between the lowest and highest intensity level. The lowest intensity of the greyscale represents the low contrast images which would be improved by raising the dynamic range to the highest potential limit [103] which is managed by the bits number employed to signify each pixel that is also named as the bit depth.

To raise the dynamic range of the image from 0 to 255, the image intensity needs to be multiplied by an enhancement factor which is represented in Equation 5.2:

$$Ef = \frac{2^n-1}{Gray_{max}-Gray_{min}} \tag{5.2}$$

where n represents the number of bits for the greyscale image; 0 taking to account as that was the reason 1 was deducted from the nominator. Here greyscale images are 8-bit images. The enhanced image, h(f), is calculated using Equation 5.3 where the initial image is zero and multiplied by the enhancement factor.

$$h(f) = (g(f) - grey_{\min})(Ef) \tag{5.3}$$

This is a filter application in a spatial domain. A filter mask is a neighbourhood coefficient which is usually a 3×3 rectangle. The coefficients are varied and are selected based on the filter type. The weighted average filter uses the image centre for the highest weight coefficient and the rest of the coefficients are weighted inversely as a distance function [103]. The weighted average filter is a low-pass filter which is used to wave low frequencies and eliminate noises, while minimizing blurring that results in edge preservation improvement [103]. The weighted average filter is calculated using Equation 5.4 which is obtained by dividing the mask into its summation. The weighted average filter is obtained by Equation 5.5 which is the two-dimensional correlation filtering (m x n) of the initial image; this indicates the summation of the coefficient multiplied by the local pixel value to calculate the filtered value in the filter location centre for each image pixel.

$$w(x,y) = \frac{1}{16}\begin{bmatrix} 1 & 2 & 1 \\ 2 & 4 & 2 \\ 1 & 2 & 1 \end{bmatrix} \tag{5.4}$$

$$R = w(1,1)f(x+1,y+1) + w(1,0)f(x+1,y) + \cdots + w(0,0)f(x,y) + \cdots w(-1,-1)f(x-1,y-1) \tag{5.5a}$$

$$g(x,y) = \sum_{-\frac{m}{2}}^{\frac{m}{2}} \sum_{-\frac{n}{2}}^{\frac{n}{2}} w(u,v) f(x+u, y+v) = w(x,y) \times f(x,y) \quad (5.5b)$$

Figure 5-1 illustrates the mechanics of spatial filtering. The procedure contains simple movement of the filter mask from one point to another in an image. The response of each point is calculated by a predefined relationship. Weighted smoothing filter is more effective compared with the simple smooth spatial filters. It is employed when pixels closer to the centre pixel carry higher weighting compared with other pixels which are further away from the centre pixel.

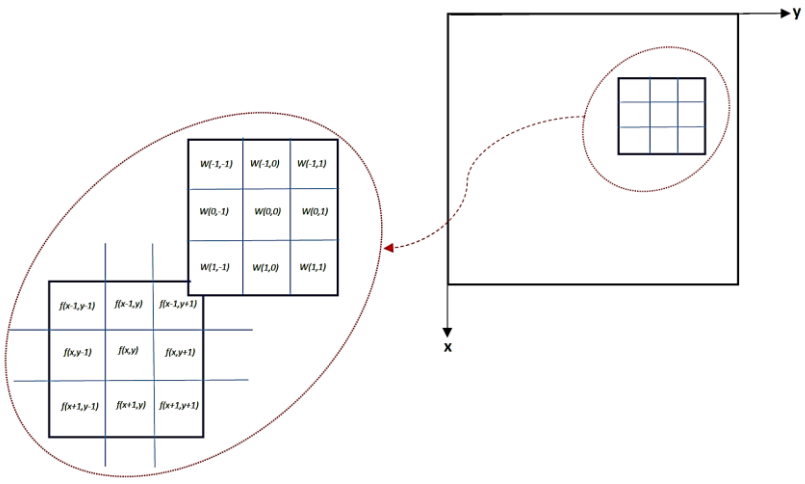

Figure 5-1 Mechanics of spatial filtering

5.2.2 ***Segmentation***

The gradient thresholding of a single image involves the intensity vector derivatives regarding x and y. The edges of the image are the place where there are sudden intensity changes [104]. Consequently, the gradient magnitude is employed to distinguish the edges by defining the threshold to find a location where the magnitude of the gradient is above the value of the threshold.

$$\nabla f = \begin{bmatrix} G_x \\ G_y \end{bmatrix} = \begin{bmatrix} \frac{\partial f}{\partial x} \\ \frac{\partial f}{\partial y} \end{bmatrix} \quad \|\nabla f\| = \sqrt{{G_x}^2 + {G_y}^2} \tag{5.6}$$

$$\theta = \tan^{-1}\left(\frac{G_x}{G_y}\right) \quad \sin\theta = \frac{G_y}{\|\nabla f\|} \quad \cos\theta = \frac{G_x}{\|\nabla f\|} \tag{5.7}$$

where (∇f) is the gradient magnitude which specifies the greatest changes in intensity at the pixel. The pixel position and orientation were computed from Equations 5.6 and 5.7.

5.2.3 ***Feature extraction***

The final stage for image processing is feature extraction. In this section, the Hough transform method is employed, which is a reliable method for identifying the shapes inside the images. This method was initially proposed by Paul Hough in 2008 to detect the lines [105]. In the current chapter a circular Hough transform method was used for feature extracting of the oocyte in the image as the shape of an oocyte is usually circular. A parametric circle equation is used and rearranged to calculate the centre point

voted by the edge points, that are planned to parametric space named as an accumulator, as shown in Figure 5-2.

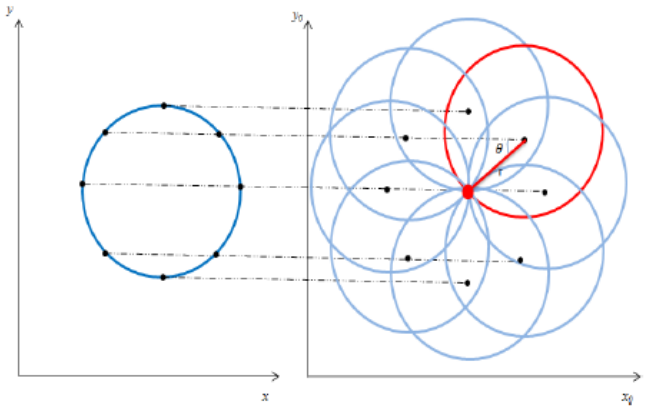

Figure 5-2. Circle Illustration in an image and applying Hough transformation to a parameter space which is defined as an accumulator

As it is shown in Figure 5-2, the edge points direct a circular object to be recognised. Equation 5.8 shows the relationship between the orientation and gradient which is employed to obtain the sinθ and cosθ for the vote received for each centre point. The obtained vote for the position in the accumulator and the votes' summation completes the plan. As a result, in the presence of any circle in the image, circle detection and centre point location would be obtained based on the centre point votes which cluster in a small accumulator region and create a maximum region. The centre point is achieved from the accumulator employing a centre point detection algorithm.

$$x_0 = x - r\cos\theta \qquad y_0 = y - r\sin\theta \tag{5.8}$$

The weighted Hough transform is a development of the Hough transform method which has a different convention for planning to the accumulator. This technique employs weighting coefficients for each vote. The gradient based systems consider the magnitude of the gradient as the coefficient to plan the accumulator. Consequently, the votes for centre point from the sharper edge would have higher weighting coefficients in comparison to the other votes which are received from blurred edges.

In addition, an elliptical fitting method is added to the WHT to recognise an elliptical object in case the cell is not a perfect circle. In this method, the centre point has been calculated and radius ranges have been defined. The gradient of the image shown as Gx and Gy calculates the encapsulated area in a square area. This is twice the maximum value for the radius surrounding the centre point of an elliptical item existing in the image. The radius vales which are indicated as a and b for an elliptical item, are determined based on the location of the maximum value in the accumulator. The values in addition to the value of the centre point are employed to fit to the item using elliptical Equations 5.9:

$$r = \sqrt{(x - x_0)^2 + (y - y_0)^2} \quad where \quad x = x_0 + a\cos\theta \quad y = y_0 + b\sin\theta \qquad (5.9)$$

5.3 ***Detecting of polar body and oocyte***

Designing of this software is based on combinations of the methods presented earlier in the last section. The images used for the software test were 8-bit JPEG compressed RGB images received from different types of inverted microscope cameras.

Then, all the images were converted to greyscale layout to save computational time for the subsequent steps. Linear contrast enhancement was employed for the purpose of raising the dynamic range of the images to achieve better and easier edge detection [106].

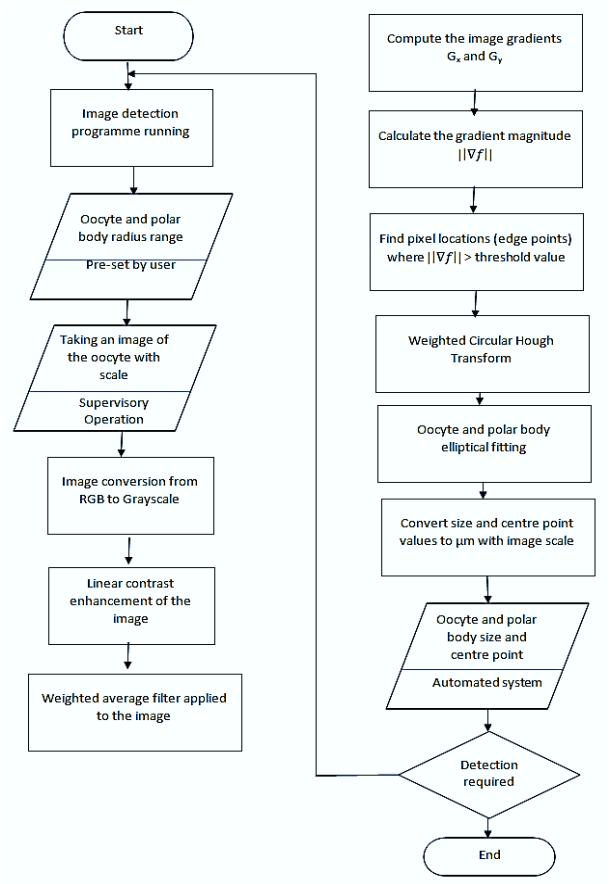

Figure. 5-3 Detection software Process

A 5X5 weighted filter was applied to the images to minimize the presented noises in the image and also restrain the granularity presence in the polar body and oocyte. This filterisation helps to reduce any possible false detection. The centre point position of the polar body and oocyte were detected by employing the weighted circular Hough transform method. The obtained gradient magnitudes were used as the weighting

coefficient. To minimize the calculation time, a limit is defined by the gradient magnitude threshold for the total of the edge points based on the centre point calculation.

As this software is designed to be compatible for different types of oocyte, the radius range for both the oocyte and polar body is to be supplied by the user. This range was obtained from the literature for each iteration. The centre point for both the oocyte and the polar body were extracted based on the developed algorithm. The microscope's lens' centre point was taken as the main reference point of the image. The circular Hough transform (CHT) was utilised for the oocyte and polar body detection in any position and for orientation in the image, which did not need to be in a close neighbourhood area in the centre of the image [107]. The elliptical Hough transform (EHT) is employed to detect an elliptical shape, in case the oocyte and/or polar body are this shape. It should be noted that WHT is also sufficient for detecting the centre point, although EHT increases the accuracy of the detection in possible elliptical shapes.

The sizes of the polar body and oocyte were detected after obtaining the location of the centre points. This was used as a combination with the elliptical fitting method, which was presented in the last section and recently developed for this specific application. The radius for the elliptical fitting for the polar body and oocyte detection was determined by considering the specified radius ranges by the user. This method does not need the edge of the polar body and oocyte to be identified and has a better fitting in comparison to a circular fitting for the elliptical and ovoid shapes; and consequently provides more accurate sizing.

The software is designed, via a graphical user interface (GUI), to get initial information from the operator and show the results based on the calculation. This GUI

asks about two parameter ranges which enable this software to be compatible with different microscopes and different types of oocytes. Then, after pushing the 'RUN' button, the specification of the oocyte and polar body is as indicated in Figure 5-4.

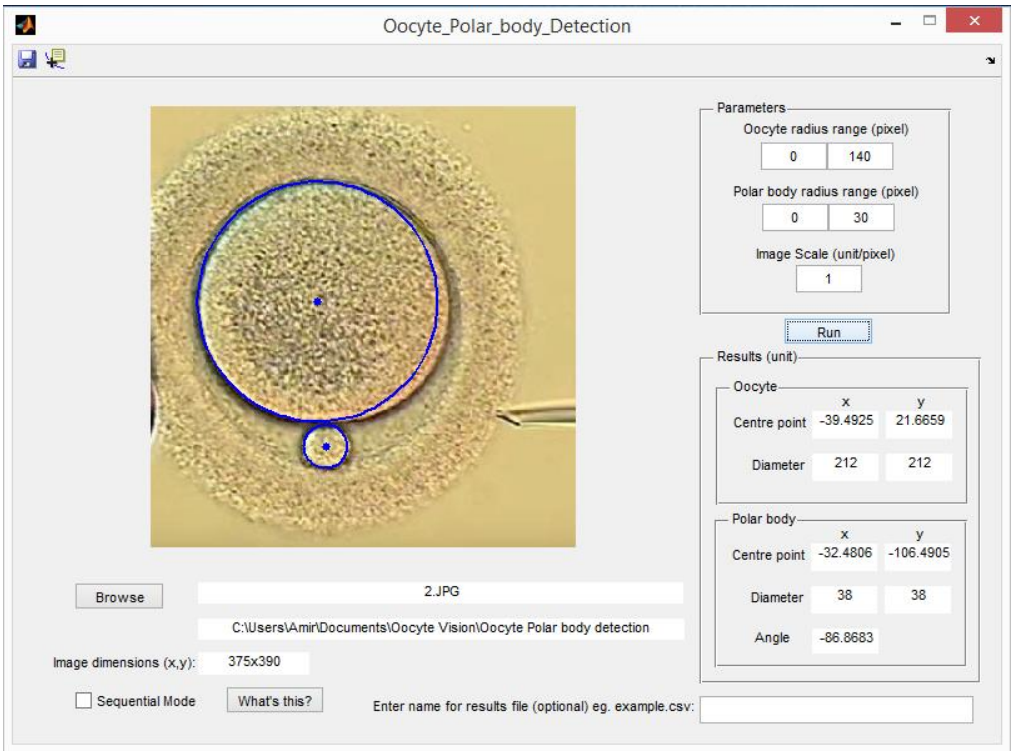

Figure 5-4. GUI for the detection software

The output information received from the algorithm fed the proposed system about the initial location and positioning of the polar body and Oocyte in global coordination. This information indicates the position and the diameter of the Oocyte and polar body centres as well as the angle where polar body's centre positioned with respect to positive direction of X-Axis. The image centre is the centre of the microscope vision field.

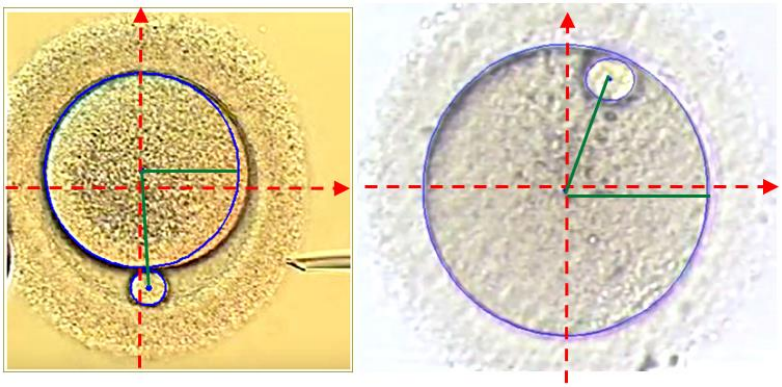

Figure 5-5. Processed images and detected oocyte and polar body as well as positional reports

5.4 *Experimental results and discussion*

The experiments were conducted for various images sourced from numerous microscopes. The images were considered as input to the software and the software first detected the polar body and oocyte. If the polar body was not in the focal zone of the microscope, then the software gave a message about not locating a polar body. After the confirmation of the correct recognition of the polar body and oocyte, the sizes of the oocyte and polar body were computed. The sizes of both the polar body and oocyte were measured manually using ImageJ software. ImageJ is a public domain image processing programme developed for image analysis in biomedical applications.

The algorithm has been tested with different factors that may have an impact on the results. eighty images have been tested for each major factor set. Table 5-1 compares 260 different images taken from different resources. The first row indicates the images taken from different microscopes with a different background colour. It shows 100% correct detection on these types of sampling test. The second row images of different

orientations of a polar body which were taken from the same microscope. The polar bodies are located in random locations in the perivitelline space. This test indicates the ability of the software to detect orientation and position of the polar body in a space. A 100% successful detection has been reported for this set as well. The third row shows different microscope zooms. This test has been done to check the ability of the software to detect the polar body and oocyte under different magnifications. This test also had a 100% success rate. The last row points out the failure of the software in this type of image; this is because the images are blurred and the clarity of the image is so poor. Also there are some disturbances in the image which are considered as noises (see Figure 5-12) and these were the cause the failures. Despite these disturbances, the oocyte was detected successfully and the failures happened just for the polar body detection.

The algorithm is capable of being adopted by different versions of the inverted microscopes. Existing extra cumulus cells are known as disturbance for the outcome of this algorithm and may cause some errors in the detection of the polar body due to its smaller size. However, the existence of these cells have not had any effect on oocyte detection.

Table 5-1 Comparison table for all tested images

Description	Total tested images	Correct Oocyte detection	Correct polar body detection	Correct Oocyte location detection	Correct polar body location detection
different background colour	80	80 100%	80 100%	80 100%	80 100%
Different position and orientation	80	80 100%	80 100%	80 100%	80 100%
Different magnification of the images	80	80 100%	80 100%	80 100%	80 100%
Existing the disturbance	20	20 100%	12 60%	20 100%	12 60%

The quality of an image is indicated by the behaviour of the associated histogram. The good quality of an image is defined when the image is bright enough and has a good contrast. As a result, the histogram data is a measure of the brightness and contrast as well as an indication of the associated dynamic range.

Each of the analysed categories of the images is indicated separately in the following sections. The results are demonstrated using two main methods. The first method illustrates the results of the detection and is shown as a naked image, its identity which is exhibited by the histogram, and the final detected result from the developed algorithm. The second method uses the box and whisker chart demonstration, which indicates the differences in the measurements made manually using imageJ and the algorithm-based measurement.

5.4.1 *Different background colour*

Different microscopes operate with different vision background colours based on the type and purpose of the operation. This should be taken into consideration in designing the vision detection software. The proposed algorithm is capable to recognise the polar body and the oocyte present in different background colours as demonstrated by the obtained results. Three different background colours are shown in Figure 5-6. The histogram of these colours concentrate on high gray value but not well spread, which is due to poor contrast. As a result, during pre-processing of an image, contrast was increased. Consequently, this figure illustrates the right detection of the oocyte and polar body in each try.

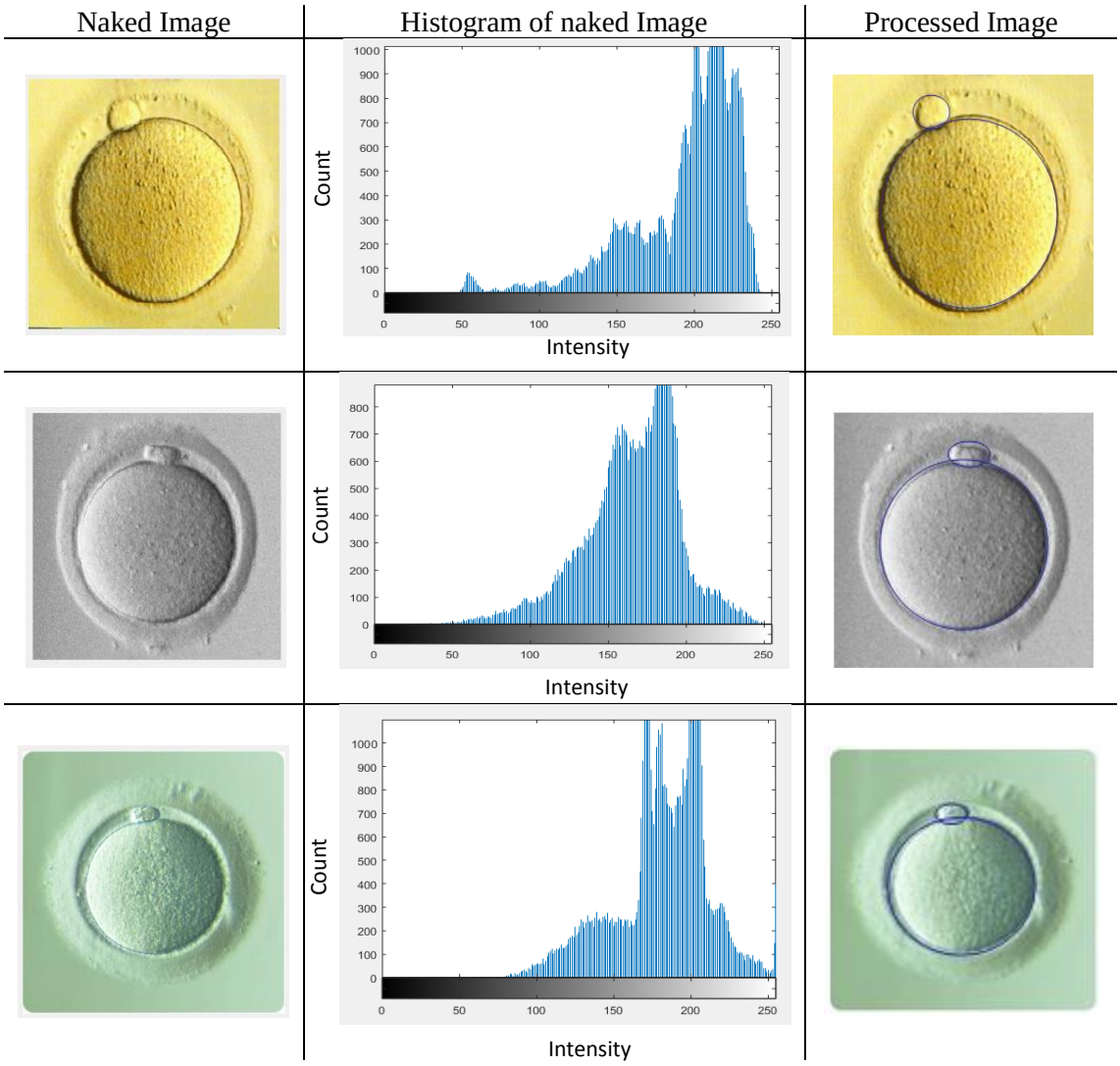

Figure. 5-6 Different background colour examined images

Figure 5-7 illustrates the highest difference in manual and software measurement belongs to oocyte diameter measurement. As the average oocyte diameter and polar body are 140 µm and 20µm respectively, the corresponding maximum error for oocyte diameter measurements are approximately 5%±2% and 10%.

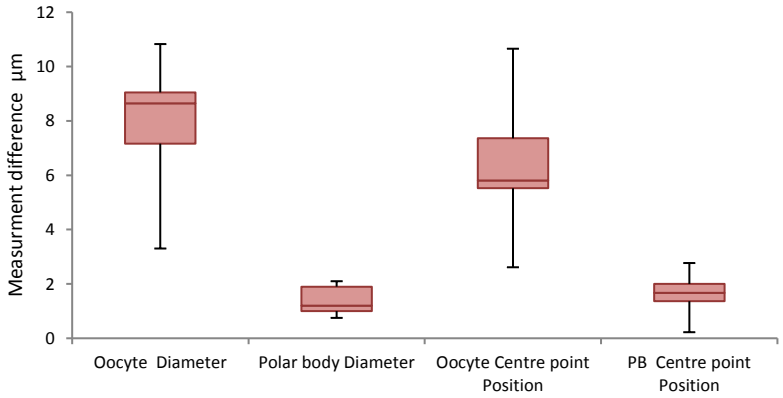

Figure 5-7. Whisker chart demonstrating differences in measurements in different background colour

5.4.2 **Different polar body position and orientation**

The oocyte is positioned on the petri dish at random, which results in the random positioning of its polar body. The proposed algorithm is capable of detecting the centre point of the oocyte and that of its polar body, together with the line that connects these two points. The results confirm 100% successful detection of all of the 80 test images. Examples of the results are illustrated in Figure 5-8, where the detected images are circled by blue lines.

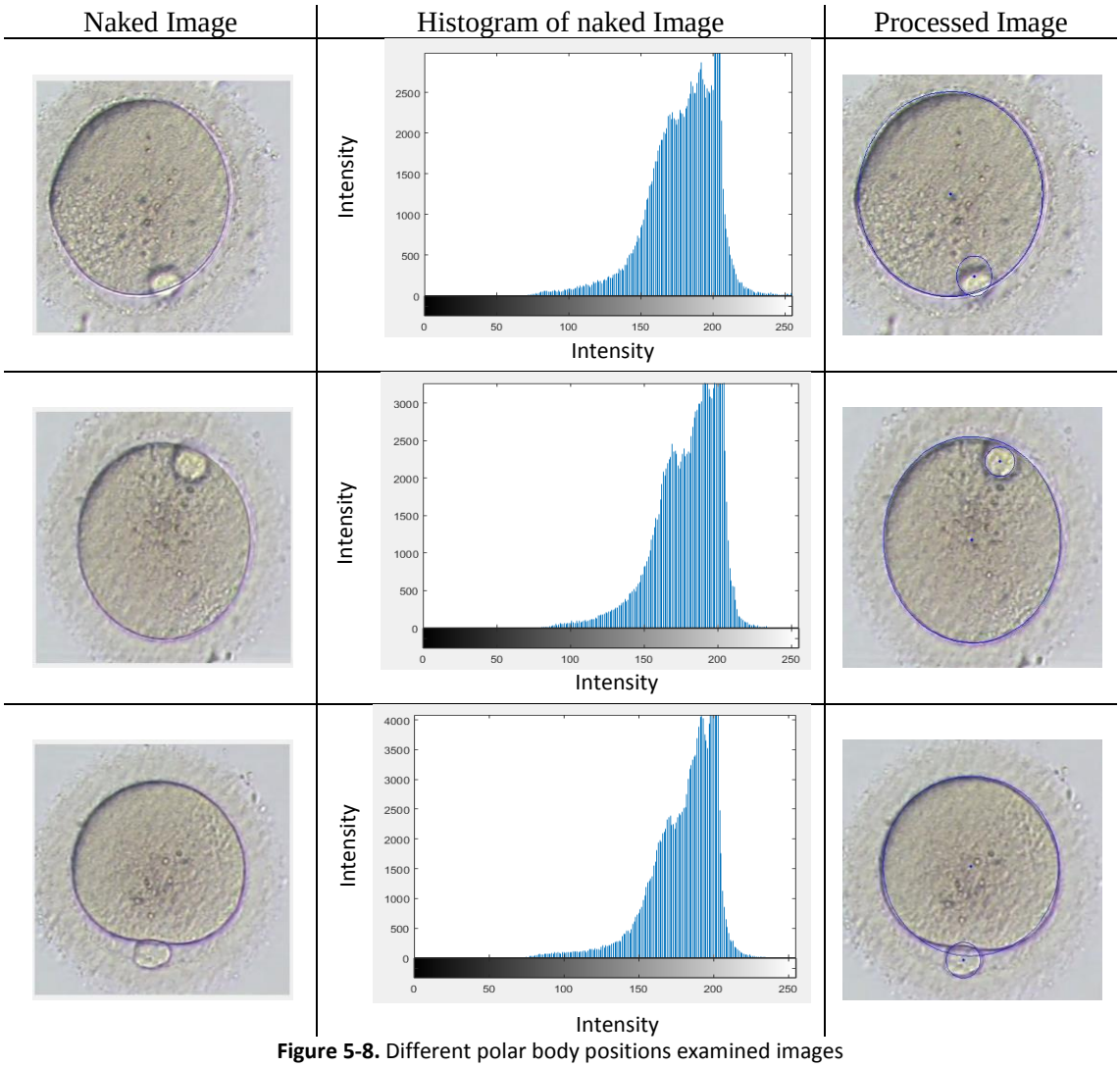

Figure 5-8. Different polar body positions examined images

Validation with ImageJ software confirms accuracy of the oocyte and polar body diameter and centre point measurements, as shown in Figure 5-9. The figure illustrates that the majority of the differences for the oocyte diameter and positioning are less than 10 µm, and for polar body are approximately 2µm. These are very satisfactory results for 100% correct detection containing less than 5% error in reporting the measurement.

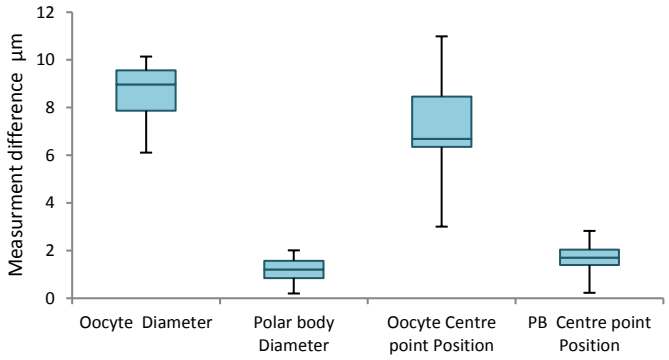

Figure 5-9. Whisker chart demonstrating differences in measurements in different polar body positions

5.4.3 **Different zoom and intensity of the images**

After random deposition of an oocyte under the focal zoom of microscope, there is a possibility of changing the zooms to find the best zoom for the visualization. Consequently, the proposed algorithm has the option of detecting the oocyte position under different zooms. Examples are given in figure 5-10.

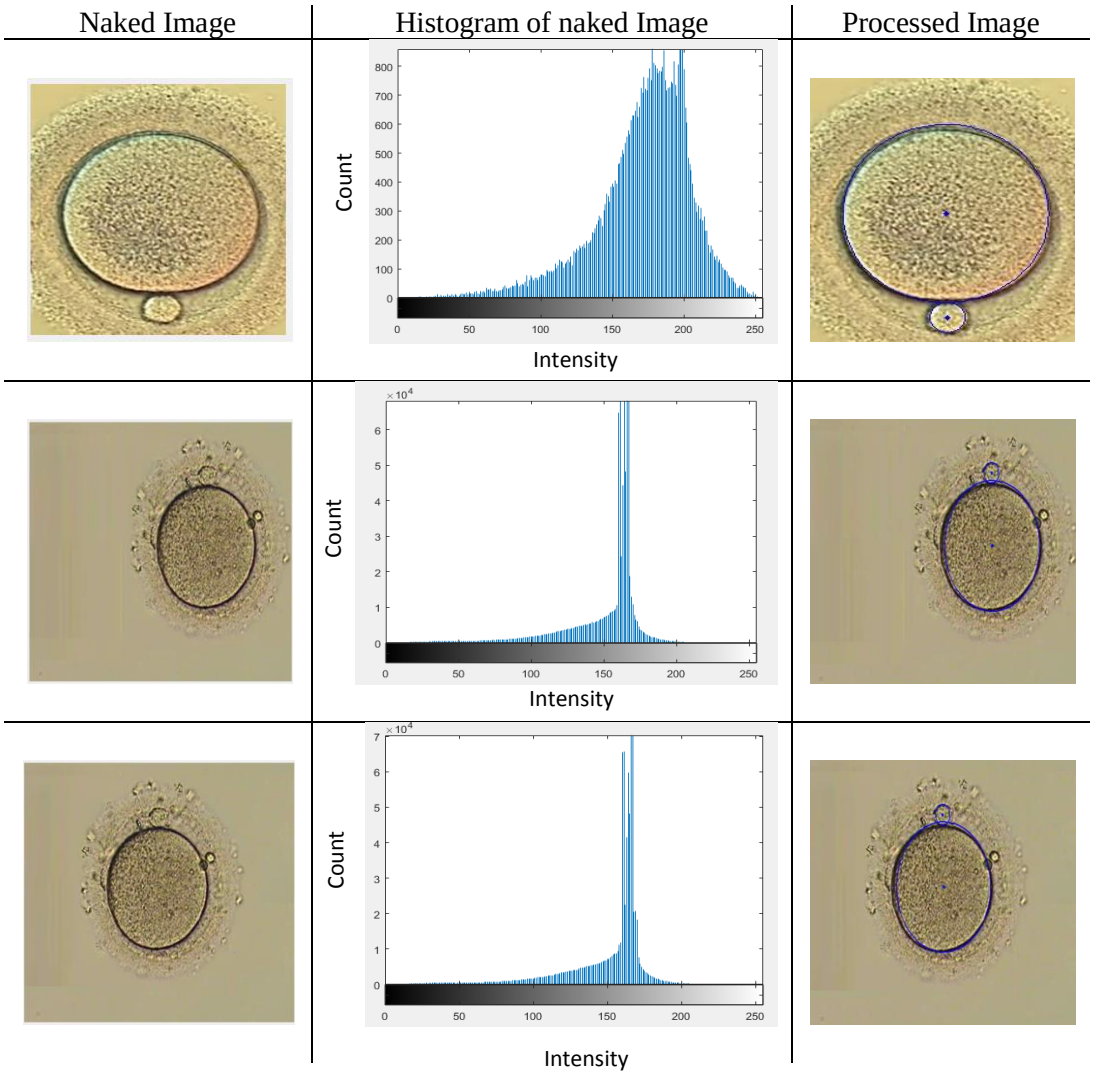

Figure 5-10. Different magnifications examined images

The effect of different magnifications used by the microscope was another important factor that needed to be considered. In smaller magnifications the histograms show less contrast and less clarity of the oocyte, although the developed algorithm successfully fully detected the polar body and oocyte and the majority of the measurements are even less than 5% for oocyte and almost 10% for the polar body. The error for the polar body may be caused by smaller size in lower magnifications and also caused by human error in manual measurements.

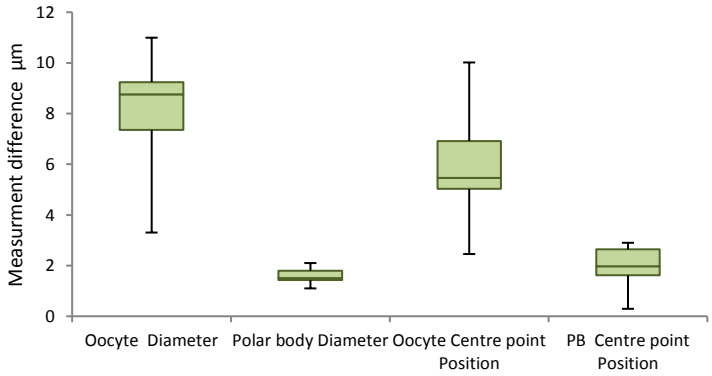

Figure 5-11. Whisker chart demonstrating differences in measurements in different magnifications

5.4.4 **Image disturbance**

Oocyte should be positioned in the focal zone of the microscope without the presence of any cumulus. Oocyte denudation is the initial step after oocyte retrieval from the patient. If this denudation is not applied properly, the existing cumulus adversely affect the quality of the image and also that of the detection. This could be considered as a disturbance. In the proposed algorithm the detection success rate for the images that include cumulus is approximately 60%. Figure 5-12 demonstrates examples of such disturbance causing false detection.

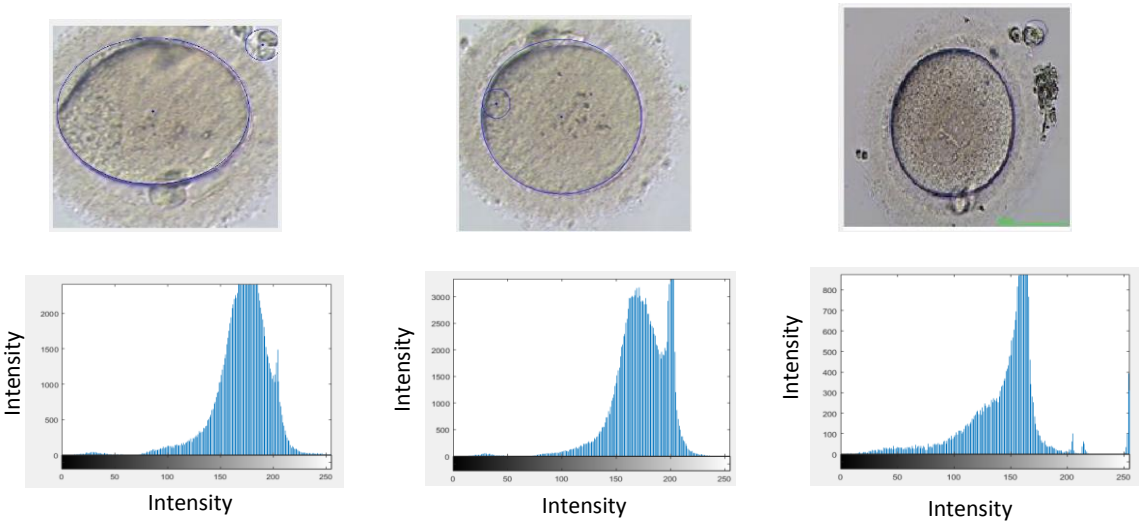

Figure 5-12. Different examined images including disturbance

Computational time is another important factor for developing this kind of software. The computational time is highly dependent on the quality and size of the image based on the pixels. After 80 experiments, the following graph was obtained showing the computational time. Figure 5-13 shows the graph of computational time with respect to the average size of the images. As it is indicated in the graph, the computational time for the images with the average amount of 900 pixels is 1±0.2 seconds. For the majority of the acceptable quality images, the computational time is 0.8 seconds, although if the number of pixels increases to more than 1000, the computational time suddenly significantly increases. This is a very acceptable computational time in comparison to similar image development software which takes 12 seconds.

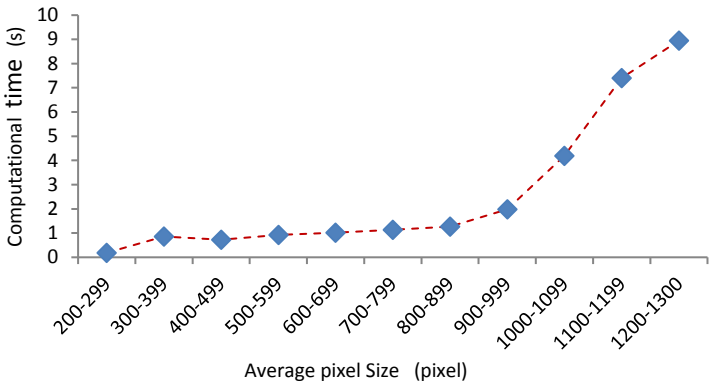

Figure 5-13. Computational time of the images based on the size of images

The data obtained from the software have been compared with the manual measurements using ImageJ. In ImageJ, the pixel size is calibrated with a reference in the image and then the measuring takes place. The differences between the manual measurement and the software measurement are indicated in Figure 5-14 for both oocyte

and polar body diameter and position measurements. In this algorithm, the maximum reported error on measuring the oocyte and polar body diameters in the detection section is slightly higher than 8 µm (~ 5% error) and less than 2 µm (~ 8%) respectively. This indicates the considerable accuracy in dimension detection. On the other hand, this figure describes a high precision in centre point detection which assists in positioning the samples after detection. Additionally, the reported errors in three considered factors are virtually similar, which indicates the independency of the algorithm from factors mentioned in Table 5-1.

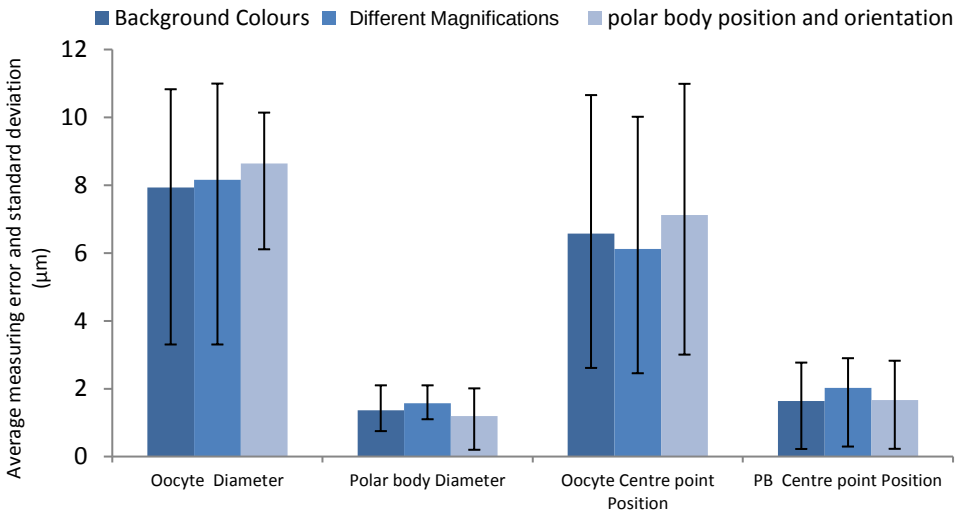

Figure 5-14 the measurement errors of the affecting factors

5.5 ***Conclusion***

In this chapter a vision detection software has been developed for detecting the polar body and oocyte position and orientation, as well as measuring their sizes. This software is designed to be integrated to the micromanipulation system which designed for automated manipulation of the metaphase II oocyte.

The developed software is well-matched with various inverted microscopes with a range of imaging factors. This is the first report of utilising the gradient weighted Hough transform in the application of ICSI which also included elliptical fitting. This software is able to detect the polar body and oocyte under different magnifications as well as with different background colours. The obtained results show a rate of 100% in detecting the oocyte and polar body. For polar body it drops to 60% in existing disturbances which is caused by disruption in the area of the image and also morphological problems of the polar bodies. In terms of measurement, there was a 6% and a 9% error in the oocyte and polar body diameter measurements. In addition, there was less than 10 μm and a 2μm error in the oocyte and polar body position measurements. The computational time decreased considerably, compared with similar software, to 1±0.2 seconds which enables the robotic systems to operate in a shorter time domain and be closer to a real time application.

CHAPTER 6

A PROPOSED AUTOMATIC 3D CELL MANIPULATION SYSTEM

6.1 *Introduction*

This chapter covers the design and control of a 3D automatic cell manipulation and cell injection integrated system. The design of manipulators for moving the oocyte through an optimum number of actions will be discussed. Additionally, it is proposed that the fully automated injection system will deliver a single sperm into an oocyte. Inverse kinematics, vibration analysis and dynamics are the main analysis tools for the design of the manipulators. In addition, the maximum work volume in the small workspace of the microscope will be considered. After discussing the design, the control methods and how the manipulators operate in real time will be analysed in the second part of this chapter.

Current ICSI operation has a number of drawbacks which cause damage such as oocyte degeneration to the cell during manipulation and injection. These are not only due to the existing injection technology, but are also dependent on the embryologist's skill. The reason for oocyte degeneration is still unclear but is speculated that the main cause of the problem is related to the mechanical injection procedure. During this, the micro needle induces damage to the zona pellucida (external membrane) by producing deformities within the structure.

Additionally, there is no agreed protocol for cell manipulation and injection. The overall procedure is expensive and the pre/post treatments are an unpleasant experience to the patients, where many time-consuming trials may be needed before a successful operation leads to fertilisation.

The operations involved during manipulation and injection of an oocyte are greatly responsible for the relatively low ICSI success rate. There is, therefore, a compelling case to increase the success rate of the ICSI operation, hence significantly reducing the treatment cost and time, while improving the patient's experience.

The problem pertains to the method of automating manipulation of an oocyte and injection of a single sperm into it during the ICSI operation through the minimisation of the mechanical damage caused by the manipulation of cell. Consequently, human errors would be decreased considerably, while speed of operation (as an important factor on successful outcome) is optimised.

The current microinjection procedure is manual (through a mechanised system) and the tracking is purely through visual observation using images from a microscope. This method has no injection force-feedback to give the embryologist (operator) a sensory feel for the injection and hence allowing sufficient control over the process. This effectively means that the operator has no information while performing the injection other than 2D visual feedback which leads to a great deal of human error during the process, particularly during the oocyte-needle interaction.

Currently, cell manipulation is achieved using the manual joysticks which control the micropipette. The manipulations take place using physical pushing of the oocyte until it is positioned at the desired location and orientation. The drawbacks include:

- frequent physical interference/impact with the oocyte;
- blind injection - lack of sensation during injection;
- high operational time;
- lack of control during injection and manipulation which cause damages to cell; and
- no awareness of accurate positional and orientational deployment of sperm into oocyte.

The designed system is capable of manipulating an oocyte from any random orientation to a final orientation ready for injection of a single sperm. The system has a 7 degree-of freedom (DoF) manipulator which delivers the oocyte such that its polar body is delivered the desired position and orientation with a minimum number of operations. In addition, the proposed system is fully automated for the entire process of the manipulation. The manipulation and injection of the oocyte is designed to be from the same side to allow for a compact design and utilisation of the same micro stage, hence saving cost and space.

The system has the capability of minimising mechanical damages to oocyte due to injection. This is achieved by calculating the optimum injection speed through its injection force feedback system, and accurately identifying the exact location within the oocyte for sperm delivery. A vision recognition algorithm has been developed to detect

the oocyte and its associated polar body such that their accurate positional information can be used by the manipulator arms to determine the optimum manipulation trajectory.

This is the first reporting of a fully automated and integrated manipulation and injection system that is capable of minimising mechanical damage to the oocyte, hence increasing the success rate. The system has the potential capability of simultaneous injection of sperms into multiple oocytes.

The main features and advantages of the proposed system are as follows:

- Greater success rates of the ICSI process due to minimised mechanical damage due to oocyte deformation.
- Elimination of human error through the introduction of fully automated system leading to increased consistency in the process.
- Measurable environment due to feedback given via sensors throughout the process.
- Capability for simultaneous injection of multiple oocytes, therefore reduced costs.
- Cell manipulation with a minimum number of operations (contact touch limitation during manipulation).
- Capability of high speed processes of detection, manipulation and injection.
- Simplification of the process to allow for less skilled operators to be employed reducing the need for the presence of embryologist.
- Fully controlled injection procedure to avoid delivery of toxic material within the cell.
- Fully adoptable to the consumables used in current practice and available in the market.

- Adaptable to all microscopes and other vision systems within ICSI laboratories.

8.2 *System architecture*

The proposed system is totally different to existing conventional ICSI systems in the market. The initial step is cell manipulation and then injection takes place after the oocyte delivery to a stationary holder.

The proposed system consists of four main sections which work in collaboration An in-house designed novel two-armed robotic manipulator is assembled on a three-dimensional micro controlled stage system (8MT167 motorised stages, Standa Ltd.) to manipulate a single oocyte and deliver it to re-position the cell in the stationary holder in the correct orientation through a minimum number of oocyte interactions and trajectories. The other section is an in-house designed integrated automated injector which conducts the injection through optimum approaches. The advantage of this system is operation of the manipulation and the injection in one unit which makes the system compact. The manipulator is attached to a controller which is controlled by in-house designed an integrated vision recognition algorithm for real-time visual servoing which detects the polar body and oocyte position and orientation and provides the initial coordinates to the controller. The manipulator delivers the oocyte after manipulation to a stationary holder (RI manual manipulator). The proposed system is fully adoptable to the consumables used in current practice and available in the market.

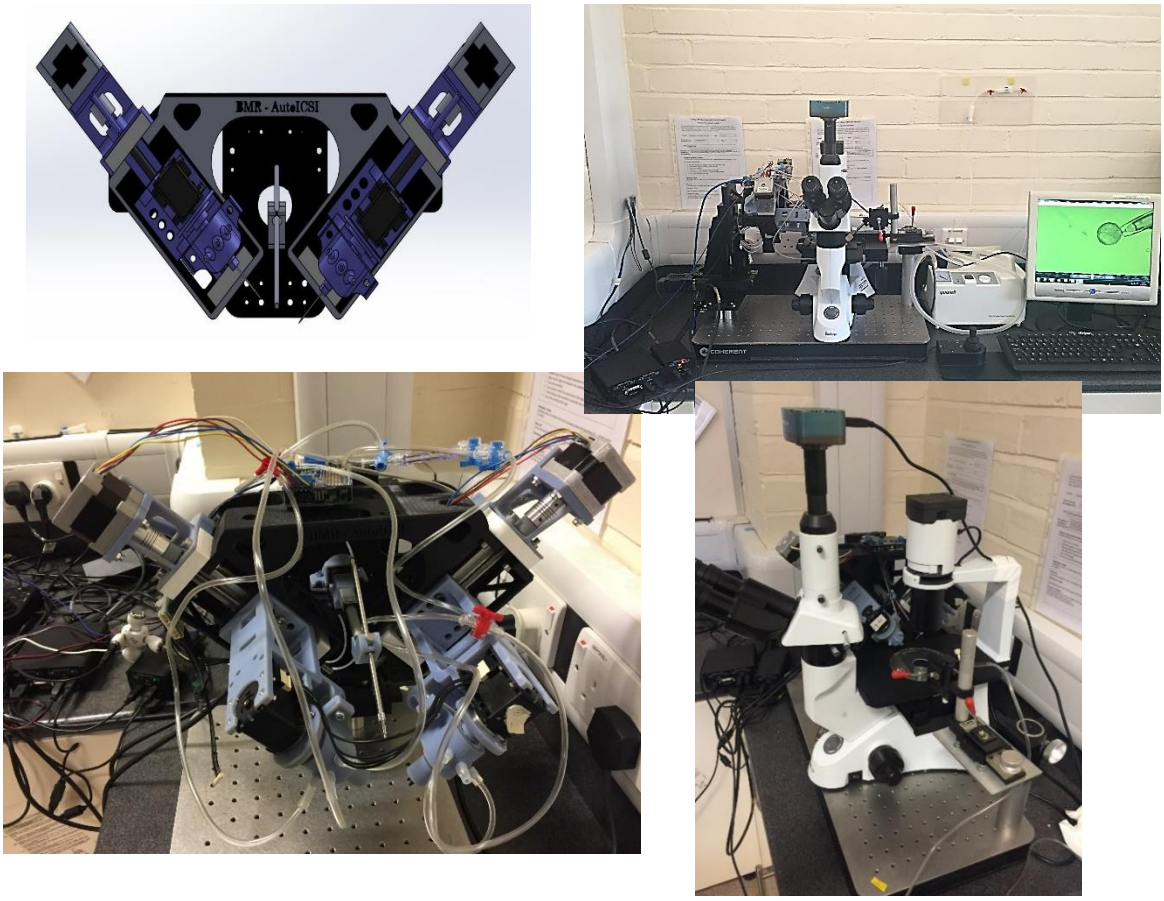

Figure 6-1. Views of the proposed Auto ICSI system: (Top right) - Schematic diagram of the system, (top left) – manipulation and injection system view, (Bottom left) - the manipulator system, (Bottom right) - the manipulator system integrated with an inverted microscope

6.2.1 **Manipulator Architecture**

The manipulator contains two identical arms. It operates on two modes of coarse and fine movement. To provide linear movement in coarse motion, a hybrid stepper motor (RVFM MY5602 Mini Hybrid Stepper Motor Size 14) is employed on the arm which is connected to a lead screw with 1 mm pitch. The main advantage of using the stepper motor is to eliminate the necessity of having an encoder, as it can be controlled in an open-loop manner by controlling the steps, as there is a chance of missing a step. The proposed and selected stepper motor is highly accurate and has low noise and low inertia. The step angle of this stepper motor is 1.8 degree/step with the holding torque of 8 N-cm.

This stepper motor is connected to the linear lead screw fastened by a coupler. A single small-sized platform has been assembled on the lead screw on top of a metallic guide to avoid any disorientation. The platform moves forward and backward by rotation of the lead screw. The lead-screw can bend 0.5 mm over 1 m.

As already mentioned, each step of the stepper motor is rotating 1.8 degrees of a circle which defines the whole circle as taking 200 steps. A micro-stepping driver can be employed in conjunction with the stepper controller in case a smaller angle is required. However, there is no need for micro stepping as that may add errors to the system which is not acceptable. As the pitch for the lead-screw is 1 mm, then each step will operate with the movement of 5μm transitionally calculated in Equation 6.1. Consequently, each step would provide a linear movement of 5μm. This is a big value for a micromanipulation operation. Therefore, the arm motion is employed for coarse motions. Fine motions are covered by the motorised stage, which has the accuracy of 1 μm and the whole manipulator is assembled on it.

$$whole\ revolution = 360\ degrees = 200\ steps = 1\ mm\ \rightarrow$$

$$single\ step = \frac{1}{200}\ mm = 5\mu m \tag{6.1}$$

The rotational movement of the cell is provided by a servo motor (Dynamixel MX-28R Robot Actuator) on each arm. Each cell is held by negative pressure with a commercial micro-holder. This holder is connected to the servo motor through a suction chamber for the purpose of rotational manipulation. The micro-holder is inserted into a hollow shaft through an adaptor made of rubber where the shaft is placed in a vacuum chamber to prevent any leakage of air. This is significant as any air loss will cause a reduction in the negative pressure and end with the loss of the cell. Thus, the vacuum area

is absolutely sealed to waive this problem. The vacuum is created in the chamber by using three suction pipes attached to the top of the chamber which is connected to the controllable dynamic suction pump. The shaft is then connected to the servo motor on the other end. This has the responsibility of providing the rotational movement of the micro-holder ±180 degrees. The vacuum chamber is assembled on the platform which is built on the lead screw with a guide which moves based on the rotation of the lead screw.

The system is designed based on clinical health and safety and ethics. Consequently, for each patient a single micro holder should be used and after the operation, the used micro-holder should be replaced with a new one. This is essential for the prevention of contamination between patients. As a result, the method of assembly and disassembly of these micro-holders should be easy for the operator.

6.2.2 **Injector Architecture**

The injector is designed on the same manipulator's case. This design enables cell injection from the same side as conducted cell manipulation. The injector is developed to operate in two modes, coarse and fine movement. The coarse movement provides a sudden expansion of an actuator (Actuonix L05 Micro Linear Actuator) after manipulation is conducted. The actuator is secured safely on the stage and the Injection Holder (for Pneumatic Injector, HI-9) is assembled on it. The fine movement of the injector is supported by the three-axis stage with the accuracy of 1um during the injection. The injection process uses the information received from the research which were conducted in Chapter 4.

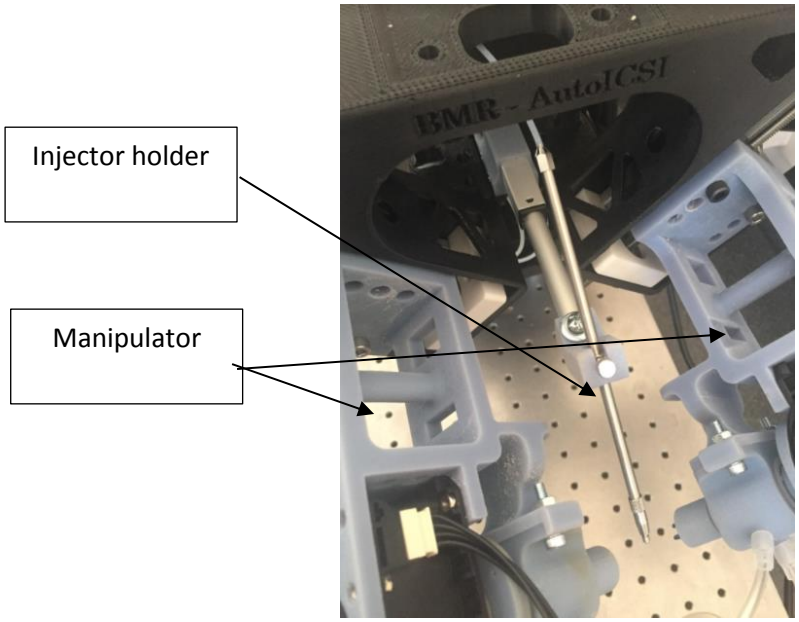

Figure 6-2 the injector assembled on the system

6.2.2 **Vision Architecture**

The detail of the vision algorithm is mentioned in Chapter 5. The vision algorithm is run in the master computer using Matlab software as the running platform where the microscope camera (Bestscope camera, BUC1B-320C) is connected. An initial photo shot is taken to identify the oocyte and polar body using the inverted microscope (BestScope BS-2090 Inverted Biological Microscope).

6.3 ***System functionality***

The proposed system is a compact design which provides manipulation and injection as one unit from one side. However, it sustains the conventional ICSI which is delivering the sperm inside an oocyte from the same side. The operation of the system is

fully automated after receiving the start order from operator. The system functionality is divided into four main steps, cell deposition, cell recognition, cell manipulation and delivery to stationary holder, and, finally, the cell injection. The sperm allocation for the injector is not covered in this thesis.

The AutoICSI operation starts when an oocyte is randomly deposited in the focal zone of microscope. It should be noted that the oocyte should be in metaphase II (which shows its maturity) and denuded from the excess cumulus prior this step. Then the automated cell recognition begins. Polar body position and orientation are recognised and the locational information of the polar body and oocyte is provided to the controller of the manipulator. This is the initial operation which contributes significantly to the success of the manipulator. Then the system requests the final orientation information from the user. This process will take up to 2 seconds for detecting and calculating the positions of the centre points for the oocyte and polar body (detailed explanation is in Chapter 4). After receiving the initial information and finalising the calculation, one of the arms which is considered to have a better approach to the cell depending on the positional situation of the polar body starts the grasping approach.

The two arms of the manipulator are perpendicular to each other as it is demonstrated in Figure 6-4. Consequently, each arm covers two rotational degrees of freedom which leads to final 3D manipulations. The system is designed to manipulate with two minimum operations if the polar body is detected correctly and a maximum of four, if not. Incorrect polarbody detection is caused by confusion in the polar body orientation which may be on either the top or bottom of the cell's hemisphere. This is because of transparency of the cell and using inverted vision system.

After 2D manipulation of the first arm, the cell is delivered to the second arm for final manipulation. This will cover another two dimensions which are perpendicular to the initial ones. For the approach trajectory, it is essential to detect the correct position of polar body. There are three possibilities for the polar body's position under the focal zone of the microscope, which are as follows:

- Polar body is visible and detected correctly by the software;
- Polar body is not visible;
- Polar body is detected wrongly.

In each of the above conditions, a specific operation is defined for the system. If the polar body is visible and detected correctly, then the standard procedure takes place and the main operation starts. If the polar body is not visible, then one of the manipulators manipulates the oocytes 90 degrees and examines the new position and orientation by taking an image again. This procedure repeats until the polar body is brought into the vision field of the microscope. Once it is detected, the main operation starts. For the last stage of polar body detection, the user needs to confirm if the system has detected the polar body correctly. If the polar body is detected incorrectly and the user does not verify the detection, the software repeats the examinations and selects the alternative potential features which could be considered if the polar body does not exist in the image. The main operation starts once a polar body is detected.

After finalising the manipulation steps of the oocyte, the cell is delivered to the host stationary holder which is defined for the system as the final point and the injection procedure starts. The injection is based on the optimum speed found in Chapter 5. Once the manipulation is concluded, the arms are returned to the home position and then the

injector deck expands to conduct the injection. It is essential to identify the final location of the sperm delivery which can be selected by the user. Sperm deposition plays an important role in the success rate of the ICSI. Once this is selected, the system delivers to the aimed location with minimum damage to the cell using optimum factors. Additionally, the delivery system controls the deposition to avoid any extra PVP (toxic material to the oocyte which is used to slow down the sperm motion) inserted into the cell.

The cell is released to be moved to an incubator after conducting the injection. The proposed system provides the injection with conditions of 100% humidity and temperature control of 37 °C.

6.4 *System operational analysis*

The main analysis of the operation was focused on developing the optimum number of essential operations to manipulate a single oocyte and deliver it to the desired place. As was indicated in the system's architecture section, the two manipulators are designed to be perpendicular to each other. Consequently, the developed system is based on two main coordinates which are global and local coordinates. The origin of the system for global coordinates is defined as the centre of the image. The observed two dimensional information is provided to the system to operate the approach trajectory for grasping considering final point. All the calculations are based on the global coordinates.

Each oocyte usually has a circular shape when viewed under the microscope. In some exceptional circumstances, the oocyte can be slightly deformed and have an elliptical shape. In this research and for manipulation purposes, it is assumed that the

oocyte is perfectly spherical and a perfect circle in the images; although the vision system is capable of detecting an elliptical cell. In the case of an exceptional condition, then the mean of the diameters of the elliptical shape is considered as the diameter of the circle.

The manipulation calculation is about the centre point of the oocyte with respect to global coordinates and the polarbody with respect to local coordinates. The polarbody centre is located on the perimeter of a sphere. Consequently, the polarbody centre point coordinate needs to be calculated in volumetric dimensions from the information received from the image analysis software. Point P in Figure 6-3 illustrates the polarbody centre point in 3D and point Q exhibited defines the projection of the polar body centre in two dimensions, which is in the view field of the microscope; θ specifies the angle of QO (which is the line from the coordinate centre to the point Q) with respect to X axis and φ shows the vertical angle of OP (which is the line from the coordinate centre to the point P) with respect to Z axis. These angles are essential to understand the exact coordinates of the point P in volumetric dimensions. The information of this point in two-dimensions is received from image software.

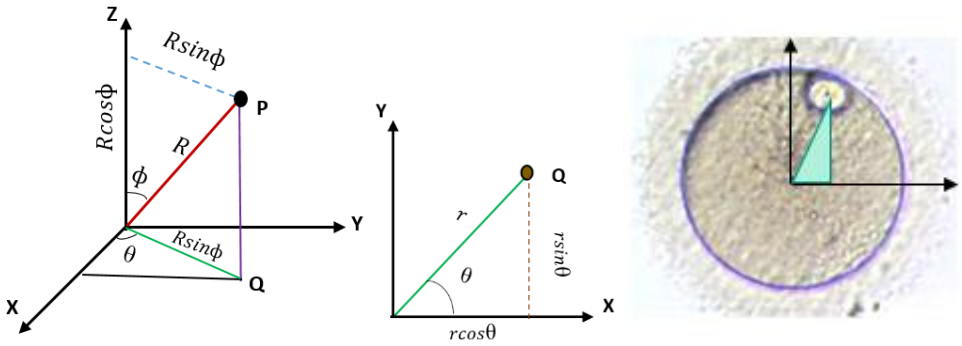

Figure 6-3. The schematic view of the location for polar body centre point in two dimensional and three dimensional coordinates

The Θ and r are calculated based on the image post processing. This process provides information about the polar body's centre on the XY plane and in the focal zone of the microscope. The dimension to be found is (ρ, Θ, ϕ). Thus ϕ is the only - unknown value left and it can be indicated as the following:

$$r = Rsin\phi \tag{6.2a}$$

$$\phi = Arcsin(\frac{r}{R}) \tag{6.2b}$$

$$x=R\sin\phi\cos\theta\ ,\quad y=R\sin\phi\sin\theta\ ,\quad Z=R\cos\phi \tag{6.2c}$$

Therefore (X, Y, Z) is the initial centre coordinate of the polar body with respect to the centre of the oocyte in volumetric coordinates. This coordinate will help in understanding the initial position of the polar body and oocyte.

As the images were recorded using an inverted microscope, the light passes through the transparent cell. Consequently, the polarbody may be located either on the top hemisphere of the cell or on the bottom one. The initial hypothesis for the polarbody positional coordinate is placed on the top hemisphere. As a result, the system assesses the initial hypothesis after the first operation.

The manipulation operates with the purpose of positioning the polar body in the desired location. Each oocyte would be manipulated by two pipettes separately. Each micro-holder rotates around its central axis while it holds the oocyte as illustrated in Figure 6-4. In terms of making the problem more understandable, we rotate the real system 45 degrees as can be seen in Figure 6-4. Each circle locates on a plane perpendicular to the manipulator with an appropriate known distance.

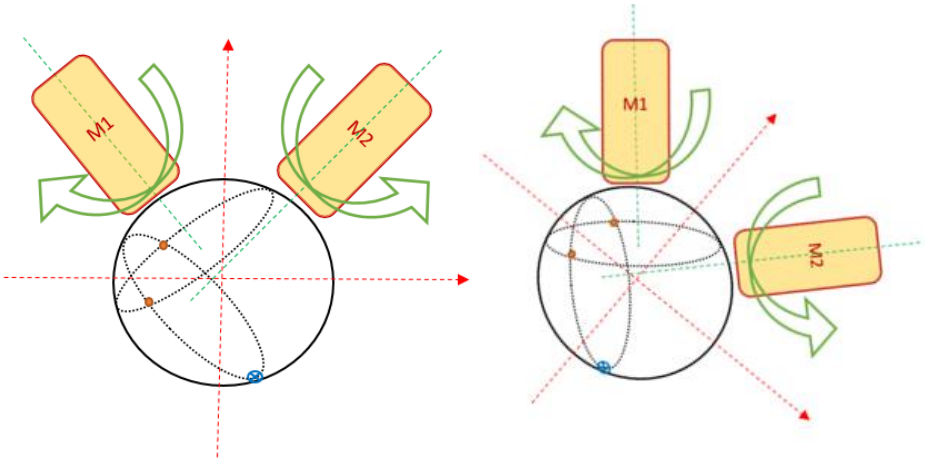

Figure 6-4. Schematic sketch of the manipulator configurations

Each manipulator's operation provides rotational motion for the cell. The centre of the polar body rotates on an imaginary circle circumference on each manipulating operation. This circle is the result of the intersection of a plane passing through this circle and the oocyte (sphere). So there will be two circles created perpendicular to each other based on the manipulation. The PB centre will move on these two circles. These two circles have intersections with three possibilities which are as follows and shown in Figure 6-5:

- Two intersection points;
- One intersection point;
- No intersection point

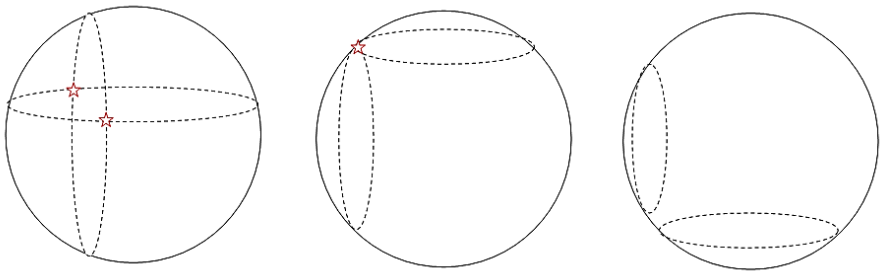

Figure 6-5. Schematic view of circles interactions a. two interaction, b. one interaction, and c. no interaction

The following equations are developed to understand the condition of these two imaginary circles with respect to each other. (X_i, Y_i, Z_i) is calculated and considered as the initial point. (X_f, Y_f, Z_f) is requested from the operator to define the final location of the polar body. As a result, two imaginary circles can be created as follows:

$$X_1{}^2 + Y_1{}^2 = (OQ)^2 = r'^2 \tag{6.3a}$$

$$X_2{}^2 + Z_2{}^2 = r"^2 \tag{6.3b}$$

The centres of the imaginary circles are located in the centre line where it passes through the manipulator. Consequently, (0, 0) is considered to be the circle centre. The distance between the planes where the circle is located to the centre of the oocyte is found from Equation 6.4.

$$R^2 = d^2 + r'^2 \qquad \rightarrow\ d^2 = R^2 - r'^2 \tag{6.4a}$$

$$R^2 = d^2 + r"^2 \qquad \rightarrow\ d^2 = R^2 - r"^2 \tag{6.4b}$$

The initial and final points are applicable in equation 6.5a and equation 6.5b respectively. So r and r' are obtained by the substitution of the initial and final coordinates into the equations. Y is the common point in both circles. So:

$$X_1{}^2 = r'^2 - Y_1{}^2 \tag{6.5b}$$

$$Z_2{}^2 = r"^2 - Y_2{}^2 \tag{6.5b}$$

where Y_1 and Y_2 is equivalent. By substituting the Equation 6.6 into the perimeter equation of the sphere which is applicable for all the points. (X0, Y0, Z0) is (0, 0, 0) which is the centre of the image.

$$(X - X_0)^2 + (Y - Y_0)^2 + (Z - Z_0)^2 = R^2 \tag{6.6}$$

Then Y is obtained as in equation 6.7 which assesses the existing interaction between circles:

$$Y = \sqrt{r'^2 + r"^2 - R^2} \qquad \begin{Bmatrix} Y > 0 \; there\; is\; two\; intersection\; point \\ Y = 0 \; there\; is\; only\; one\; intersection\; point \\ Y < 0 \; there\; is\; no\; intersection\; point \end{Bmatrix} \tag{6.7}$$

where r, r', and R are the first imaginary circle, second imaginary circle, and oocyte radius which a were obtained previously. The operation starts once the number of interactions becomes clear. For Y>0, the system selects one of these two points and develops the grasping approach and manipulation route by employing this point. This is similar case to the Y=0. However, if the Y<0, the manipulator rotates the oocyte for 45 degrees and system repeats the assessing route. The value of the rotational angle for each manipulator is calculated from the following equation:

$$\Delta\theta = \frac{\Delta S}{r_i} = \frac{2r_i}{r_i} sin^{-1}\left(\frac{d}{2r_i}\right) = 2sin^{-1}\left(\frac{d}{2r_i}\right) \tag{6.8}$$

where S is arc length, r is the circle radius and d is the straight-line distance between the two points. At the time of initial manipulation, operation of the first arm only adjusts the x' and y' coordinates and the Z coordinate remains unchanged. Once the operation of the first arm ends, the second arm operation starts and this manipulation adjusts the Y" and Z" while the X' remains unchanged. Accordingly, after terminating the operation, the centre point of polar body is (X', Y", Z") which is the required endpoint. Please note that this operation is defined only for the initial case which has two intersection points. For the other two, a course manipulation of a single arm is added and the calculation added to the computation of the centre point coordinates.

After the manipulating calculation, the system determines the grasping approach which is with respect to global coordinates.

If the cell is not perfectly circle and the manipulator wants to retrieve the oocyte, then the calculations indicate the error of:

$$R_{Circle} = \frac{A+B}{2},\ R_{Circle} - A = Error \tag{6.9}$$

where A and B are the elliptical dimeters. However, this error can be eliminated by grasping the oocyte using negative pressure (suction) through the pipette that can hold the cell. On the other hand, if the manipulator reaches the oocyte from point B, then it will push the oocyte a little, but that does not have a major effect as the push is not at high speed. The grasping data is defined to the manipulator by the following transformational matrix demonstrated in Equation 6.10.

$$\begin{bmatrix} \frac{u^2+(v^2+w^2)cos\theta}{u^2+v^2+w^2} & \frac{uv(1-cos\theta)-w\sqrt{u^2+v^2+w^2}sin\theta}{u^2+v^2+w^2} & \frac{uw(1-cos\theta)+v\sqrt{u^2+v^2+w^2}sin\theta}{u^2+v^2+w^2} & 0 \\ \frac{uv(1-cos\theta)+w\sqrt{u^2+v^2+w^2}sin\theta}{u^2+v^2+w^2} & \frac{v^2+(u^2+w^2)cos\theta}{u^2+v^2+w^2} & \frac{uw(1-cos\theta)-u\sqrt{u^2+v^2+w^2}sin\theta}{u^2+v^2+w^2} & 0 \\ \frac{uw(1-cos\theta)-v\sqrt{u^2+v^2+w^2}sin\theta}{u^2+v^2+w^2} & \frac{vw(1-cos\theta)+v\sqrt{u^2+v^2+w^2}sin\theta}{u^2+v^2+w^2} & \frac{w^2+(u^2+v^2)cos\theta}{u^2+v^2+w^2} & 0 \\ 0 & 0 & 0 & 1 \end{bmatrix}$$

(6.10)

This matrix indicates rotation of the point (x, y, z) about the vector ⟨u, v, w⟩ by the angle θ, where the vector is ⟨0, 1, 0⟩ and θ= ±45°. The outcome of this matrix would be a point indicating the position of the centre of the polar body with respect to the new rotated origin. Please note that the global origin does not transfer, it just rotates by 45 Counter Clock Wise (CCW) and Clock Wise (CW).

Once the manipulation has concluded, the cell is delivered to the stationary holder to initiate the injection procedure. After cell deposited to the stationary holder, the manipulators return back to home position and the injector expands and the injection operates. The expansion of the injector is done by the actuator; however, the final sperm deposition is conducted by the movement of the stage with the accuracy of 1µm. The injection is happening with the optimum speed obtained in Chapter 4.

6.5 ***Results and discussion***

This section focuses on the results of the system after the detection conduction. Before the operation starts, the final point is received from the operator to devise the essential number of operations and the angles of rotation. Table 6-1 indicate the calculation received from the software to find the rotational angle. The obtained figures from software after the experiments are compared to manual measurements using ImageJ software as shown in Figure 6-6.

Table 6-1 Inverse kinematic calculations received from system

Variable	Unit	Obtained results
r	µm	49.677
R	µm	67.786
θ	deg	67.066
ϕ	deg	47.12589
X	µm	19.35766
Y	µm	45.75025
Z	µm	46.1209

Obtained from vision recognition

Obtained from Equation 6.2 in this chapter

Calculated by the system as a part of manipulation calculation

Variable	Unit	Obtained results
r'	µm	49.677
r''	µm	67.786
d'	µm	46.1209
d''	µm	49.677

Obtained from Equation 6.3 in this chapter

Obtained from Equation 6.4 in this chapter

Intersection point		
Y	µm	49.677
X	µm	0
Z	µm	46.1209

Initial to Middle action point		
X_i	µm	19.35766
Y_i	µm	45.75025
X_m	µm	0
Y_m	µm	49.677
d	µm	19.75192
r	µm	49.677
rotation	rad	0.400274
	deg	**22.934**

Obtained from vision recognition

Calculated by system to obtained rotational angle for this arm is CCW

Calculated by system to find the intersection point

Middle to Final action point		
X_m	µm	0
Z_m	µm	46.1209
X_f	µm	67.786
Z_f	µm	0
d	µm	81.98829
r	µm	67.786
Rotation	rad	1.298925
	deg	**74.4229**

The end point requested from user

Calculated by system to obtain rotational angle for this arm which is CW

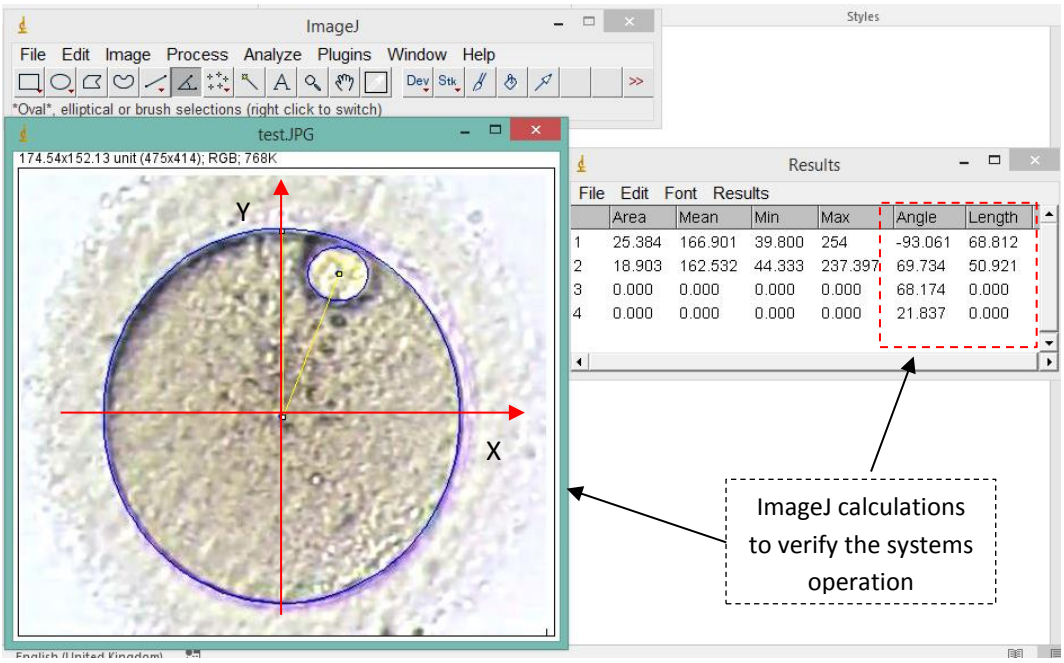

Figure 6-6. Manual Analysis of the manipulation calculation

Table 6-2 Comparison of obtained results between manual measurement and system reports

Variable	Unit	System Measurements	Manual Measurements	Variation
R	µm	67.786	68.812	1.026
r	µm	49.677	50.921	1.244
θ	deg	67.066	68.174	1.108
Rotation	deg	22.934	21.837	1.097

The system operation has been examined for repeatability, accuracy and resolution. Each manipulation arm has been separately tested on a rig to ensure the accuracy and repeatability as illustrated in Figure 6-7. The fixation method for the test rig is similar to the fixation on the case to avoid any environmental effect on the results.

Three different distances were examined with three different speeds selected for the motion of the manipulator as slow, medium and high. The results indicate the maximum error of 5% in resolution tests. Table 6-3 emphasizes the reliability as the errors are absolutely negligible.

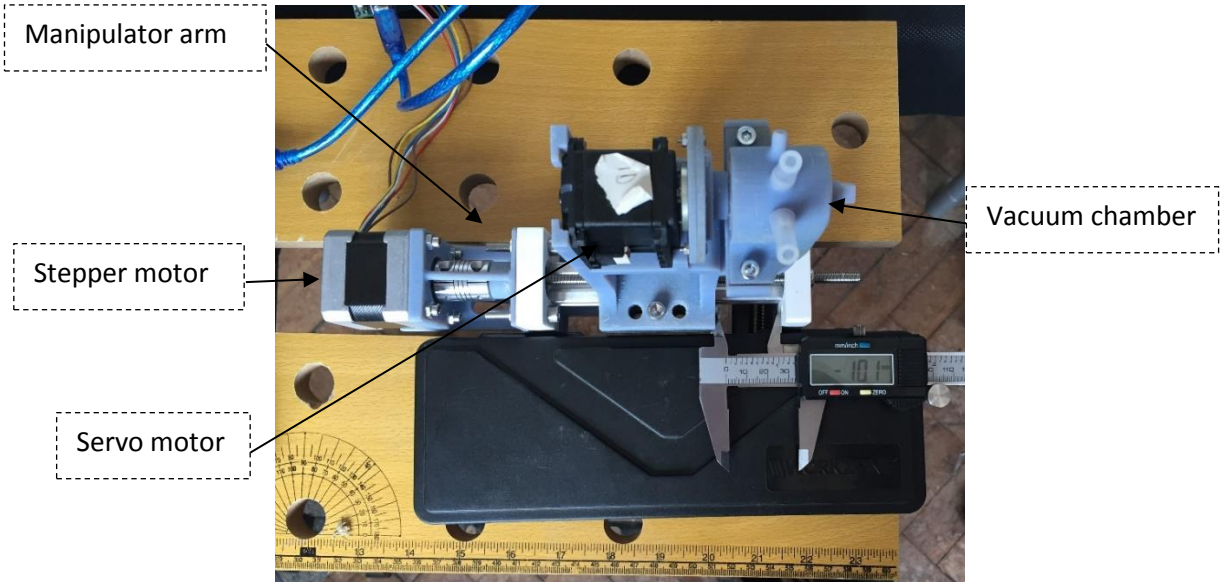

Figure 6-7. Demonstration of a single arm for coarse motion and test repeatability, accuracy and resolutions

Table 6-3 Resolution assessment of the system when it is ordered to move a certain displacement and the real movement is assessed by ImageJ

Speed	Theory	Average Experiment	Average Error
0.42	1	0.986	1%
	5.5	5.458	1%
	10	9.926	1%
0.75	1	0.974	3%
	5.5	5.454	1%
	10	9.988	0%
1.34	1	0.99	1%
	5.5	5.478	0%
	10	9.978	0%

The results indicate the satisfactory resolutions of the manipulator. It should be noted that the arm is designed to control the coarse motion and the fine motion is done by the stage with the resolution of 1um. The same tests are applied to examine the injector. Figure 6-8 indicates the graph of expected displacement of the manipulator based on the order and recorded displacement for various expected displacements and different speeds. The consistency of the manipulator between different speeds and different periods of operation (by examining various travel distance) prove a trusted manipulator for coarse motion. The obtained data indicates that a higher speed has a tiny effect on increasing the resolution of the system. However, the magnitude of the error for the low speed is still insignificant.

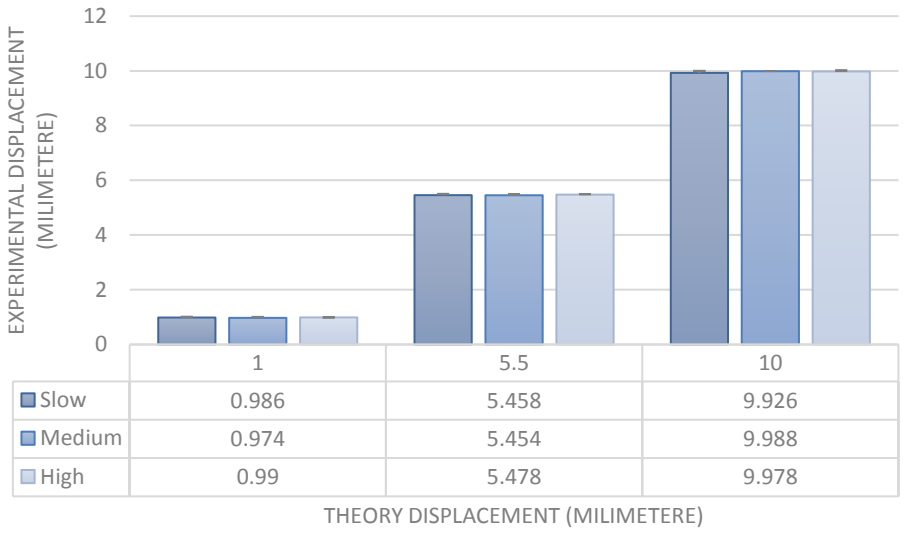

Figure 6-8. Comparison between theory and experimental displacement to analyse repeatability, accuracy and precision of the system

The repeatability test examines the error which may occur during repeating operations. Consequently, the manipulator was ordered to move forward and backward for 10 times and for a distance of ±15 mm and the variances of the initial and final location

of the stage were recorded. The results indicate differences of 0.01 mm, 0.2mm and 1 mm for initial and final points for low, medium and high-speed movement respectively after the movement of ten loops.

Figure 6-8 indicates the repeatability and accuracy and resolution test of the injection when it is requested to achieve the target aim. The target aim is defined as a location where the success rate is higher based on a reported research. Figure 6-9(c) indicates the current sperm deposition in practice. However, the allocated area which has the highest success rate is unapproachable using manual injection due to lack of sensation. The proposed system can deposit the sperm in the selected area by operator with the higher resolution in compare to the current proposed systems as in figure 6-9 C [138].

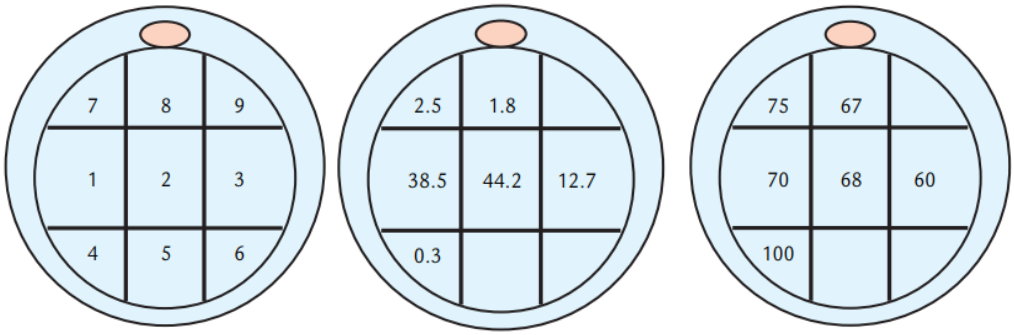

Figure 6-9. a. cell division for sperm deposition, b. deposition of the sperm by practitioners, and c. the fertilization success rate % [138]

The system validity tests of the injection section for the set up were conducted using microscope scaled micro-ruler and ImageJ analysis. For this experiment, a conventional injection pipette (MIC-SLM-35- Origio) assembled to a micropipette holder (HI-7, Narishige) and the microscope was focused on 20X zoom on the micro-ruler. The target point was defined for the stage. The approach is defined as a straight line, in two dimensional and three-dimensional forms. The operation is photographed and the results

are obtained from the images as exhibited in Figure 6-10 to demonstrate spatial resolution. The images are taken with the same size lens and combined using vision analysis software. The distance of displacement is measured by using the scale in the image.

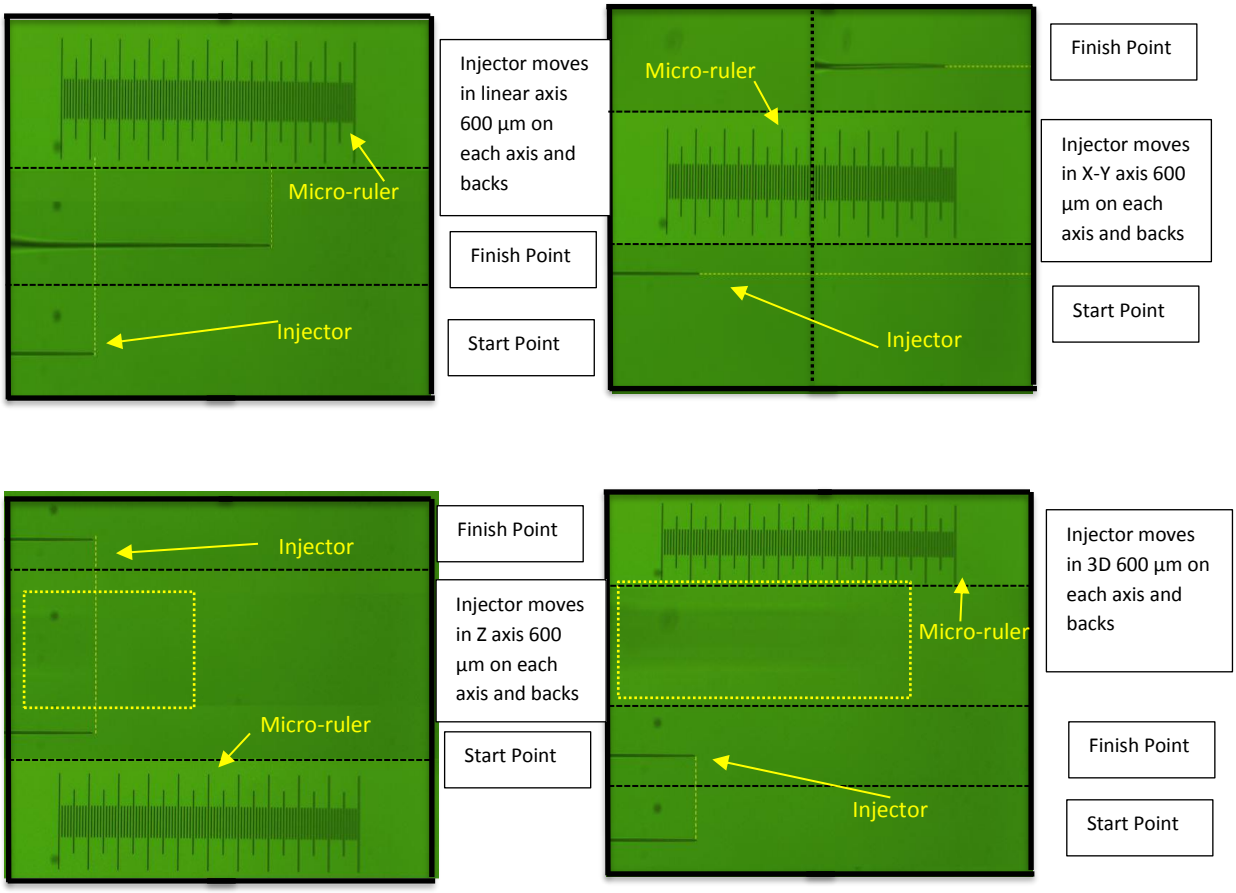

Figure 6-10. Accuracy, repeatability and precision tests of the system using injection micropipette, a. the linear motion assessment, b. 2D displacement assessment, c. z-axis displacement and return assessment, d. 3D displacement and return assessment

Table 6-4 Resolution assessment of the proposed system

Resolution (Aim 600µm)						
Category	Low Speed		Medium speed		High Speed	
	Value	Variation	Value	Variation	Value	Variation
Linear	602.32	2.32	602.59	2.59	601.22	1.22
Two-dimensional motion	601.78	1.78	602.12	2.12	600.56	0.56
Three-Dimensional motion	601.99	1.99	601.98	1.98	602.12	2.12

Analysing the accuracy and resolution of the manipulator is not visually possible due to the angle between manipulator arm and the horizontal stage. However, these already mentioned factors have been analysed for coarse motion. The fine motion is controlled with the same accuracy as mentioned for the injection pipette as the injector and manipulator are controlled with the same source in their fine operation. Table 6-4 indicates the average resolution of the system when it is aimed to achieve the 600µm in each axis assessing the variation of linear, two dimensional (which is X and Y) and three dimensional movements with three different speeds of low, medium and high which are 0.2 mm/s, 0.4 mm/s and 1 mm/s. The experiments were conducted 5 times on each variable and the figures obtained by vision analysis software. However, the maximum variation for the system is reported as 2.59µm in resolution which belongs to two-dimensional movement.

Table 6-5 Accuracy assessment of the proposed system

Accuracy (0-600µm)						
Category	Low Speed		Medium speed		High Speed	
	Value	Variation	Value	Variation	Value	Variation
Linear	598.65	1.35	601.25	1.25	602.33	2.33
Two-dimensional motion	602.01	2.01	603.20	3.20	603.99	3.99
Three-Dimensional motion	601.30	1.30	603.56	3.56	603.23	3.23

The system is operated in a planned order for a loop of 10 times to approach to 600µm and return to the home position to evaluate the repeatability of the system. Similar to the resolution, this assessment was conducted for linear, two-dimensional and three-dimensional evaluation of the repeatability employing three different speeds low, medium and fast. The visual results exhibited a high accuracy of the system after the loops and the software results report the maximum of 3.99µm variation in the final position.

Figure 6-11 and 6-12 indicates the repeatability of the system aiming for 600 µm. the majority of the results are accommodated between 598-602 µm. The path control for this experiment is Point-to-Point. Figure 6-12 confirms a good repeatability and good accuracy for the system.

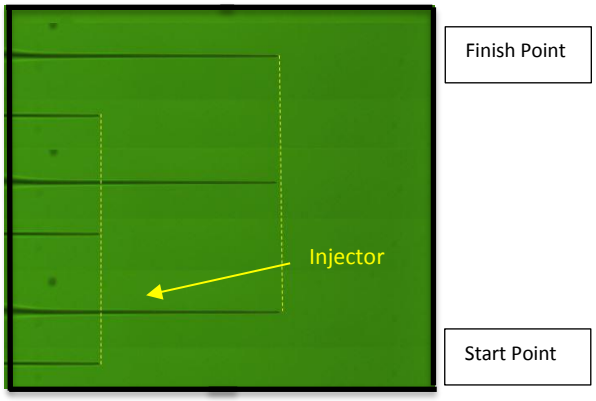

Figure 6-11. Three example of Repeatability assessment

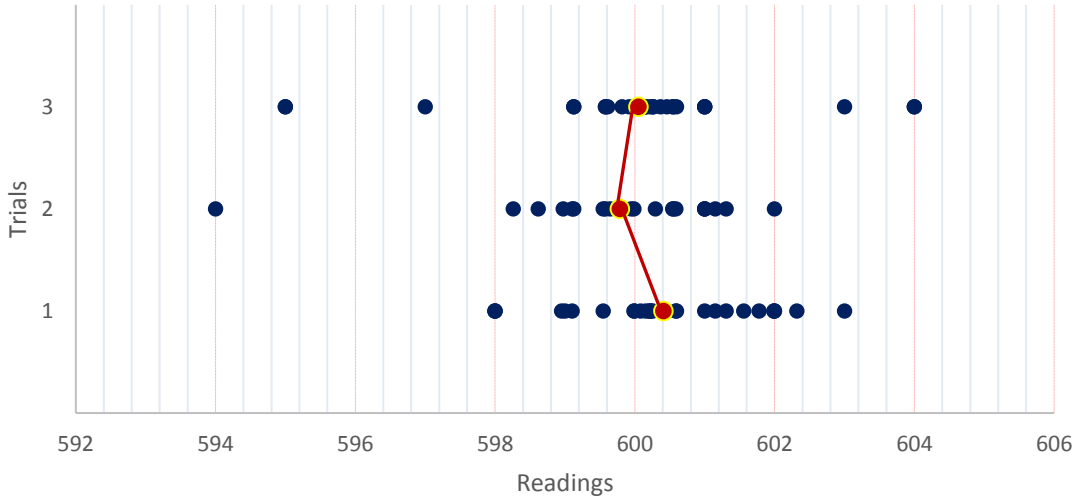

Figure 6-12. Repeatability test for three different speeds as 1) slow, 2) medium, and 3) fast aiming for 600 µm

The obtained results indicate the high accuracy, repeatability and resolution of the system in its fine motion as well as the coarse motion. However, the coarse motion is

intended to speed up the grasping approach. The total manipulation and injection operated with a high level of accuracy with a maximum error in repeatability of almost 4% for humans and less than 1% for Zebrafish, and resolution of 2 % and <1% for human oocyte (approximately 100µm in diameter) and zebrafish embryo (approximately 800µm in diameter) respectively.

8.8 *Conclusion*

This chapter focused on developing a seven degree-of-freedom micro manipulating set-up with the purpose of manipulating an oocyte in the application of ICSI. Currently, embryologists manipulate the oocyte manually to position the polar body in the desired position and orientation. The proposed manipulating system is configured with two main arms which are equipped with actuators and drive systems. The robotic manipulation arms are designed in-house and are perpendicular with respect to each other and 45 degrees to the horizontal. Both manipulator arms are identical and operate independently but collaboratively. The accuracy of the system is 1µm in translation and 0.5 degree for rotation.

This system operates using an in-house designed integrated vision recognition algorithm for real-time visual servoing which controls the novel two-armed robotic manipulator and an integrated automated injector, both in house-designed.

The designed system is capable of manipulating an oocyte from any random orientation to a final orientation ready for injection of a single sperm. The system has a 7 degree-of-freedom (DoF) manipulator which delivers the oocyte such that its polar body1 assumes the desired position and orientation with a minimum number of operations. In addition,

the proposed system is fully automated for all steps of the manipulation. The manipulation and injection of the oocyte is designed to be from the same side to allow for a compact design and utilisation of the same micro stage, hence saving cost and space.

The system has the capability of minimising mechanical damage to the oocyte due to injection. This is achieved by calculating the optimum injection speed through its injection force feedback system, and accurately identifying the exact location within the oocyte for sperm delivery. A vision recognition algorithm2 has been developed to detect the oocyte and its associated polar body such that their accurate positional information can be used by the manipulator arms to determine the optimum manipulation trajectory.

The operation of the system has been discussed in detail in this chapter. The system analysis indicates that it operates with high accuracy and high resolution.

CHAPTER 7

CONCLUSION AND FUTURE WORK

7.1 *Introduction*

An automated micromanipulation and microinjection system has been proposed in this thesis. This proposed system is a unique system that can operate for both manipulation and injection to the human oocyte for the application of an intra-cytoplasmic sperm injection to minimise the damages and errors occurring during the injection procedure.

Deformation creation on the oocyte at the injection time was the major deficiency of the current systems. In this thesis, deformation analysis was carried out and different methods proposed to minimise this deformation. Also different aspects considering the mechanical and dynamical factors were analysed.

The research aimed to minimise damages by developing a new automated set-up. The proposed set-up has 7 degrees of freedom and is able to operate fully automated. The manipulation happens based on the information received from sensors and vision analysis software; which have been created and developed for this specific application. The main objectives of this research are:

- analytical analysis of deformation creation;
- analysis of the effect of the injection speed on deformation creation (analytically and experimentally);
- design an FE model to analyse the speed of injection on force and deformation;
- develop vision detection software for detecting the oocyte and polar body's position and orientation;
- develop a conceptual design and analysis of the operation for an automated cell manipulation set-up for the application of ICSI.
- develop a prototype of the design and conduct elementary dynamical tests

7.2 *Developed methodology and main results*

This thesis proposed a new automated system for cell manipulating initially and then for injecting for the deployment of sperm into the desired location in an oocyte in ICSI. The main aim of proposing this set-up is to design a system that can minimise the damages applied to the oocyte. This system consists of two main manipulators which are able to manipulate a single cell. These manipulations proceed using the information received from visions software.

Thus, initially in this thesis, cell deformation at the injection time has been analysed in detail and a few methods proposed to minimise this deformation; such as angled injection and injection through suctions.

The speed of the injection is one of the most important factors affecting the creation of deformation, as a dynamic factor. So a series of experiments have been done on zebrafish embryos with seven different speeds and the injection force and deformation have been measured. It is concluded that a higher speed will result in less deformation; although vibrations at very high speed would cause damage to the cell during the injection. The penetration force of the injection related to the speed has been recorded. It is illustrated that a higher speed causes higher force, which in turn may cause higher stress to the membrane.

New software has been developed to recognise the polar body's and oocyte's position and orientation. This software is designed to be compatible with different sources of microscopes and can recognise the oocyte and polar body accurately. The data obtained from this software will feed the manipulation system for operation decisions and route planning for the manipulation of the oocyte.

Due to the limitation of access to samples for testing, and to different methods of injection as well as different factors of the injections that affects damages, for speed, an FE model was proposed and validated using experimental data. This software is highly accurate for predicting the deformation creation during the injection process.

Finally, a new proposed micromanipulator including a microinjecting system was designed by considering the factors which have been analysed through this thesis. The micromanipulator is designed to operate with the minimum number of operations to bring the polar body into the desired place. Then the injection procedure is carried out considering the injecting factors investigated here to minimise the deformation. The fabricated porotype of the design is tested dynamically.

7.3 *Contribution of this thesis*

This thesis focused on analysis of deformation as a main mechanical factor of the degeneration of the oocyte after a sperm injection in intra-cytoplasmic sperm injection application. Following the main aim of minimising this damage, a new proposed system has been developed. The research contributions are listed as follows:

- A conceptual design of a novel automated system to manipulate and inject the oocyte in ICSI;
- Cell deformation and cytoplasm emission analysis;
- Injection speed analysis for deformation creation to find the optimum injection speed; Five different speeds were analysed and concluded that 600 µm/s is the most appropriate injection speed as injection with this speed causes less damages in comparison with lower speeds and less vibration of the cells in compare to the higher speeds;
- A newly designed and developed vision software for recognising the oocyte and polar body; This proposed software is capable of detecting oocyte with a success rate of 100% and also detecting the polar body with success rate of 90%. This software is also able to recognise the position of the oocyte and polar body in three dimensional coordinate system;
- An FE model developed to analyse different speeds of the injection. This developed software, was used to analyse different speed of injection and was validated using the experimental results. The obtained results from FE was

reasonable based on the experimental results. This software eliminating the need of real experiment for speed analysis.

7.4 *Future directions*

The proposed system presented in this thesis has been reported for the first time. There is no similar system reported which is able to operate both an injection and manipulation in an integrated system. Consequently, it should be further developed and enhanced in a number of ways:

a) By expanding the analysis of the system dynamically and assessing the vibrations
b) By expanding the methods of injections and experimental validation.
c) With the integration of an automated sperm selection system (lab-on-a-chip device) to the proposed system.
d) By developing the FE model further to be applicable for other samples, like sheep oocytes.
e) By operating the same speed test for sheep oocytes and expanding the models related to it to compare with zebrafish embryos.
f) The system is now in prototyping stage. Dynamical modelling of the micropipette for vibrational analysis needs to be considered [139-140]. However this was out of the scope for this research but is essential for further development.

References

[1] J. Datta, M.J. Palmer, C. Tanton, L.J. Gibson, K.G. Jones, W. Macdowall, A. Glasier, P. Sonnenberg, N. Field, C.H. Mercer, A.M. Johnson, K. Wellings; Prevalence of infertility and help seeking among 15 000 women and men, Human Reproduction, Volume 31, Issue 9, 1 September 2016, Pages 2108–2118,

[2] Marcia C. Inhorn, Pasquale Patrizio; Infertility around the globe: new thinking on gender, reproductive technologies and global movements in the 21st century, Human Reproduction Update, Volume 21, Issue 4, 1 July 2015, Pages 411–426,

[3] Bungum, M., P. Humaidan, M. Spano, K. Jepson, L. Bungum, and Aleksander Giwercman. "The predictive value of sperm chromatin structure assay (SCSA) parameters for the outcome of intrauterine insemination, IVF and ICSI." *Human Reproduction* 19, no. 6 (2004): 1401-1408.

[4] Andersen, A. Nyboe, V. Goossens, L. Gianaroli, R. Felberbaum, J. De Mouzon, and K. G. Nygren. "Assisted reproductive technology in Europe, 2003. Results generated from European registers by ESHRE." Human Reproduction (2007).

[5] Fertility Treatments. (n.d.). Retrieved 11 06, 2016, from Newlife IVF: https://www.newlife-ivf.co.uk/fertility-treatments.php

[6] Hill, M.A. (2016) Embryology Oocyte Development. Retrieved November 5, 2016, From https://embryology.med.unsw.edu.au/embryology/index.php/Oocyte_Development

[7] Gerris, Jan MR. "Single embryo transfer and IVF/ICSI outcome: a balanced appraisal." *Human Reproduction Update* 11, no. 2 (2005): 105-121.

[8] Ladjal, Hamid, Jean-Luc Hanus, and Antoine Ferreira. "Microrobotic simulator for assisted biological cell injection." In *2011 IEEE/RSJ International Conference on Intelligent Robots and Systems*, pp. 1315-1320. IEEE, 2011.

[9] Ladjal, Hamid, Jean-Luc Hanus, and Antoine Ferreira. "Micro-to-nano biomechanical modeling for assisted biological cell injection." *IEEE Transactions on Biomedical Engineering* 60, no. 9 (2013): 2461-2471.

[10] Kastrop, P. M. M., S. M. Weima, R. J. Van Kooij, and E. R. Te Velde. "Comparison between intracytoplasmic sperm injection and in-vitro fertilization (IVF) with high insemination concentration after total fertilization failure in a previous IVF attempt." *Human Reproduction* 14, no. 1 (1999): 65-69.

[11] Ebner, Thomas, Cemil Yaman, Marianne Moser, Michael Sommergruber, Klaus Jesacher, and Gernot Tews. "A prospective study on oocyte survival rate after ICSI: influence of injection technique and morphological features." *Journal of assisted reproduction and genetics* 18, no. 12 (2001): 623-628.

[12] Dumoulin, John CM, Edith Coonen, Marijke Bras, J. Marij Bergers-Janssen, Rosie CM Ignoul-Vanvuchelen, Lucie CP van Wissen, Joep PM Geraedts, and Johannes LH Evers. "Embryo development and chromosomal anomalies after ICSI: effect of the injection procedure." *Human Reproduction* 16, no. 2 (2001): 306-312.

[13] Montag, Markus, Thomas Schimming, and Maria Köster. "Analysis of the Zona Pellucida as an Indicator of Oocyte Developmental Potential." In *Human Gametes and Preimplantation Embryos*, pp. 9-16. Springer New York, 2013.

[14] Agarwal, Ashok, Kartikeya Makker, and Rakesh Sharma. "Review article: clinical relevance of oxidative stress in male factor infertility: an update." *American Journal of Reproductive Immunology* 59, no. 1 (2008): 2-11.

[15] De Kretser, D. M. "Male infertility." *The lancet* 349, no. 9054 (1997): 787-790.

[16] Gordon, Jon W., and Beth E. Talansky. "Assisted fertilization by zona drilling: a mouse model for correction of oligospermia." *Journal of Experimental Zoology* 239, no. 3 (1986): 347-354.

[17] Bowen, Jennifer R., Frances L. Gibson, Garth I. Leslie, and Douglas M. Saunders. "Medical and developmental outcome at 1 year for children conceived by intracytoplasmic sperm injection." *The Lancet* 351, no. 9115 (1998): 1529-1534.

[18] Palermo, Gianpiero, Hubert Joris, Paul Devroey, and André C. Van Steirteghem. "Pregnancies after intracytoplasmic injection of single spermatozoon into an oocyte." The Lancet 340, no. 8810 (1992): 17-18.

[19] Van Steirteghem, André C., et al. "Higher success rate by intracytoplasmic sperm injection than by subzonal insemination. Report of a second series of 300 consecutive treatment cycles." Human Reproduction 8.7 (1993): 1055-1060.

[20] Gabrielsen, A., S. Lindenberg, and K. Petersen. "The impact of the zona pellucida thickness variation of human embryos on pregnancy outcome in relation to suboptimal embryo development. A prospective randomized controlled study." *Human Reproduction* 16, no. 10 (2001): 2166-2170.

[21] Authorithy, H. F. (2010). Trends and figures. UK: Authorithy, Human Fertilization and EMbryology

[22] http://www.hfea.gov.uk/ivf-figures-2006.html. (n.d.). IVF figures: 2009 and 2010. Retrieved 11 06, 2016, from Human Fertilization and Embryology Authority: http://www.hfea.gov.uk/ivf-figures-2006.htm

[23] G. D. Palermo et al., 'Oolemma characteristics in relation to survival and fertilization patterns of oocytes treated by intracytoplasmic sperm injection.', Hum. Reprod., vol. 11, no. l, pp. 172–176, 1996.

[24] M. A. Danfour and M. S. Elmahaishi, 'Human oocyte oolemma characteristic is positively related to embryo developmental competence after ICSI procedure', Middle East Fertil. Soc. J., vol. 15, no. 4, pp. 269–273, 2010.

[25] M. Khalilian, M. R. Valojerdi, M. Navidbakhsh, M. Chizari, and P. Eftekhari-Yazdi, 'Estimating zona pellucida hardness under microinjection to assess oocyte/embryo quality: Analytical and experimental studies', Adv. Biosci. Biotechnol., vol. 4, pp. 679–688, 2013.

[26] K. Yanagida, H. Katayose, H. Yazawa, Y. Kimura, K. Konnai, and A. Sato, 'The usefulness of a piezo-micromanipulator in intracytoplasmic sperm injection in humans.', Hum. Reprod., vol. 14, no. 2, pp. 448–453, 1998.

[27] J. M. R. Gerris, 'Single embryo transfer and IVF/ICSI outcome: A balanced appraisal', Hum. Reprod. Update, vol. 11, no. 2, pp. 105–121, 2005.

[28] Y. Kawase, T. Iwata, Y. Toyoda, T. Wakayama, R. Yanagimachi, and H. Suzuki, 'Comparison of intracytoplasmic sperm injection for inbred and hybrid mice', Mol. Reprod. Dev., vol. 60, no. 1, pp. 74–78, 2001.

[29] Y. Kawase et al., 'Effect of partial incision of the zona pellucida by piezo-micromanipulator for in vitro fertilization using frozen-thawed mouse spermatozoa on the developmental rate of embryos transferred at the 2-cell stage.', Biol. Reprod., vol. 66, no. 2, pp. 381–5, 2002.

[30] K. Ediz and N. Olgac, 'Effect of Mercury Column on the Microdynamics of the Piezo -Driven Pipettes', J. Biomech. Eng., vol. 127, no. 3, pp. 531–535, 2005.

[31] A. F. Ergenc, M. W. Li, M. Toner, J. D. Biggers, K. C. K. Lloyd, and N. Olgac, 'Rotationally oscillating drill (Ros-Drill©) for mouse ICSI without using mercury', Mol. Reprod. Dev., vol. 75, no. 12, pp. 1744–1751, 2008.

[32] A. F. Ergenc and N. Olgac, 'New technology for cellular piercing: Rotationally oscillating µ-injector, description and validation tests', Biomed. Microdevices, vol. 9, no. 6, pp. 885–891, 2007.

[33] L. Rienzi, E. Greco, F. Ubaldi, M. Iacobelli, F. Martinez, and J. Tesarik, 'Laser-assisted intracytoplasmic sperm injection', Fertil. Steril., vol. 76, no. 5, pp. 1045–1047, 2001.

[34] S. Abdelmassih, J. Cardoso, V. Abdelmassih, J. a Dias, R. Abdelmassih, and Z. P. Nagy, 'Laser-assisted ICSI: a novel approach to obtain higher oocyte survival and embryo quality rates.', Hum. Reprod., vol. 17, no. 10, pp. 2694–2699, 2002.

[35] Y. Murayama et al., 'Elasticity Measurement of Zona Pellucida Using a Micro Tactile Sensor to Evaluate Embryo Quality', J. Mamm. Ova Res., vol. 25, no. 1, pp. 8–16, 2008.

[36] Y. Murayama, C. E. Constantinou, and S. Omata, 'Micro-mechanical sensing platform for the characterization of the elastic properties of the ovum via uniaxial measurement', J. Biomech., vol. 37, no. 1, pp. 67–72, 2004.

[37] Y. Murayama et al., 'Mouse zona pellucida dynamically changes its elasticity during oocyte maturation, fertilization and early embryo development.', Hum. cell Off. J. Hum. Cell Res. Soc., vol. 19, no. 4, pp. 119–125, 2006.

[38] M. Khalilian, M. Navidbakhsh, M. R. Valojerdi, M. Chizari, and P. E. Yazdi, 'Estimating Young's modulus of zona pellucida by micropipette aspiration in combination with theoretical models of ovum', J. R. Soc. Interface, vol. 7, no. 45, pp. 687–694, 2010.

[39] Yu Sun, Kai-Tak Wan, K. P. Roberts, J. C. Bischof, and B. J. Nelson, 'Mechanical property characterization of mouse zona pellucida', IEEE Trans. Nanobioscience, vol. 2, no. 4, pp. 279–286, 2003.

[40] Y. Hiramoto and S. Nakamura, 'Mechanical properties of the cell surface in starfish eggs', vol. 20, no. 4, pp. 317–327, 1978.

[41] A. Pillarisetti, J. P. Desai, H. Ladjal, A. Schiffmacher, A. Ferreira, and C. L. Keefer, 'Mechanical Phenotyping of Mouse Embryonic Stem Cells: Increase in Stiffness with Differentiation', Cell. Reprogramming (Formerly 'Cloning Stem Cells'), vol. 13, no. 4, pp. 371–380, 2011.

[42] B. V Derjaguin, V. M. Muller, and Y. U. P. Toporov, 'Effect of contact deformation on the adhesion of particles.', J. Colloid Interface Sci., vol. 53, no. 2, pp. 314–326, 1975.

[43] Z. Zhang, M. A. Ferenczi, and C. R. Thomas, 'A micromanipulation technique with a theoretical cell model for determining mechanical properties of single mammalian cells', Chem. Eng. Sci., vol. 47, no. 6, pp. 1347–1354, 1992.

[44] H. Huang, J. K. Mills, C. Lu, and D. Sun, 'A universal piezo-driven ultrasonic cell microinjection system', Biomed. Microdevices, vol. 13, no. 4, pp. 743–752, 2011.

[45] Y. Xie, D. Sun, C. Liu, and S. H. Cheng, 'An adaptive impedance force control approach for robotic cell microinjection', 2008 IEEE/RSJ Int. Conf. Intell. Robot. Syst. IROS, pp. 907–912, 2008.

[46] Y. Xie, D. Sun, C. Liu, S. H. Cheng, and Y. H. Liu, 'A force control based cell injection approach in a bio-robotics system', Proc. - IEEE Int. Conf. Robot. Autom., pp. 3443–3448, 2009.

[47] S. D. Tan Y Huang W, Cheng SH., 'Mechanical modeling of biological cells in microinjection.', IEEE Trans Nanobioscience, vol. 7, no. 4, pp. 257–266, 2008.

[48] G. Gilardi and I. Sharf, 'Literature survey of contact dynamics modelling', Mech. Mach. Theory, vol. 37, no. 10, pp. 1213–1239, 2002.

[49] Lu, Zhe, Peter CY Chen, Hong Luo, Joohoo Nam, Ruowen Ge, and Wei Lin. "Models of maximum stress and strain of zebrafish embryos under indentation." Journal of biomechanics 42, no. 5 (2009): 620-625.

[50] Vassilev, V.M., Kostadinov, K.G., Mladenov, I.M., Shulev, A.A., Stoilov, G.I. and Djondjorov, P.A., 2011, April. Cell Membranes Under Hydrostatic Pressure Subjected to Micro- Injection. In AIP Conference Proceedings (Vol. 1340, No. 1, pp. 234-240). AIP.

[51] Lin, Y.L., Wang, D.M., Lu, W.M., Lin, Y.S. and Tung, K.L., 2008. Compression and deformation of soft spherical particles. Chemical Engineering Science, 63(1), pp.195-203.

[52] Westerfield, M., 1995. The zebrafish book: a guide for the laboratory use of zebrafish (Brachydanio rerio). University of Oregon press.

[53] S. Takeuchi, H. Minoura, T. Shibahara, X. Shen, N. Futamura, and N. Toyoda, 'Comparison of piezo-assisted micromanipulation with conventional micromanipulation for intracytoplasmic sperm injection into human oocytes', Gynecol. Obstet. Invest., vol. 52, no. 3, pp. 158–162, 2001.

[54] P. Collas and F. L. Barnes, 'Nuclear transplantation by microinjection of inner cell mass and granulosa cell nuclei', Mol. Reprod. Dev., vol. 38, no. 3, pp. 264–267, 1994.

[55] K. Yanagida, H. Katayose, H. Yazawa, Y. Kimura, K. Konnai, and a Sato, 'The usefulness of a piezo-micromanipulator in intracytoplasmic sperm injection in humans.', Hum. Reprod., vol. 14, no. 2, pp. 448–453, 1999.

[56] Z. Lu, X. Zhang, C. Leung, N. Esfandiari, R. F. Casper, and Y. Sun, 'Robotic ICSI (Intracytoplasmic Sperm Injection)', IEEE Trans. Biomed. Eng., vol. 58, no. 7, pp. 2102–2108, 2011.

[57] W. Wang, X. Liu, D. Gelinas, B. Ciruna, and Y. Sun, 'A fully automated robotic system for microinjection of zebrafish embryos', PLoS One, vol. 2, no. 9, 2007.

[58] A. Ghanbari, X. Chen, W. Wang, B. Horan, H. Abdi, and S. Nahavandi, 'Haptic microrobotic intracellular injection assistance using virtual fixtures', 11th Int. Conf. Control. Autom. Robot. Vision, ICARCV 2010, pp. 781–786, 2010.

[59] A. Sieber et al., 'A novel haptic platform for real time bilateral biomanipulation with a MEMS sensor for triaxial force feedback', Sensors Actuators, A Phys., vol. 142, no. 1, pp. 19–27, 2008.

[60] M. Ammi and A. Ferreira, 'Biological cell injection visual and haptic interface', Adv. Robot., vol. 20, no. January 2015, pp. 283–304, 2006.

[61] Y. Kimura and R. Yanagimachi, 'Intracytoplasmic sperm injection in the mouse', Biol Reprod, vol. 52, no. 4, pp. 709–720, 1995.

[62] D. Kim, B. Kim, S. Yun, and S. Kwon, 'Cellular force measurement for force reflected biomanipulation', IEEE Int. Conf. Robot. Autom. 2004. Proceedings. ICRA '04. 2004, no. April, p. 2412–2417 Vol.3, 2004.

[63] J. P. Desai, A. Pillarisetti, and A. D. Brooks, 'Engineering Approaches to Biomanipulation', Annu. Rev. Biomed. Eng., vol. 9, no. 1, pp. 35–53, 2007.

[64] Z. Lu, P. C. Y. Chen, H. Luo, J. Nam, R. Ge, and W. Lin, 'Models of maximum stress and strain of zebrafish embryos under indentation', J. Biomech., vol. 42, no. 5, pp. 620–625, 2009.

[65] M. Asgari, H. Abdi, C. P. Lim, and S. Nahavandi, 'Formulation and simulation of a 3D mechanical model of embryos for microinjection', Proc. - 2013 IEEE Int. Conf. Syst. Man, Cybern. SMC 2013, pp. 2219–2224, 2013.

[66] Z. Lu, P. C. Y. Chen, J. H. Nam, R. Ge, and W. Lin, 'A micromanipulation system for automatic batch microinjection', J. Micromechanics Microengineering, vol. 17, pp. 314–321, 2007.

[67] A. Pillarisetti, S. Member, M. Pekarev, A. D. Brooks, J. P. Desai, and A. Member, 'Evaluating the Effect of Force Feedback in Cell Injection', vol. 4, no. 3, pp. 322–331, 2007.

[68] Y. Xie, D. Sun, C. Liu, H. Y. Tse, and S. H. Cheng, 'A Force Control Approach to a Robot-assisted Cell Microinjection System', Int. J. Rob. Res., vol. 29, no. 9, pp. 1222–1232, 2010.

[69] Deok-Ho Kim, Seok Yun, and Byungkyu Kim, 'Mechanical force response of single living cells using a microrobotic system', IEEE Int. Conf. Robot. Autom., pp. 5013–5018, 2004.

[70] Xinyu Liu, K. Kim, Yong Zhang, and Yu Sun, 'Nanonewton Force Sensing and Control in Microrobotic Cell Manipulation', Int. J. Rob. Res., vol. 28, no. 8, pp. 1065–1076, 2009.

[71] P. C. Y. Chen et al., 'Speed optimization in automated microinjection of zebrafish embryos', Int. J. Control. Autom. Syst., vol. 13, no. 5, pp. 1233–1241, 2015.

[72] Kim, D.H., Sun, Y., Yun, S., Kim, B., Hwang, C.N., Lee, S.H. and Nelson, B.J., 2004, September. Mechanical property characterization of the zebrafish embryo chorion. In Engineering in Medicine and Biology Society, 2004. IEMBS'04. 26th Annual International Conference of the IEEE (Vol. 2, pp. 5061-5064). IEEE.

[73] Hajiyavand, A.M., Saadat, M. and Bedi, A.P.S., 2016, July. Polar body detection for ICSI cell manipulation. In Manipulation, Automation and Robotics at Small Scales (MARSS), International Conference on (pp. 1-6). IEEE.

[74] Hogan, Brigid, Frank Costantini, and Elizabeth Lacy. Manipulating the mouse embryo: a laboratory manual. Vol. 34. Cold Spring Harbor, NY: Cold spring harbor laboratory, 1986.

[75] Hogg, R.C.; Bandelier, F.; Benoit, A.; Dosch, R.; Bertrand, D. An automated system for intracellular and intranuclear injection. Journal of neuroscience methods 2008, 169, 65-75.

[76] Wang, Z.; Latt, W.T.; Tan, S.Y.M.; Ang, W.T. Visual servoed three-dimensional cell rotation system. IEEE Transactions on Biomedical Engineering 2015, 62, 2498-2507.

[77] Lu, Z.; Zhang, X.; Leung, C.; Esfandiari, N.; Casper, R.F.; Sun, Y. Robotic icsi (intracytoplasmic sperm injection). IEEE Transactions on Biomedical Engineering 2011, 58, 2102-2108.

[78] Feng, L.; Turan, B.; Ningga, U.; Arai, F. Three dimensional rotation of bovine oocyte by using magnetically driven on-chip robot, Intelligent Robots and Systems (IROS 2014), 2014 IEEE/RSJ International Conference on, 2014; IEEE: pp 4668-4673.

[79] Zhao, Q.; Sun, M.; Cui, M.; Yu, J.; Qin, Y.; Zhao, X. Robotic cell rotation based on the minimum rotation force. IEEE Transactions on Automation Science and Engineering 2015, 12, 1504-1515.

[80] Nan, Z. and Xu, Q., 2017, July. Multiple-cell recognition and path planning for robotic microinjection system. In Control Conference (CCC), 2017 36th Chinese (pp. 6691-6696). IEEE

[81] Wang, Z., Feng, C., Ang, W.T., Tan, S.Y.M. and Latt, W.T. Autofocusing and polar body detection in automated cell manipulation. IEEE Transactions on Biomedical Engineering, 2017, 64(5), pp.1099-1105.

[82] Boukallel, M.; Gauthier, M.; Dauge, M.; Piat, E.; Abadie, J. Smart microrobots for mechanical cell characterization and cell convoying. IEEE transactions on biomedical engineering 2007, 54, 1536-1540.

[83] Janocha, H. In Microactuators-principles, applications, trends, Proc. MICRO. tec 2000, VDE World Microtechnology Congress, 2000; pp 25-27.

[84] Bellouard, Y. Microrobotics: Methods and applications. CRC Press: 2009.

[85] Leung, C.; Lu, Z.; Zhang, X.P.; Sun, Y. Three-dimensional rotation of mouse embryos. IEEE Transactions on Biomedical Engineering 2012, 59, 1049-1056.

[86] Nguyen, B.V.; Wang, Q.G.; Kuiper, N.J.; El Haj, A.J.; Thomas, C.R.; Zhang, Z. Biomechanical properties of single chondrocytes and chondrons determined by micromanipulation and finite-element modelling. Journal of the Royal Society Interface 2010, 7, 1723-1733.

[87] Mohanty, S.K.; Gupta, P.K. Laser-assisted three-dimensional rotation of microscopic objects. Review of scientific instruments 2004, 75, 2320-2322.

[88] Shen, Y.; Fukuda, T. State of the art: Micro-nanorobotic manipulation in single cell analysis. Robotics and Biomimetics 2014, 1, 21.

[89] Chronis, N.; Lee, L.P. Polymer mems-based microgripper for single cell manipulation, Micro Electro Mechanical Systems, 2004. 17th IEEE International Conference on.(MEMS), 2004; IEEE: pp 17-20.

[90] Jager, E.W.; Inganäs, O.; Lundström, I. Microrobots for micrometer-size objects in aqueous media: Potential tools for single-cell manipulation. Science 2000, 288, 2335-2338.

[91] Ichikawa, A.; Sakuma, S.; Shoda, T.; Arai, F.; Akagi, S. On-chip enucleation of oocyte using untetherd micro-robot with gripping mechanism, Micro-NanoMechatronics and Human Science (MHS), 2013 International Symposium on, 2013; IEEE: pp 1-3.

[92] Zhang, Y.; Tan, K.K.; Huang, S. Vision-servo system for automated cell injection. IEEE Transactions on Industrial Electronics 2009, 56, 231-238.

[93] Shin, Y.K.; Kim, Y.; Kim, J. Automated microfluidic system for orientation control of mouse embryos, Intelligent Robots and Systems (IROS), 2013 IEEE/RSJ International Conference on, 2013; IEEE: pp 496-501.

[94] Otsu, N. A threshold selection method from gray-level histograms. IEEE transactions on systems, man, and cybernetics 1979, 9, 62-66.
[95] Wang, Y.; Zhao, X.; Zhao, Q.; Lu, G. Illumination intensity evaluation of microscopic image based on texture information and application on locating polar body in oocytes, Proceedings of China Automation Conference, Beijing, China, 2011; pp 7-10.
[96] Chen, D., Sun, M. and Zhao, X. Oocytes polar body detection for automatic enucleation. Micromachines, 2016, 7(2), p.27.
[97] Zhao, Q., Cui, M., Zhang, C., Yu, J., Sun, M. and Zhao, X., 2014, April. Robotic enuleation for oocytes. In Nano/Micro Engineered and Molecular Systems (NEMS), 2014, 9th IEEE International Conference on (pp. 23-27). IEEE.
[98] Sun, Y.; Nelson, B.J. Biological cell injection using an autonomous microrobotic system. The International Journal of Robotics Research 2002, 21, 861-868.
[99] Du, Q.; Zhang, Q.; Tian, L.; Wu, Z. Object detection and tracking for a vision guided automated suspended cell injection process, Mechatronics and Automation (ICMA), 2010 International Conference on, 2010; IEEE: pp 1760-1764.
[100] Blake, A.; Isard, M. Active contours: The application of techniques from graphics, vision, control theory and statistics to visual tracking of shapes in motion. Springer Science & Business Media: 2012.
[101] Rienzi, L.; Balaban, B.; Ebner, T.; Mandelbaum, J. The oocyte. Human Reproduction 2012, 27, i2-i21.
[102] Al-amri, S.S.; Kalyankar, N.; Khamitkar, S. Linear and non-linear contrast enhancement image. International Journal of Computer Science and Network Security 2010, 10, 139-143.
[103] Rafael Gonzalez, C.; Woods, R. Digital image processing. Pearson Education 2002.
[104] Priya, S.; Kumar, T.A.; Paul, V. A novel approach to fabric defect detection using digital image processing, Signal Processing, Communication, Computing and Networking Technologies (ICSCCN), 2011 International Conference on, 2011; IEEE: pp 228-232.
[105] VC, H.P. Method and means for recognizing complex patterns. Google Patents: 1962.
[106] Caponetti, L.; Castellano, G.; Basile, M.T.; Corsini, V. Fuzzy mathematical morphology for biological image segmentation. Applied intelligence 2014, 41, 117-127.
[107] Hamarneh, G.; Althoff, K.; Abu-Gharbieh, R. Automatic line detection. Project Report for the Computer Vision Course Lund, Simon Fraser University 1999.
[108] Ng, Soon-Chye, Ariff Bongso, and Shan S. Ratnam. "Microinjection of human oocytes: a technique for severe oligoasthenoteratozoospermia." Fertility and sterility 56, no. 6 (1991): 1117-1123.
[109] Palermo, Gianpiero, Hubert Joris, Paul Devroey, and André C. Van Steirteghem. "Pregnancies after intracytoplasmic injection of single spermatozoon into an oocyte." The Lancet 340, no. 8810 (1992): 17-18.
[110] Palermo, G., H. Joris, P. Devroey, and A. C. Van Steirteghem. "Induction of acrosome reaction in human spermatozoa used for subzonal insemination." Human Reproduction 7, no. 2 (1992): 248-254.
[111] Van Steirteghem, André C., Zsolt Nagy, Hubert Joris, Jiaen Liu, Catherine Staessen, Johan Smitz, Arjoko Wisanto, and Paul Devroey. "High fertilization and implantation rates after intracytoplasmic sperm injection." Human Reproduction 8, no. 7 (1993): 1061-1066.
[112] Cohen, Jacques, Mina Alikani, Henry E. Malter, Alexis Adler, Beth E. Talansky, and Zev Rosenwaks. "Partial zona dissection or subzonal sperm insertion: microsurgical fertilization alternatives based on evaluation of sperm and embryo morphology." Fertility and sterility 56, no. 4 (1991): 696-706.
[113] Malter, Henry E. "Micromanipulation in assisted reproductive technology." Reproductive biomedicine online 32, no. 4 (2016): 339-347.

[114] D. Beebe, M. Wheeler, H. Zeringue, E. Walters, and S. Raty, "Microfluidic technology for assisted reproduction," Theriogenology, vol. 57, no. 1, pp. 125–135, 2002.

[115] Hogg, Ron C., Florence Bandelier, Audrey Benoit, Roland Dosch, and Daniel Bertrand. "An automated system for intracellular and intranuclear injection." Journal of neuroscience methods 169, no. 1 (2008): 65-75.

[116] Wang, Zenan, Win Tun Latt, Steven Yih Min Tan, and Wei Tech Ang. "Visual Servoed Three-Dimensional Cell Rotation System." IEEE Transactions on Biomedical Engineering 62, no. 10 (2015): 2498-2507.

[117] Lu, Zhe, Xuping Zhang, Clement Leung, Navid Esfandiari, Robert F. Casper, and Yu Sun. "Robotic ICSI (intracytoplasmic sperm injection)." IEEE Transactions on Biomedical Engineering 58, no. 7 (2011): 2102-2108.

[118] S. Muntwyler, F. Beyeler, and B. J. Nelson, "Three-axis micro-force sensor with sub-micro-newton measurement uncertainty and tunable force range," J. Micromech. Microeng., vol. 20, no. 2, 2010, Art. no. 025011.

[119] F. Beyeler et al., "Monolithically fabricated microgripper with integrated force sensor for manipulating microobjects and biological cells aligned in an ultrasonic field," J. Microelectromech. Syst., vol. 16, pp. 7–15, Feb. 2007

[120] K. Kim, X. Liu, Y. Zhang, and Y. Sun, "Nanonewton force-controlled manipulation of biological cells using a monolithic MEMS microgripper with two-axis force feedback," J. Micromech. Microeng., vol. 18, no. 5, 2008, Art. no. 055013.

[121] B. Solano and D. Wood, "Design and testing of a polymeric microgripper for cell manipulation," Microelectron. Eng., vol. 84, nos. 5–8, pp. 1219–1222, 2007.

[122] B. Solano, A. Gallant, and D. Wood, "Design and optimisation of a microgripper: Demonstration of biomedical applications using the manipulation of oocytes," in Proc. Symp. Design, Test, Integr. Packag., Apr. 2009, pp. 61–65.

[123] S. Raty et al. "Embryonic development in the mouse is enhanced via microchannel culture," Lab Chip, vol. 4, pp. 186–190, 2004.

[124] Leung, Clement, Zhe Lu, Xuping P. Zhang, and Yu Sun. "Three-dimensional rotation of mouse embryos." IEEE Transactions on Biomedical Engineering59, no. 4 (2012): 1049-1056.

[125] R. Ma et al., "In vitro fertilization on a single-oocyte positioning system integrated with motile sperm selection and early embryo development," Anal. Chem., vol. 83, no. 8, pp. 2964–2970, 2011.

[126] C. Han et al., "Integration of single oocyte trapping, in vitro fertilization and embryo culture in a microwell-structured microfluidic device," Lab Chip, vol. 10, pp. 2848–2854, 2010.

[127] Benhal, Prateek, J. Geoffrey Chase, Paul Gaynor, Björn Oback, and Wenhui Wang. "AC electric field induced dipole-based on-chip 3D cell rotation." Lab on a Chip 14, no. 15 (2014): 2717-2727.

[128] Arnold, W. Michael, Rita K. Schmutzler, Andreas G. Schmutzler, Hans van der Ven, Safaa Al-Hasani, Dieter Krebs, and Ulrich Zimmermann. "Electro-rotation of mouse oocytes: single-cell measurements of zona-intact and zona-free cells and of the isolated zona pellucida." Biochimica et Biophysica Acta (BBA)-Biomembranes 905, no. 2 (1987): 454-464.

[129] Liang, Yuan-Li, Yuan-Peng Huang, Yen-Sheng Lu, Max T. Hou, and J. Andrew Yeh. "Cell rotation using optoelectronic tweezers." Biomicrofluidics4, no. 4 (2010): 043003.

[130] Jager, Edwin WH, Olle Inganäs, and Ingemar Lundström. "Microrobots for micrometer-size objects in aqueous media: potential tools for single-cell manipulation." Science 288, no. 5475 (2000): 2335-2338.

[131] Chiou, Eric PY, and Ming C. Wu. "OPTOELECTRONIC TWEEZERS." Micro/Nano Technology Systems for Biomedical Applications: Microfluidics, Optics, and Surface Chemistry (2010): 317.

[132] Thakur, Atul, Sagar Chowdhury, Petr Švec, Chenlu Wang, Wolfgang Losert, and Satyandra K. Gupta. "Indirect pushing based automated micromanipulation of biological cells using optical tweezers." The International Journal of Robotics Research (2014): 0278364914523690.

[133] W. T. Coakley, D. W. Bardsley, M. A. Grundy, F. Zamani, and D. J. Clarke, "Cell manipulation in ultrasonic standing wave fields," J. Chem. Technol. Biotechnol., vol. 44, no. 1, pp. 43–62, 1989.

[134] Sun, Yu, and Bradley J. Nelson. "Biological cell injection using an autonomous microrobotic system." The International Journal of Robotics Research 21, no. 10-11 (2002): 861-868.

[135] Huang, Haibo B., Dong Sun, James K. Mills, and Shuk Han Cheng. "Robotic cell injection system with position and force control: toward automatic batch biomanipulation." IEEE transactions on robotics 25, no. 3 (2009): 727-737.

[136] Lu, Zhe, Peter CY Chen, Joohoo Nam, Ruowen Ge, and Wei Lin. "A micromanipulation system with dynamic force-feedback for automatic batch microinjection." Journal of micromechanics and microengineering 17, no. 2 (2007): 314.

[137] Lu, Zhe, Xuping Zhang, Clement Leung, Navid Esfandiari, Robert F. Casper, and Yu Sun. "Automated cell manipulation: Robotic ICSI." In Robotics and Automation (ICRA), 2011 IEEE International Conference on, pp. 2540-2545. IEEE, 2011.

[138] Yanaihara, A., Iwasaki, S., Negishi, M. and Okai, T., 2005. Intracytoplasmic Sperm Injection: Technical Improvement. Taiwanese Journal of Obstetrics and Gynecology, 44(4), pp.314-317.

[139] Bahadur, I.M. and Mills, J.K., 2012, July. Dynamic model of micropipettes in piezo-assisted icsi. In Complex Medical Engineering (CME), 2012 ICME International Conference on (pp. 191-196). IEEE.

[140] Bahadur, I.M. and Mills, J.K., 2013, May. A mechanical perforation procedure for embryo biopsy. In Complex Medical Engineering (CME), 2013 ICME International Conference on (pp. 313-318). IEEE.

APPENDICES

Appendix A: Measurement differences between manual and experimental

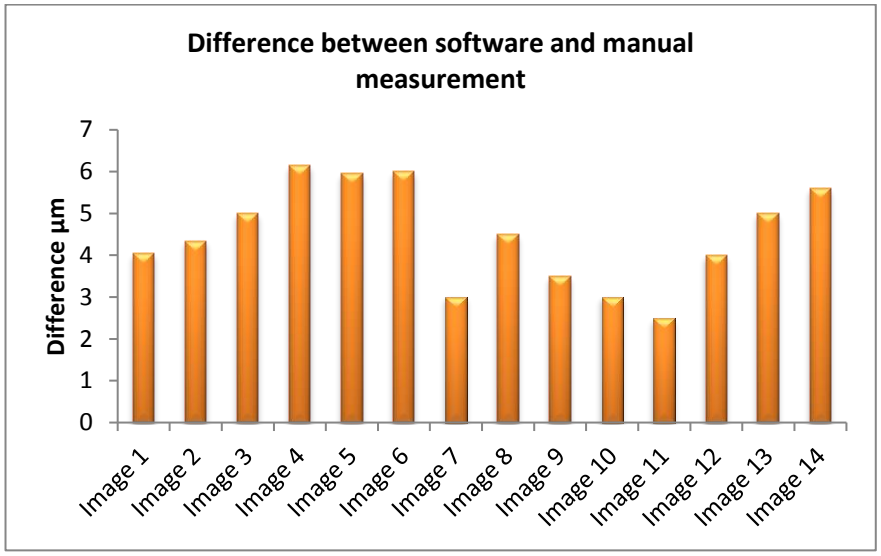

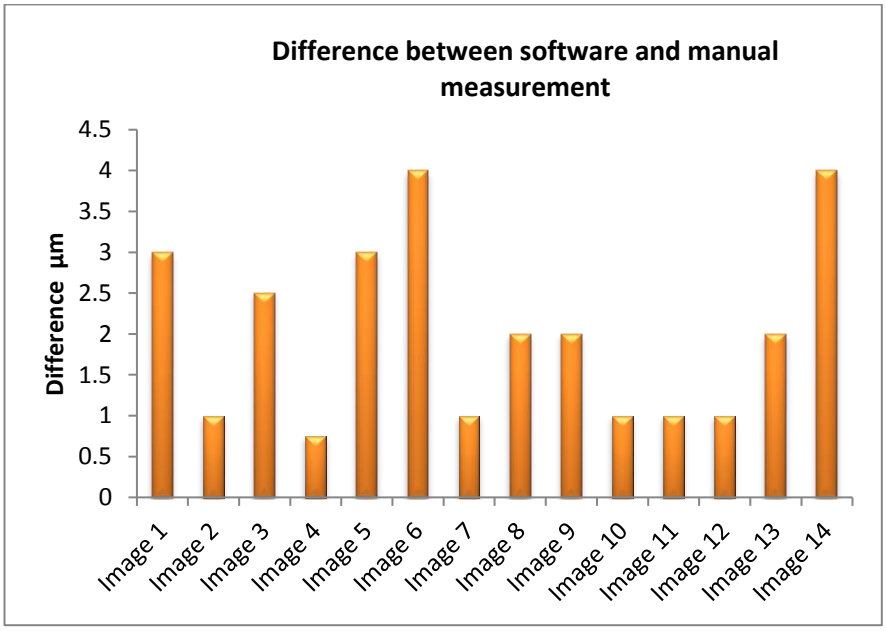

Appendix B: Measurement data for 10 zebrafish embryo experiments

NO	Constant speed mm/s	Tests										Mean
		T1	T2	T3	T4	T5	T6	T7	T8	T9	T10	
1	0.05	377	383	376	388	382	385	381	380	379	371	380.2
2	0.1	344	358	355	352	344	346	347	346	352	350	349.4
3	0.2	331	333	325	328	334	325	328	325	330	332	329.1
4	0.4	315	312	326	322	321	314	319	322	325	325	320.1
5	0.6	290	291	296	299	289	294	292	299	298	294	294.2
6	1	265	260	259	260	267	262	263	263	266	265	263
7	1.2	244	242	235	239	241	242	236	239	238	244	240

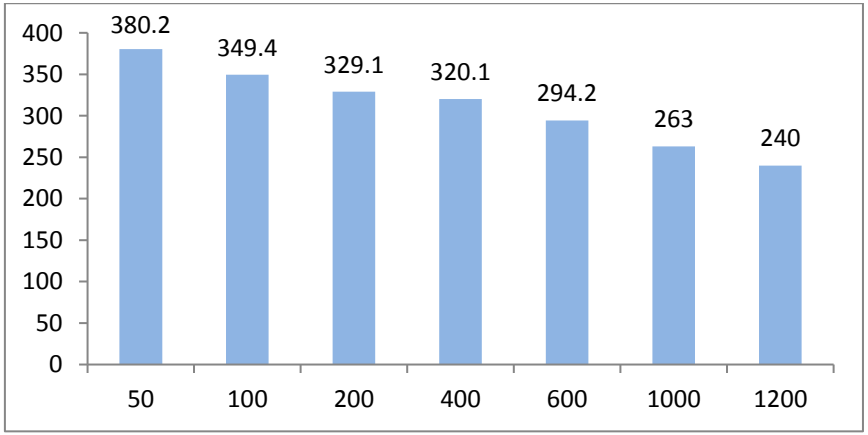

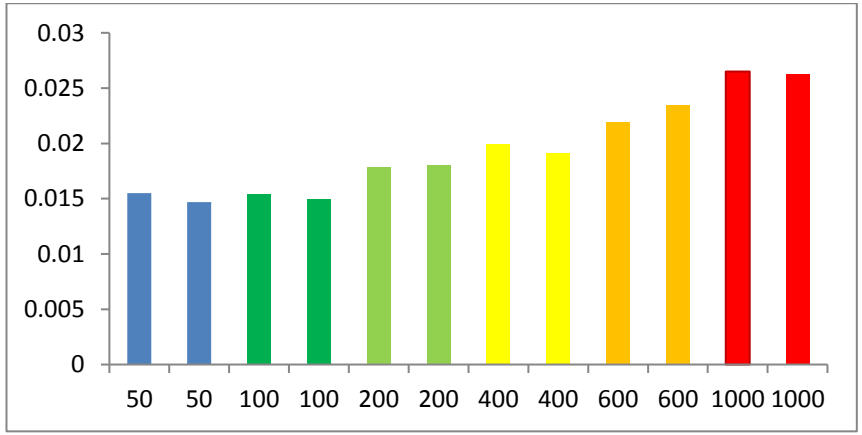

Appendix C: Deformation creation for 10 experiments for each speed with different embryos

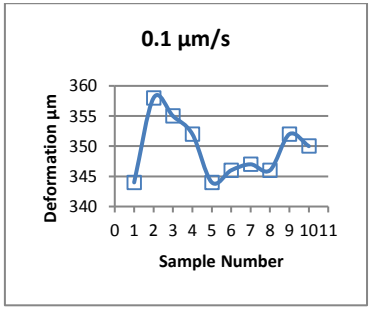

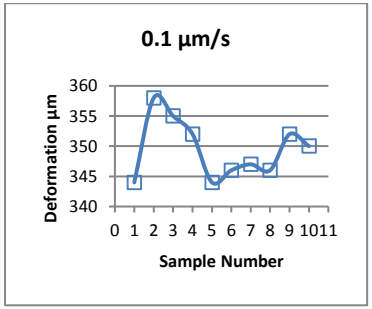

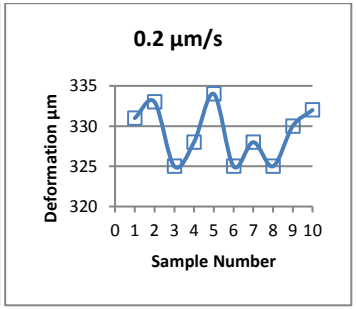

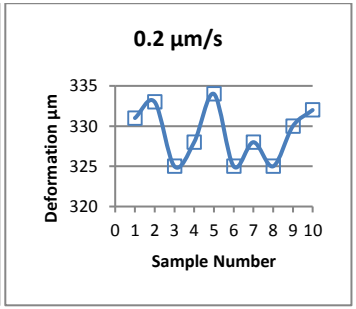

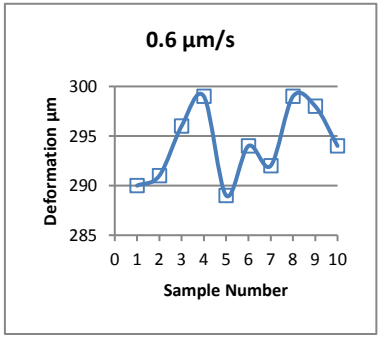

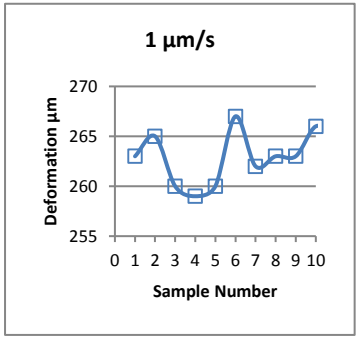

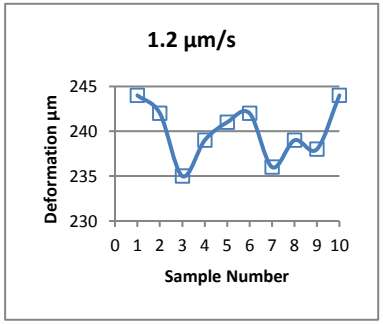

Deformation versus indentation force for different speeds

Experiment No	Speed mm/s	Deformation	Indentation force
Series 1	0.05	375 µm	1.17 µN
Series 2		384 µm	1.12 µN
Series 3	0.1	343 µm	1.22 µN
Series 4		339 µm	1.24 µN
Series 5	0.2	331 µm	1.2 µN
Series 6		326 µm	1.18 µN
Series 7	0.4	313 µm	1.26 µN
Series 8		319 µm	1.26 µN
Series 9	0.6	279 µm	1.31 µN
Series 10		284 µm	1.36 µN
Series 11	1	251 µm	1.4 µN
Series 12		247 µm	1.42 µN

Appendix D: Manual measurement of deformation using ImageJ

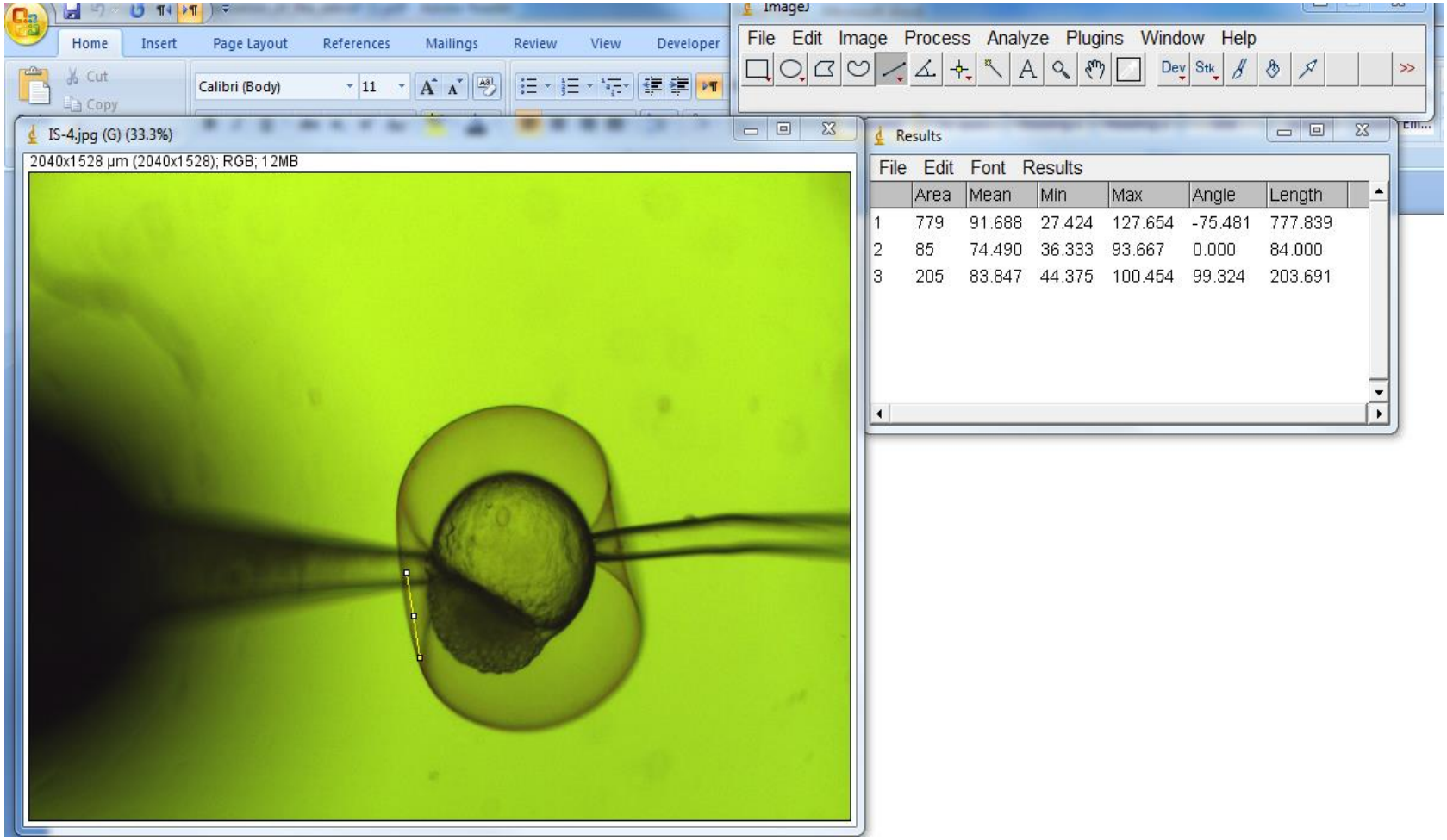

Appendix D: Manual measurement of deformation using ImageJ, Continued

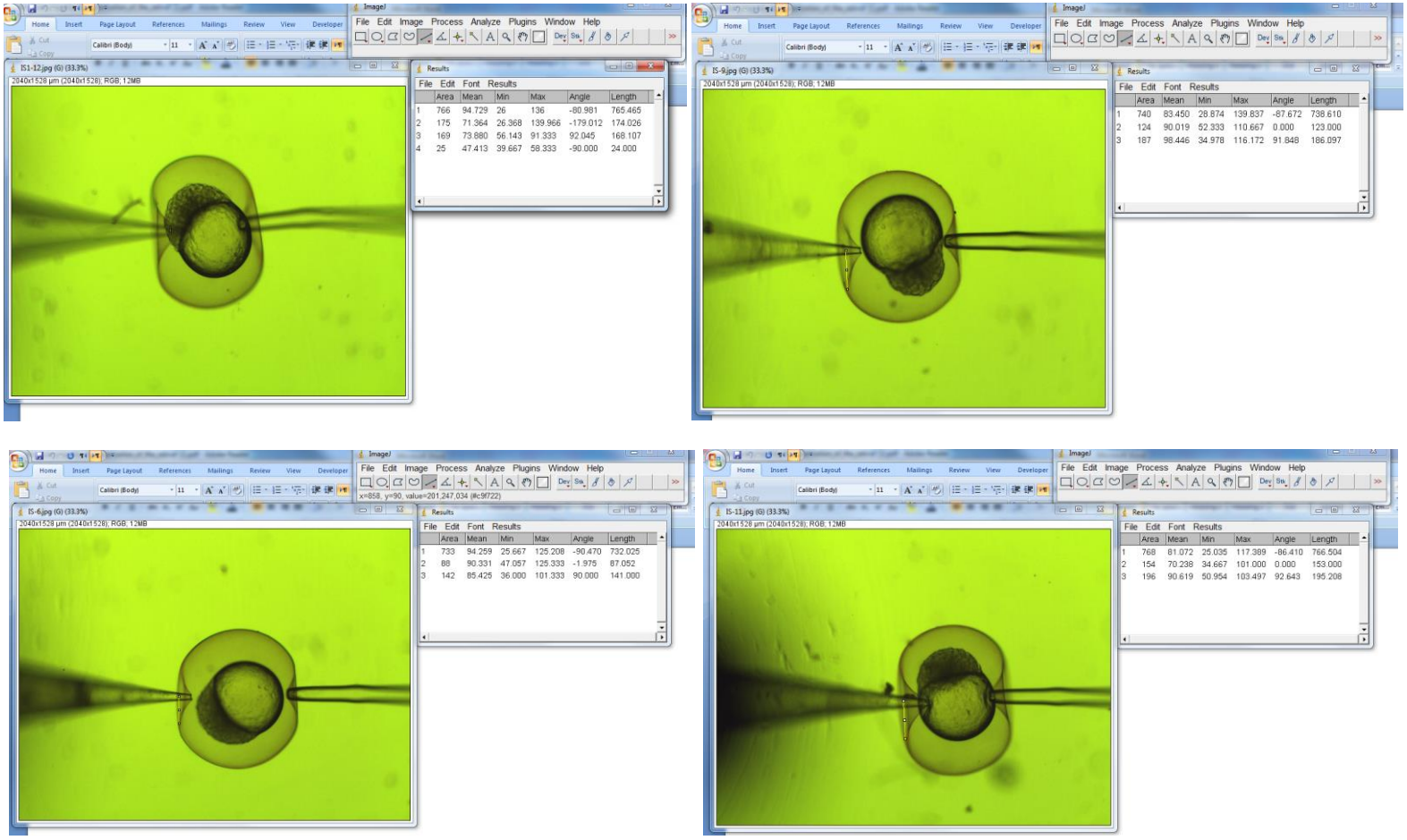

Appendix D: Manual measurement of deformation using ImageJ, Continued

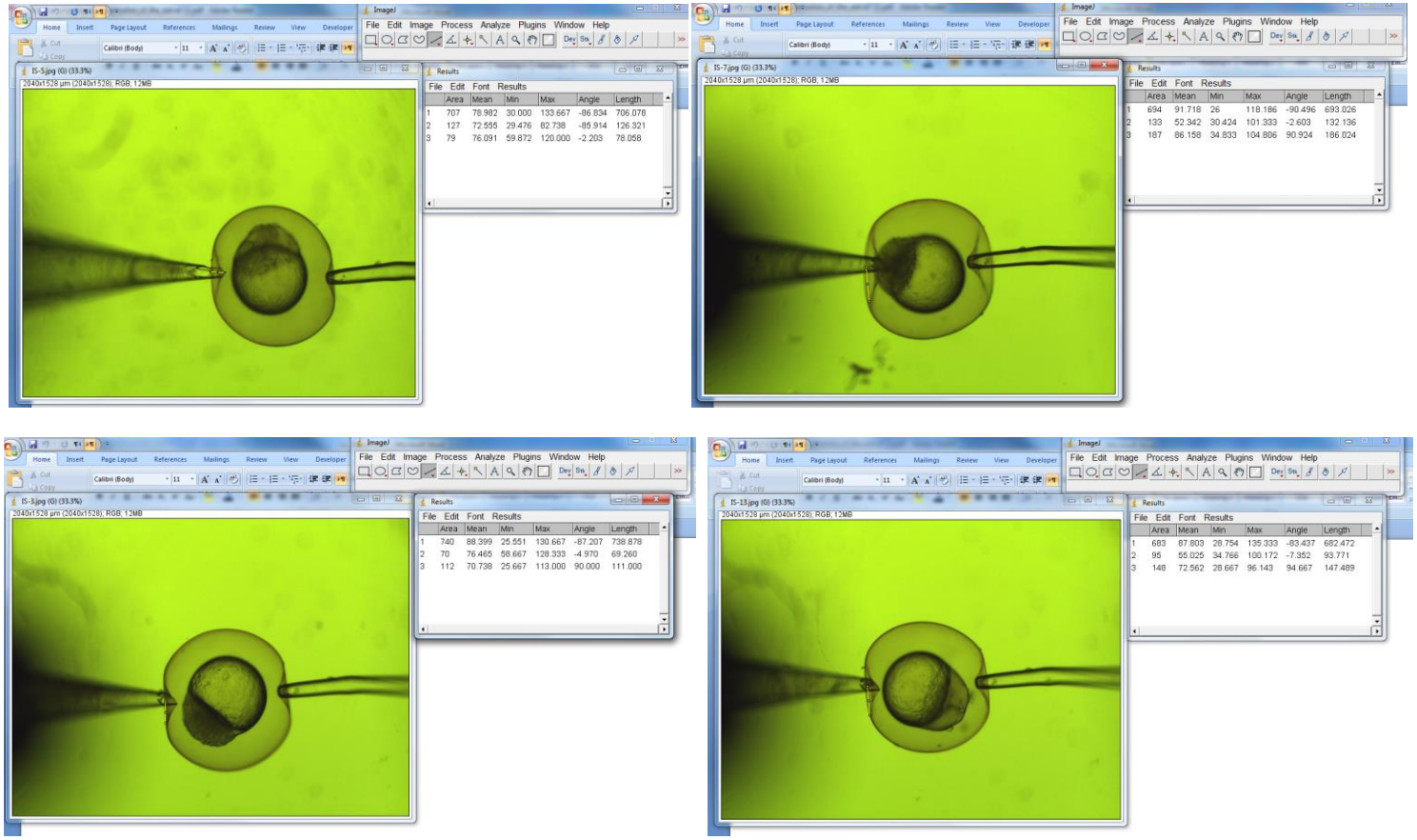

Appendix D: Manual measurement of deformation using ImageJ, Continued

	Diameter µm	F mN	H µm	W_d µm	a µm	c µm	E Pa
Image 1	682.472	0.39	3	93.771	147.489	20	**1.45E+06**
Image 2	747.024	0.38	3	132.034	210.086	20	**1.52E+06**
Image 3	738.61	0.43	3	123.000	186.097	20	**1.47E+06**
Image 4	732.025	0.35	3	87.052	141.000	20	**1.40E+06**
Image 5	766.504	0.61	3	153.000	195.208	20	**1.26E+06**
Image 6	706.078	0.23	3	78.058	126.321	20	**8.89E+05**
Image 7	693.026	0.62	3	132.136	186.24	20	**1.72E+06**
Image 8	738.878	0.34	3	69.200	111.000	20	**1.21E+06**

Appendix L: Images from FE model for 100 µm/s

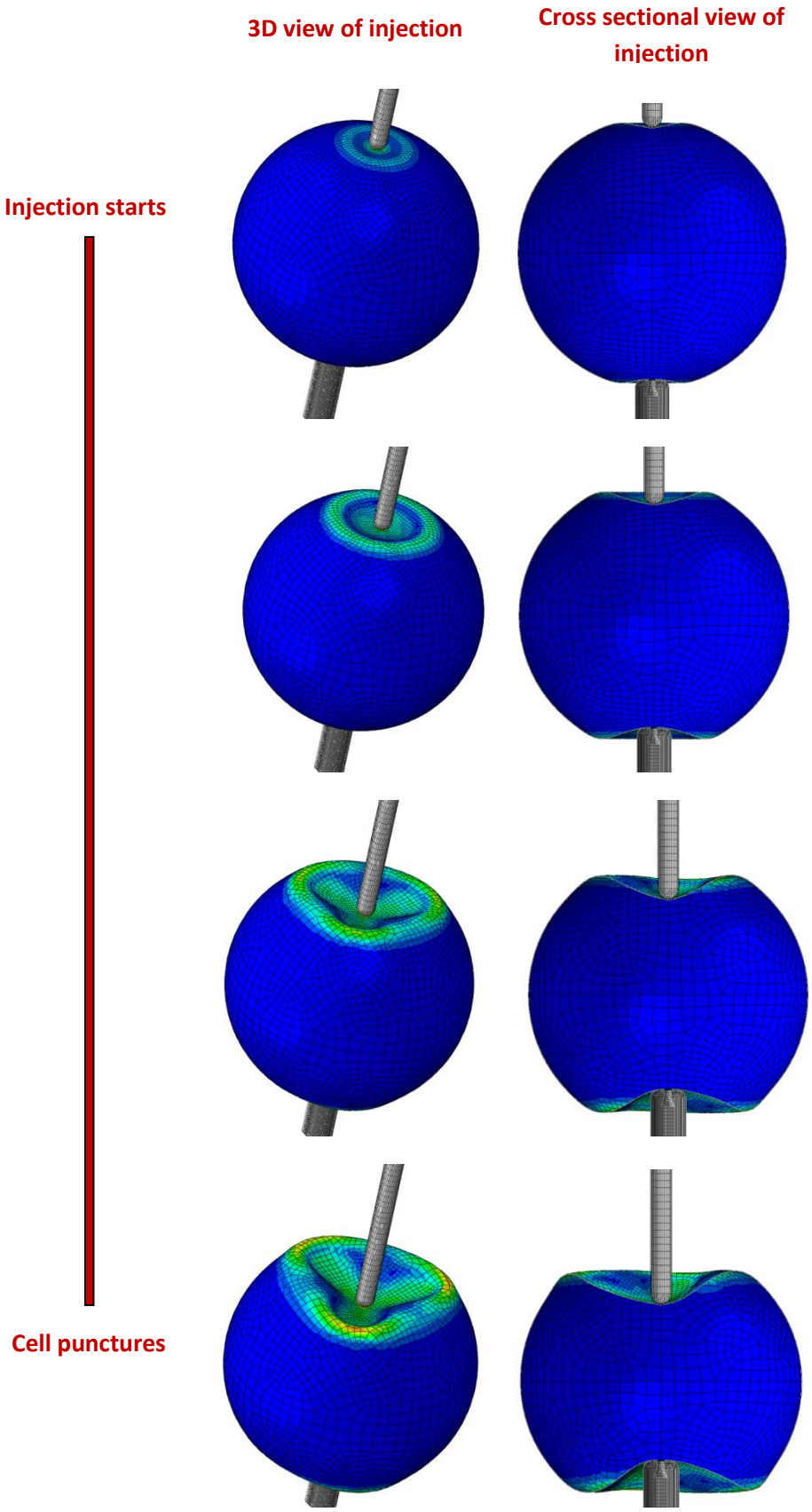

Appendix M: Images from FE model for 600 µm/s

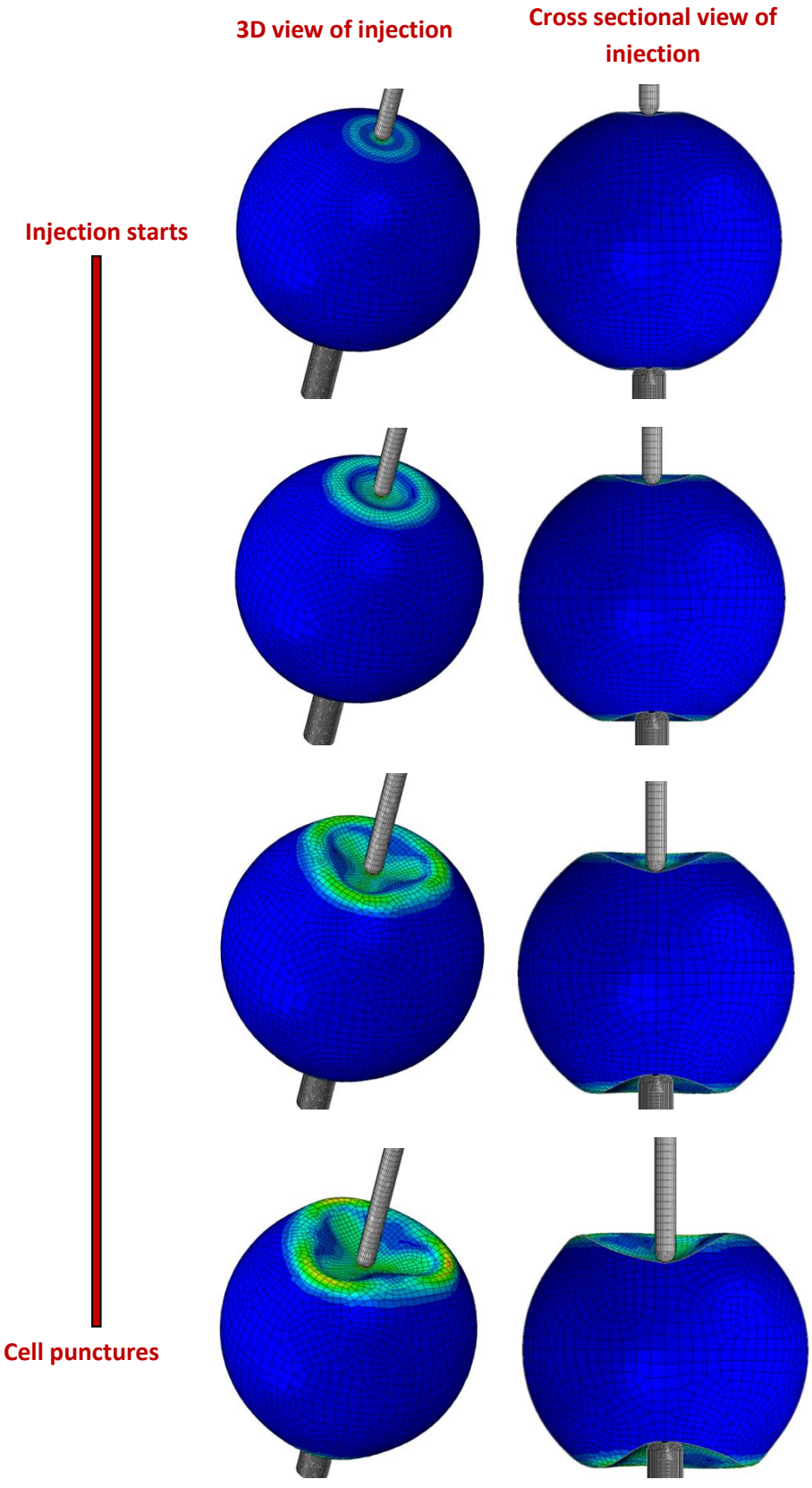

Appendix N: Images from FE model for 1000 µm/s